UC Davis
UC Davis Electronic Theses and Dissertations

Title
Numerical Modeling of Floodplains: Evaluating Ecological Outcomes

Permalink
https://escholarship.org/uc/item/7x2240nw

Author
Tomkovic, Lily Ann

Publication Date
2022

Peer reviewed|Thesis/dissertation

eScholarship.org Powered by the California Digital Library
University of California

Numerical Modeling of Floodplains: Evaluating Ecological Outcomes

By

LILY ANN TOMKOVIC

DISSERTATION

Submitted in partial satisfaction of the requirements for the degree of

DOCTOR OF PHILOSOPHY

in

Civil and Environmental Engineering

in the

OFFICE OF GRADUATE STUDIES

of the

UNIVERSITY OF CALIFORNIA

DAVIS

Approved:

_____

Fabián A. Bombardelli, Chair

_____

S. Geoffrey Schladow

_____

John L. Largier

Committee in Charge

2022

Copyright © 2022 by
Lily Ann Tomkovic
All rights reserved.

Contents

List of Figures

List of Tables

Abstract

Numerical Modeling of Floodplains: Evaluating Ecological Outcomes

Rivers and their floodplains are a complex system that presents numerous challenges when coupled with human adaptation. The many adaptations humans have made to the landscape have come at the cost of aquatic ecology. Efforts have gone underway to mitigate those costs and begin to repair our relationship with the aquatic landscape via restoration and re-engineering systems to benefit habitat. Of the myriad of tools at our disposal to investigate different restoration strategies, this thesis explores the application of hydrodynamic models to ecosystems and how the linkages between numerical models can evaluate ecological outcomes.

The application of this thesis has centered around the Sacramento-San Joaquin Delta, a focal point of California's Central Valley and a critical ecosystem in the state. The Sacramento-San Joaquin Delta has many "islands" which are essentially parcels of land that have levees surrounding them to protect against flooding from the Delta's channels. One island in the Delta is the McCormack-Williamson Tract, which lies just below the confluence of the Cosumnes and Mokelumne Rivers. The McCormack-Williamson Tract is the study area for Chapters 2 and 3, where a hydrodynamic model was developed and calibrated to investigate natural phenomena. The models were calibrated against observed flood events and then used to compare against field data collected in the study systems within the model calibration period. By pairing observed field data with replicated modeling data, linkages between source water distribution, age, and general hydrodynamic features were drawn. These linkages provide useful tools in the field of floodplain restoration engineering.

Chapter 2 demonstrates a hydrodynamic model's ability to resolve the spatio-temporal distribution of the water from the convergence of the Mokelumne and Cosumnes Rivers as they advance through the McCormack-Williamson Tract and its surrounding channels and sloughs. This modeling effort was coupled with an isotopic mixing model using water sampling in the study area, and shows that the two methods agree on source water

distribution.

The subsequent chapter (Chapter 3) that focuses on the McCormack-Williamson Tract evaluates a modeled water age against field-collected zooplankton abundance. Although this study did not find a robust relationship between the two variables, the chapter lays out the methodology used to investigate the relationship.

The second study area centered around a key feature in the Delta's hydrography - the Yolo Bypass. The Yolo Bypass is a major floodplain to convey flood waters from the Feather, American, and Sacramento Rivers around major cities and dwellings and into the Delta. Chapter 4 outlines the development and calibration of a model of the Yolo Bypass and discusses the applications the model can have to answer ongoing questions about the study system.

Acknowledgments

Firstly, I'd like to thank my advisor, Fabián A. Bombardelli for guiding me all the way from my Bachelor's Degree through the completion of my PhD. Additionally, I'd like to thank him for submitting my application to the ARCS Foundation award along with my sincerest gratitude to the ARCS Foundation for the award I received in 2016. Without that award I can't say that my time in graduate school would have been as smooth as it was. I also had the pleasure of receiving the Farrer/Patten Award from Thomas and Nancy Patten in 2017 and will always be grateful for their fund. I received additional funding from Yolo County and the Delta Stewardship Council Grant #1471.

I owe an enormous debt of gratitude to Lauren Worrell, the Civil Environmental Engineering department's Graduate Program Coordinator, because of all of the thoughtful and thorough attention she gave my graduate career. I've really enjoyed getting to know her as a person and coordinate with her on graduate social programs like intramural sports. Without Lauren, finishing this thesis would have been much more difficult.

I received a great deal of mentoring from Ed Gross and can truly say that I wouldn't have gotten as far as I did without him and his guidance. During my Masters and in completion of my Chapter 4 I received excellent mentoring from Bill Fleenor and am so grateful for his guidance, positivity, and puppies. Rusty Holleman taught me many things about Deltares and coding that I will always carry with me in my career.

The Center for Watershed Sciences (CWS) had so much to offer and I'd like to thank everyone in their various roles. I received a lot of technical support from George Scheer and Nick Santos, thank you for helping me when I was in the computational weeds. Thomas Handley provided bathymetric support and was one of my first modeling buddies at CWS. I also want to thank Alessia for being my co-modeler on the Yolo Bypass work. For the years I was able to work with them I'd like to thank Ludmila Rechiman and Sophie Munger for their modeling collaboration, may Ludmila rest in peace. The prin-

cipal investigator of the McCormack-Williamson Tract project, Carson Jeffres, deserves my eternal gratitude for his guidance with Chapters 2 and 3, for his guidance in life, for his mentorship in my career, and for his friendship. Carson's co-lab director, Rachel Johnson, also offered sage words and loving support of my research. I'd like to thank my officemates Lauren Adams, Ann Willis, and Rob Lusardi for being great co-workers and friends. I developed many deep friendships at CWS and would like to acknowledge Mollie Ogaz, Miranda Bell Tilcock, Nick Corline, and Eric Holmes for their companionship and support of me as a human. It wasn't just the humans at CWS, however, I'd like to shout out to Louie, Rico, Luna, Gus, Tippy, Oliver, and Emmy for helping keep me sane in the office space.

I couldn't mention all those dogs without mentioning the dog that means the world to me, my child, my darling, my Guppy puppy. You're the wind beneath my wings, I love you so much you sweet little angel.

Speaking of *my* child, I'd like to thank my parents that I'm a child *of*, Lorraine Fiamengo and Bill Tomkovic for their love and support for my entire life. I wouldn't be the person I am without your DNA and parenting. Thank you so much I love you very much. My sister, Brandyn Carden, might be the only person in my family who actually knows what I did for my seven years in grad school and I really appreciate your love and support. Thank you for listening to me complain about model parameterization. Thank you to my brother-in-law, Matt Carden, for loving and caring for my sister and for SCUBA diving with me in Catalina, you're the best. Shout out to Tennie, Delta, Tango, and Foxtrot, you're all wonderful animals.

Thank you to my high school friends that I still hold very dear, Sam Howell and Camille Rowan and their families that have treated me as one of their own for so long. Thank you Whittaker Strain for loving Camille and providing us with little Eamon Strain. Love you all so much. Also, thank you Camille for introducing me to Emily Ziegler, and thank you

Emily for being one of my very best friends and to Nick Fowler for loving her so very much.

During grad school I discovered whitewater rafting courtesy of the Ecogeomorphology graduate course. I'd like to thank Roy Shlemon for his fund which subsidizes that trip and impacts so many students lives. On that trip I met a number of people and want to say thank you to my boating community: Avinash Patil, Ali Grechko, Matt Abshire, Ann W., Ryan Peek, Eric H., Devon Lambert, Zach Stelly-Riggs, Aliyah Cohen, Ben Dove, Clayton Herrmann, Jeff Mount, Larry Guenther, and last but certainly not least Jordy Margid. Jordy and his wife Catherine Rudiger have been like surrogate parents for me and Davis and are very dear friends of mine that I will hold onto for a lifetime. Thank you Laura, Gloria, and Vanna for being such an important part of Jordy and Catherine's lives.

On that boating trip I learned how much I like making music with other people and joined a band with John Mola, Joanna Sollins, Luke Peterson, and Ryan Peek. We were Awkward Endings and we made pretty decent music! Our jams and performances kept my spirit light throughout grad school and earned me musical skills that I'll carry forward for the rest of my life. Thank you all for being one of my highlights of grad school. Thank you also to Ellen Bruno for keeping jazz flute in my life. And thank you to my current band mates Abbey Hart, Griffin Capehart, Ryan P., and Joanna S. for still wanting to play music with me. And thank you to

Thank you to my various housemates in Davis. Everyone at the Caternity, you enriched my life and introduced me to so many amazing people and we just had so much fun together! Thank you Devin Humpal, Ernst Bertone Oehninger, Matt Blain-Hartung, Jessica Garcia, Curtis Morrill, and Ali Hill for being the best Caternity members ever and for lock-ins. My housemates Hannah and Edie were such amazing souls to live with and I'm so excited to get to live with you again and further deepen our friendship. I love you two beans. I also love their pets, Tyson and Paddles (RIP). During my final days as a graduate student I had the pleasure of being housemates with my dear friends

Jon Mortimer and Lola Quasebarth and their cat Smuckers. Jon, Lola, Smuckers - I will always think fondly of our time together and look forward to our music and friendship in the future.

Finally, the activities that kept me sane for the last few years of grad school were many. I'd like to specifically mention my canal shark community: Jon M., Lola Q., Chris and Madeline Schomburg, Kate Tiedeman and Brendan Barrett, Julia Michaels and Kyle Schoenberger, Jordan Hollarsmith and Kyle Neumann, Caroline Larsen-Bircher and Rebecca Bircher, and Sophie Irvin. Chomp chomp! I'd also like to mention all the love I have for the little shark pups out there: Ezra and Avi Schomburg, Tobi Tiedeman, and Baby Hollarmann. Another one of my favorite activities is climbing and I want to thank Derek Roberts and Ali Hill for being such amazing climbing buddies and going on so many adventures with me to various climbing areas. Also thank you Ash Z., Luke P., and Lauren A. for keeping my climbing stamina up in the gym!

While I acknowledge that my Acknowledgements section is quite long, I feel like I could keep going for twice as long to give credit where it's due for enriching my life in every little way that someone can while I completed my PhD at UC Davis. Without this degree I would probably have the same career options, but I would have missed all the golden friendships that developed while I toiled away at this degree. I'm eternally grateful to have every single one of you (and others I may have missed) in my life.

During the course of my tenure as a graduate student at UC Davis in the Civil Engineering Department I had the honor of receiving the Farrer/Patten Award in 2017 and the ARCS Award for the 2016-17 academic year. These awards were very important components of my success at UC Davis with not only financial support but most importantly the push to excel because of the distinction of being selected.

Thank you all.

Chapter 1

Introduction

As rivers have evolved throughout the natural history of our planet, one of their key features has been their floodplains. Adjacent to the incised channel cut by years of consistent flow is the floodplain, where water flows when the channel is overwhelmed by the river's discharge. A river and its floodplain have an innate interdependence on one another due to hydraulic dynamics and sediment availability, and they leave their fingerprint on each other in a geomorphic context [1]. These largely flat alluvial landforms are often the location of rich vegetation due to years of deposition of river sediments and decomposed plant matter, offering a nutrient-rich soil as well as ample and frequent soil saturation [2]. Tree species such as cottonwood have adapted to take advantage of the disturbance that floods provide as well as the slowly-waning ground water table as the flood waters recede, and have historically found success in floodplains [3]. From a natural history context, floodplains have been a pivotal component in aquatic and riparian ecology and due to their intertwined evolution with rivers have guided the evolution of riverine species with frequent floodplain access.

Naturally, it follows that floodplains have notable utility to fish [4]–[6]. Fish which migrate up- and down-river as a feature of their life cycle, anadromous fish, have particularly adapted to take advantage of an overflowing river in order to increase chances of survival and successful reproduction. Adult fish migrating upstream to spawn are able to use floodplains as a break from the currents they swim against, and if they are feeding then

they can feed on the strong presence of lower trophic level prey. Similarly, out-migrating juvenile anadromous fish that spend time in floodplains on their way downstream are able to rest and build biomass by consuming the zooplankton and other invertebrate populations that thrive in the shallow and slow moving aquatic environment [6]–[8]. Of course the ecological benefit does not stop at fish. Terrestrial birds have proven to utilize floodplain habitat during drought as a refuge [9]. Likewise, the riparian forests often found in floodplains can be home to numerous fauna, creating a rich and diverse ecosystem.

Although floodplains create bountiful habitat, they present an obstacle to humans who are adapted to dry land. Modern civilization has adapted to settlement in historically flooded regions by creating more consistently dry land with structures and diversions. As Jacob Katz of California Trout puts it "Humanity appears to abhor a puddle", and most features of modern society such as houses, school yards, streets and more are specifically designed to shed water or prevent the accumulation of water. Throughout modern settlements humanity has done its best to eliminate floodplains from the landscape so that they could be used for livestock grazing, farming, and structural developments. Essentially modifying the environment to suit human habitation. People still want to live near water for a myriad of reasons, 13.3% of the United States' population lives on land that has a 1% annual exceedance probability [10], but they don't want to suffer flood damage. This proximity to rivers and floodplains has lead humanity to adapt and utilize water resources in ecologically consequential ways.

Dams serve many purposes for humanity, including hydro-power generation, water storage and flood protection. All of the anthropocentric goals for dam operations eliminate the natural variability of a river system's hydrograph, with reduction of peak flows and increased magnitude of seasonal low-flows [11] (Figure 1.1). Although flood protection is not a dam's only purpose, their construction in conjunction with levee developments reduce the likelihood of infrastructure damages due to flood debris and undesirable submergence of properties during larger flow events. This civil infrastructure has created

a very effective way of living near rivers and other water resources with reduced risk of suffering losses in flood conditions. All of these recent developments that prioritize human safety and prosperity have drastically altered the conditions for riverine species both terrestrially and aquatically.

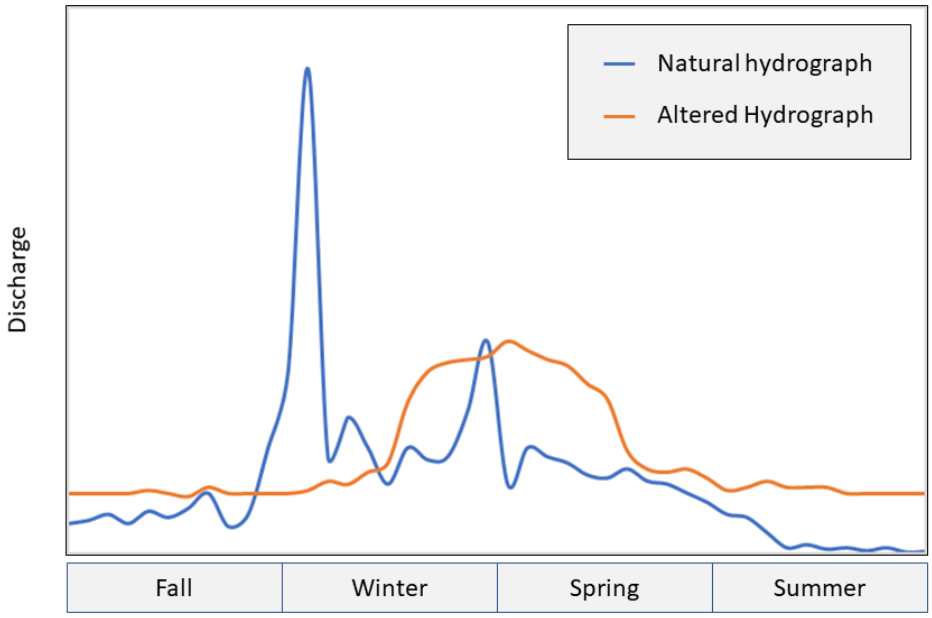

Figure 1.1: Typical natural hydrograph juxtaposed against an altered or managed system with dams or other flow regime modifications. (Adapted from Yarnell et al. 2015 [11] and Mount et al. 2017 [12])

Due to people-focused priorities in early modern settlement humans have greatly altered riverine ecological structures by removing a vast amount of wetlands and floodplains from the global landscape [13], [14] and eliminating vital habitat from the world's aquatic ecology. In many cases these major alterations have gone past the tipping point where the system can be recovered to a pre-settlement state. As society has progressed, however, scientific bodies have learned more about the ecological function that floodplains hold and the impact that their removal has had. This new consensus has prompted a surge in shallow-water-habitat restoration in areas critically affected by anthropogenic modifications.

Of course this habitat restoration comes with the balance of current demand for clean

freshwater extraction for human use as well as protection of human infrastructure and livelihood from flood waters. These co-equal goals set the framework for the limitations and constraints of proposed restoration strategies. There are multiple ways of evaluating what potential impacts of restoration construction could be, with the current standard being some sort of numerical modeling of the hydroscape.

Models are a tool which scientists use in order to investigate potential linkages and causalities in a system without the need of altering the system itself. With numerical models of river systems, one can evaluate a myriad of factors relating to the spatio-temporal patterns of incoming river discharge fate. Two varieties of models often used are hydrologic and hydrodynamic models. Hydrologic models interrogate the magnitude and timing of the bulk river discharge and can predict spatially discretized stage and discharge hydrographs. Hydrologic models are often founded on empirical equations determined from observed patterns in overland flow, rain interception, soil infiltration, evaporation, and channelized flow. Hydrologic models are particularly useful with regards to reservoir operations management, water extraction limitations, and determining necessary system capacity design flows. Hydrologic models are limited by their ability to predict more discrete parameters of a flow event like velocity, depth, and time of inundation in one specific location versus another.

Hydrodynamic or hydraulic models use equations derived from physics to spatially characterize an entire area during a flow event. The Navier-Stokes equations are used [15], which are derived from the principles of conservation of mass and momentum (Equations 1.1 & 1.2, respectively), and are written in vector notation as:

$$\nabla \cdot \mathbf{u} = 0 \tag{1.1}$$

$$\underbrace{\frac{\partial \mathbf{u}}{\partial t}}_{\substack{\text{rate of change} \\ \text{of velocity with time}}} + \underbrace{(\mathbf{u} \cdot \nabla)\,\mathbf{u}}_{\text{convective term}} = \underbrace{-\frac{\nabla P}{\rho}}_{\text{pressure gradient term}} - \underbrace{\nabla g z}_{\text{body force term}} + \underbrace{\nu \nabla^2 \mathbf{u}}_{\text{shear stress term}} \tag{1.2}$$

where ∇ is the Nabla operator, $\mathbf{u}$ is the velocity vector, P is the fluid pressure, and ν is the kinematic viscosity. The momentum equation (Equaiton 1.2) has five distinct terms: the rate of change of velocity with time, the convective term, the pressure gradient term, the body force or gravitational term, and the shear stress term. The magnitude and significance of these terms may vary significantly depending on the nature of the system and fluid being described by them. In hydrodynamic models, the Navier-Stokes equations aren't solved explicitly, instead they use the Reynolds-Averaged Navier-Stokes (RANS) equations. The RANS equations average out the turbulent fluctuations by Reynolds decomposition. In hydrodynamic models, some form of the conservation of mass and momentum equations are paired with observed physical characteristics of the study system - such as topography and bathymetry, inflow magnitudes, downstream water levels, wind speeds, and surface roughness - in order to replicate a system event.

Hydrodynamic models can be used to predict inundation patterns and durations of river flow events such as floods for a variety of reasons. Models can be one-, two-, or three-dimensional depending on what degree of detail is desired. One-dimensional models are cross-sectionally averaged, solving for only momentum in the direction of flow. Two-dimensional models are depth-averaged and allow for the solution of a velocity field in a plane. The equations used in the two-dimensional model are known as the Saint Venant equations with the assumption is that there is a hydro-static pressure distribution and they are broken into continuity or mass conservation (Equation 1.3), and momentum (Equations 1.4 & 1.5):

$$\frac{\partial H}{\partial t} + \frac{\partial (hu)}{\partial x} + \frac{\partial (hv)}{\partial y} = 0 \tag{1.3}$$

$$\frac{\partial u}{\partial t} + u\frac{\partial u}{\partial x} + v\frac{\partial u}{\partial y} = -g\frac{\partial H}{\partial x} + \nu_t \left(\frac{\partial^2 u}{\partial x^2} + \frac{\partial^2 u}{\partial y^2} \right) - c_f u + fv \tag{1.4}$$

$$\frac{\partial v}{\partial t} + u\frac{\partial v}{\partial x} + v\frac{\partial v}{\partial y} = -g\frac{\partial H}{\partial y} + \nu_t\left(\frac{\partial^2 v}{\partial x^2} + \frac{\partial^2 v}{\partial y^2}\right) - c_f v + fu \tag{1.5}$$

$$c_f = \frac{n^2 g|V|}{R^{4/3}} \tag{1.6}$$

where H is the water surface elevation in units of length, h is the water depth, u and v are the depth-averaged velocity components in the x and y directions, respectively, ν_t is the depth-averaged eddy viscosity, and f is the Coriolis parameter. The bottom friction coefficient, c_f is defined using Equation 1.6, where n is Manning's n and has units of $s/m^{1/3}$, $|V|$ is the magnitude of the velocity vector, and R is the hydraulic radius.

Three-dimensional models solve for mass and momentum in the x, y, and z directions, derived from the Reynolds averaged Navier-Stokes equations (RANS) derived from the full Navier-Stokes Equations (Equations 1.1 & 1.2). Three dimensional models can be necessary when there is vertical variability in the fluid density, strong wind forcings, or the hydro-static pressure assumption is broken. There are good cases to use either one-, two-, or three-dimensional models with the understanding that as more dimensions are accounted for in the momentum equations there will be higher computational complexity, resulting in longer simulation run times. Hydrodynamic models in whichever number of dimensions have been critical tools in evaluating riverine systems with respect to flood risk analysis, dam-break studies, and proposed modifications including restoration projects.

The hydrodynamic models solve for the hydraulic features of the flow event in space and time, and allow for the coupling of additional modules in order to model other variables affected by hydraulics. With sediment transport models the flow timesteps can be solved along with the density to determine important sedimentation patterns within a system [16], [17]. They can also be used as a determination of habitat suitability analysis for a set of desirable hydraulic conditions [18]. Variables like concentration of constituents and temperature are commonly modeled with the flow field using the advection-diffusion-

reaction equation (Equation 1.7). Modeling salinity and temperature is required for systems which stratify thermally [19] or those which have vertical salinity gradients that can induce baroclinic circulations [20]. These variables are also useful for study sites where salinity intrusion is an issue or where certain temperature ranges are a concern for targeted species. Similarly, the modeled hydraulic solution can inform a water quality or nutrient cycling model to investigate biogeochemical patterns in an area of concern.

Models implement tracers to evaluate any hydraulic bi-product desired using transport equations, and often employ an advection-diffusion equation - written here in 1D [21]:

$$\underbrace{\frac{\partial C}{\partial t}}_{\text{concentration variation in time}} = \underbrace{-\frac{\partial}{\partial x}(uC)}_{\text{advective term}} + \underbrace{\frac{\partial}{\partial x}\left(K_x \frac{\partial C}{\partial x}\right)}_{\text{diffusive term}} + \underbrace{\lambda}_{\text{source/sink term}} \tag{1.7}$$

where C is the concentration of the constituent, u is the depth-averaged velocity in the direction x, K_x is the diffusivity coefficient, and λ is the source/sink term. With the solution of the hydrodynamic model and its tracer a complete spatiotemporally varying description of the model domain is produced. This means one can evaluate the variation of a constituent concentration in time at a single location, or evaluate the spatial variation of a constituent at a single moment in time, or combine a spatial and temporal evaluation of the variability and distribution of a constituent throughout the model domain. Tracers employed by hydrodynamic models can also be aged throughout the model simulation to arrive at a transport time scale, indicating the length of time a water parcel or tracer has been in the system of interest. There are numerous transport time scales one can evaluate, such as flushing time [22], [23], residence time [22]–[25], exposure time [24], [26], and age [22], [27], among others. All of these tracers and hydrodynamic modeling approaches mentioned above can be very helpful in determining the drivers of floodplain health, as well as evaluating potential improvements that might be incurred as a result of a floodplain restoration effort.

This dissertation utilizes the modeling principles mentioned above to interrogate novel

approaches to coupling hydrodynamic models with field data in the goal of improving restoration modeling predictions and conclusions. The studies finished in the completion of this dissertation were done hand-in-hand with field work in the study area that allowed for unique exploration of a model's efficacy in predicting ecological outcomes. This application of evaluating the observed biota of a system alongside hydrodynamic models provides new insight into a models utility in the ecology of a system as well as the current limitations of that utility.

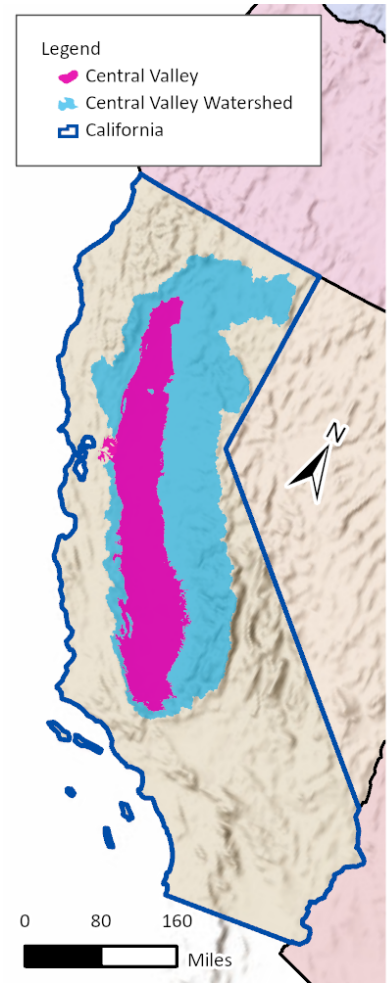

Figure 1.2: California's Central Valley shown in pink, with its surrounding watershed shown in shaded blue.

All three chapters in this body of work are centered on systems within a region known as the Central Valley (Figure 1.2), which is a large valley located in the center of California, a west-coast state in the United States of America. The Central Valley is nestled between two mountain ranges and is the drainage for their rivers, predominantly the Sacramento and San-Joaquin Rivers. The Central Valley can be divided into two Valleys corresponding to their main rivers - the Sacramento and San-Joaquin Valleys. Prior to settlement, the Central Valley would be fully inundated by its rivers in wet winters [28], giving it the nickname "The Inland Sea" [29]. This flooding was not desirable for European settlers and in due time the landscape was transformed with a system of dams and levees, disconnecting the rivers from their floodplains in the Valley.

Two key features arose from this era of settlement in the Central Valley: bypass systems for flood control, and "islands" within the low-lying streams. The first, bypass

systems, were engineered to take advantage of previously flooded basins in order to divert flood flows away from the Sacramento River and nearby cities. The Sutter and Yolo Bypasses are key features in Sacramento Valley flood control. The second, "islands", exist in what is known as the Sacramento-San Joaquin Delta (Delta) and are plots of land that are surrounded by channels and have used levees to completely enclose the land and protect it from flooding from the surrounding channels. The Delta islands have subsided in the years since they were leveed and disconnected from their channels from farming. Two of the chapters of this dissertation (Chapters 2 & 3) are centered on the McCormack-Williamson Tract (Figure 1.3) which is an island just downstream of the confluence of the Cosumnes and Mokelumne Rivers. The final chapter (Chapter 4) focuses on the Yolo Bypass (Figure 1.3). The systems are related, but the chapters focus on distinct contributions to the field of water resource engineering.

The first chapter, Chapter 2, uses three distinct conservative tracers in a two-dimensional hydrodynamic model to evaluate the source water fraction of water throughout the study system - the flooded McCormack-Williamson Tract (MWT). The MWT is located in the North-Eastern Sacramento-San Joaquin Delta at the junction of the Cosumnes and Mokelumne Rivers. The Cosumnes River is a major unregulated river off the Sierra Nevada and the Mokelumne River water that reaches the study area is coming directly out of the Camanche Dam. These two distinct hydrographic beginnings make for distinct signatures of the stable isotopes $\delta^{18}O$ and $\delta^{2}H$. Chapter 2 shows the efficacy of finding source water fraction from either stable isotope analysis or from hydrodynamic modeling with conservative tracers. This chapter has been published in Water, an MDPI journal, as Tomkovic et al. "Comparing Field Isotopes to Hydrodynamically Modeled Tracers" 2020 [30].

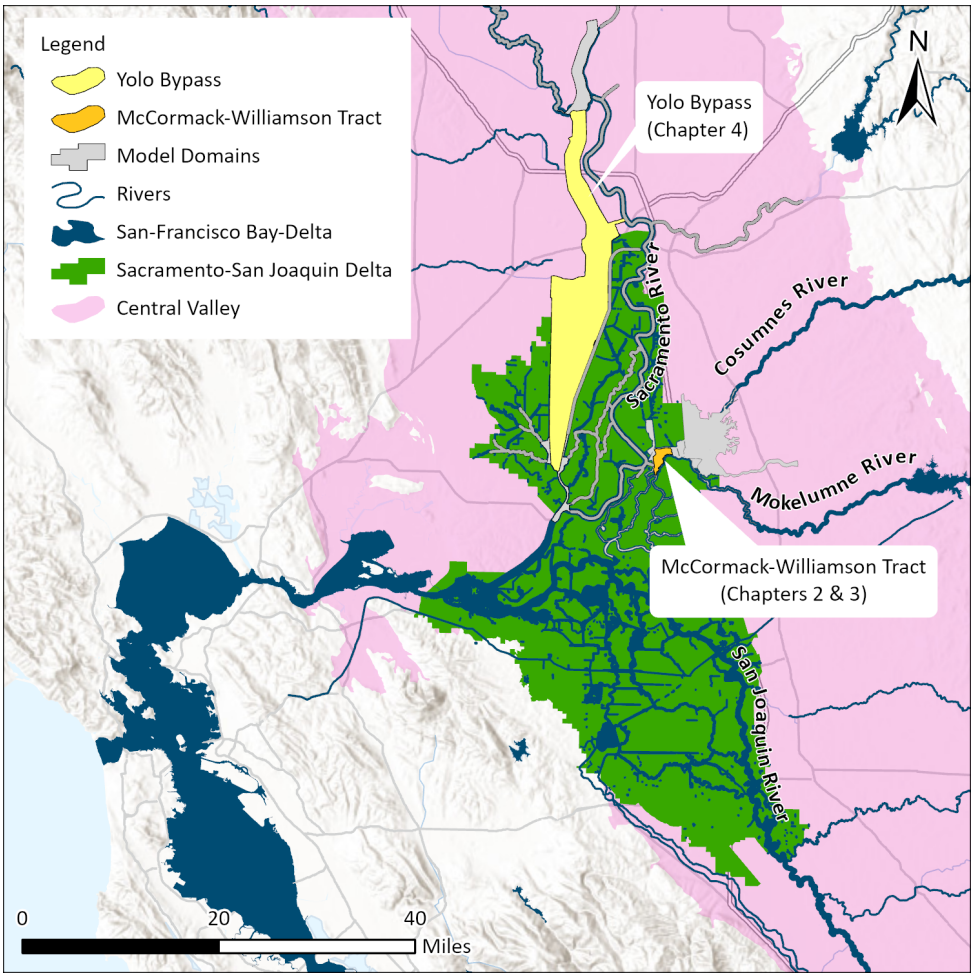

Figure 1.3: Map of the two study areas for this dissertation: the Yolo Bypass and the McCormack-Williamson Tract, set in the Sacramento-San Joaquin Delta adjacent to the San Francisco Bay.

Chapter 3 evaluates the effects of surface water age on a group of aquatic organisms known as zooplankton. The impetus arose from a study by Baranyi et al. on the Danube River in 2002 [31] where zooplankton biomass was shown to correlate positively with age. This chapter utilizes the framework and inputs of the two-dimensional hydrodynamic model from Chapter 2, but uses three dimensions and an applied wind field to replicate the flood event where zooplankton samples were taken and determine the age of the flood waters to compare modeled age to observed zooplankton abundance. This chapter evaluates the mechanisms behind producing the zooplankton versus age relationship as well as any sensitivities that can affect the outcomes of the relationship. Suggestions for future

attempts at investigating this relationship are also provided in order to further the science established by Baranyi et al.

Chapter 4 is a case study of a two-dimensional hydrodynamic model developed in a software that is free and publicly available. This chapter follows the development of a calibrated model of the Yolo Bypass - a managed floodplain in the Sacramento Valley - which can be employed in numerous scientific fields such as agriculture, economics, ecology, and flood risk. The establishment of this model reduces a barrier to entry for anyone investigating modifications to the Yolo Bypass, or for those who are interested in how climate change scenarios might affect the hydrography of the Yolo Bypass.

Chapter 2

Source Water Apportionment of a River Network: Comparing Field Isotopes to Hydrodynamically Modeled Tracers

Abstract: Tributary source water provenance is a primary control on water quality and ecological characteristics in branching tidal river systems. Source water provenance can be estimated both from field observations of chemical characteristics of water and from numerical modeling approaches. This paper highlights the strengths and shortcomings of two methods. One method uses stable isotope compositions of oxygen and hydrogen from water in field-collected samples to build a mixing model. The second method uses a calibrated hydrodynamic model with numerical tracers released from upstream reaches to estimate source-water fraction throughout the model domain. Both methods were applied to our study area in the eastern SacramentoSan Joaquin Delta, a freshwater tidal system which is dominated by fluvial processes during the flood season. In this paper, we show that both methods produce similar source water fraction values, implying the usefulness of both despite their shortcomings, and fortifying the use of hydrodynamic tracers to model transport in a natural system.

Keywords— hydrodynamic model, stable isotopes, source water fingerprinting, floodplain

2.1 Introduction

Across the globe, people have settled and established communities beside estuaries and river deltas that have proven to be ideal habitats for humans, flora, and fauna [32]. Estuaries are unique habitats in a myriad of waysthey are the location where tidal influence extends into the riverine landscape, where saline seawater and fresh river water mix, and where geomorphic effects from marine processes meet fluvial erosion and deposition. All of these factors produce an ecosystem that is specially adapted to growth and success in this confluence of conditions. Even though estuaries support a large diversity of species, they are threatened habitats [33], [34]. Numerous anthropogenic effects have impacted the quality of estuarine habitat [35]. For example, pollutants and anthropogenic inputs in the form of chemicals, human and agricultural wastes, and sediment have been introduced into the watersheds along their reaches [36], [37]. Projected sea level rise [38] and massive diversions from natural riverine inputs [39] have impacted salinity dynamics, affecting ecosystem health [40]. Entire landscapes have been shifted from land to sea [13], [14], affecting numerous processes from the headwaters of tributaries down to their deltas, all impacting the health of the estuary.

To combat these problems, humans have sought ways to balance their needs for the natural resources provided by estuaries with the long-term survival and fitness of those habitats. Better practices have been established to control pollution into rivers, estuaries, and marine environments. Furthermore, restoration efforts have been made in order to address the degradation of physical habitat surrounding river deltas and estuaries. Combinations of these efforts have been undertaken in order to produce multi-pronged benefits within these habitats. Often, the goal of restoration and management actions are to allow for the physical and biological processes important in estuaries to resume functioning. For instance, the restoration of off-channel habitat in the tributaries leading into an estuary provides the physical parameters (such as turbidity, dissolved oxygen, temperature, and light availability) to generate primary and secondary producers (phyto- and zoo-plankton) [7]. With proper connectivity, that productivity can flow into riverine habitat and be transported downstream throughout the estuary. Following the overall impacts of estuarine restoration is complicated, however, because of the complex physical properties of deltas and estuaries, such as reconnecting or braided river networks, tidal pumping effects [41], and salinity gradients.

Understanding where water flows and where it originates is useful for understanding what impacts a restoration project has as well as what the character of water is coming into a potential restoration site. Identifying source water fraction (SWF) of a river network addresses the spatiotemporal distribution of source waters and allows the investigation of tributary water fate. The properties of tributaries, such as the stable isotope compositions of water, have been used to identify source water distribution, but these studies have typically been applied to lakes or groundwater [42]–[45]. Other studies have used isotope signatures to identify which tributaries have dominant effects on geochemical properties of the mainstem [46], to investigate snow-melt versus rainfall contribution [47], and to identify water origin [48]. Our study aimed to use two methods to find the SWF at each location within the study area over time; one method used is similar to that of Halder et al. [49] and Marchina et al. [48], which evaluates stable hydrogen (2H) and oxygen (18O) isotopes at sample locations and compares those to the tributary source waters of interest.. Another direct application of using physical properties of tributary water to find the distribution of source waters in a river network was presented by Peter et al. [50] in a physically modeled hypothetical watershed. In the study, high-resolution mass spectrometry of organic contaminants was used to confirm the source hydrology of a hypothetical river system with known flows, and thus known mixtures. This physical model study demonstrated the potential of using physical and chemical signatures in water to identify source water, but was limited to systems with an exact knowledge of tributary discharge and mixing patterns, limiting the study to a discussion of methodology instead of an application of a real-world scenario in a river network. We address this limitation using a separate method to investigate the hydraulics and transport processes of a system in order to provide estimated flows and mixing patterns.

Hydrodynamic models are numerical tools that solve equations of motion in fluid mechanics and are widely used to replicate flood events and complex physical processes in river networks. Sridharan et al. [51] used a one-dimensional streamline-following junction model to evaluate particle paths through the SacramentoSan Joaquin Delta of California (Delta), giving insight to source-water fate at a large and broad scale. Bai et al. [52] used a three-dimensional hydrodynamic and water quality model to source-apportion different tributary contributions to nitrogen and phosphorous loads. The source-apportionment indicates the chemical impact of

tributaries, but not their relative volume at any particular location. In order to test the validity of a field-based approach to identifying SWF in a river network, we developed a hydrodynamic model coupled with a transport model. This studys comparison of methods can help address limitations of stable isotope methods of finding the SWF of a particular site, as well as demonstrating a field validation of source water tracking using hydrodynamic models.

This study centered on the McCormack-Williamson Tract (MWT), an island protected by a ring levee in the Delta, and the surrounding area. Slated for restoration, the site lies downstream of several other floodplain restoration sites along the Cosumnes River and Dry Creek, making understanding the distribution of incoming source waters helpful to improve the overall efficacy of the MWT restoration. Specifically, water that has had access to floodplains would likely carry more allochtonous material, providing more carbon and nutrients to kick-start in situ production at the study site. In this paper, we characterize the spatiotemporal distribution of SWF at different sites in and around the island while it was flooded. In the absence of measurements of individual tributary flows into the study area, indirect methods must be applied to estimate source water distribution. Our study aimed to evaluate the utility of the two methods discussed, to compare hydrodynamically derived values to in situ data, and to discuss the implication of these approaches to the Delta, as well as other riverine systems.

2.2 Methods

2.2.1 Study Area

The SacramentoSan Joaquin Delta (Delta), located in California, USA is a large, reconnecting, freshwatertidal river network that leads into the San Francisco Bay Estuary. The Delta is a major economic asset to the state of California. Its major diversions of freshwater, mainly from the Sacramento River, provide irrigation for the states thriving agricultural industry, as well as drinking water for its cities [53]. These large diversions from the Delta, supported by an extensive system of reservoirs, have altered transport and seasonal salt intrusion trends in the estuary [54], [55]. The nutrient-rich soils in the off-channel habitat of the Delta have been predominantly converted to agricultural plots [13], while at the same time over 95% of floodplain and intertidal habitat [56] have been channelized, thereby eliminating shallow-water habitat from the ecosystem. These and many other anthropogenic impacts on the Delta have motivated

restoration efforts to mitigate the altered ecosystem. The restoration of shallow-water habitat can boost productivity, and understanding the transport of these enriched source waters is an important factor in maximizing restoration efforts [29], making Delta an ideal location for this study.

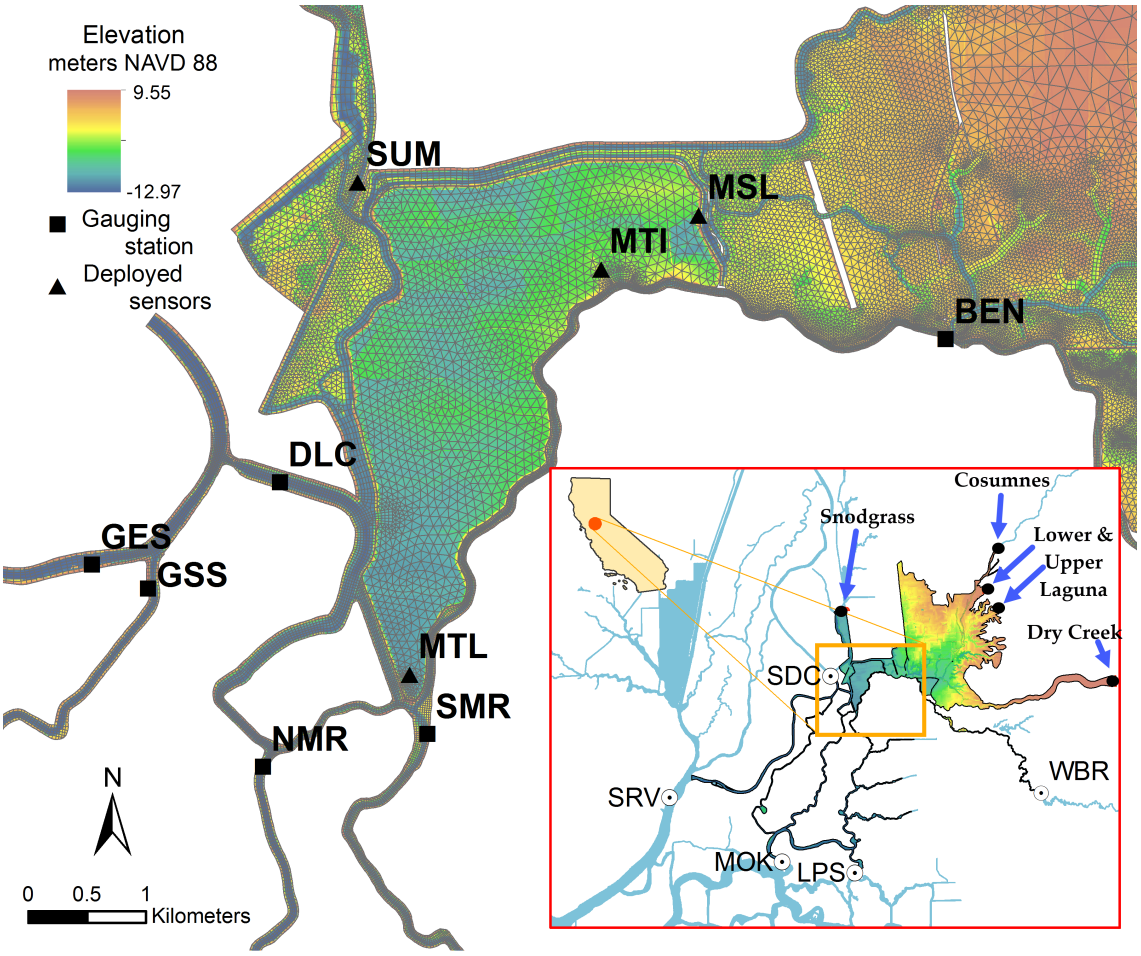

Figure 2.1: Study area with calibration gage stations shown as black points. Sensors deployed specifically for this study are triangles, and agency gages (either United States Geological Survey (USGS) or the California Department of Water Resources (DWR)) are squares. The model domain is shown (bottom right, location shown as red dot in California) overlying the Delta waterways in blue. Boundary gages are shown in the bottom right figure with agency gages shown as white and black icons and estimated boundaries labeled with blue arrows.

The specific area studied in this paper is in the North-East Delta near the confluence of the Mokelumne and Cosumnes Rivers (see Figure 2.1). It is a freshwater tidal system dominated by

fluvial processes during the flood season by the upstream Dry Creek, Cosumnes, and Mokelumne watersheds. A major feature of the study site just west of the confluence is the McCormack-Williamson Tract (MWT), which was historically wetland habitat [57] but is now a 1400-acre ring-leveed property used for agricultural purposes. The MWT is slated for restoration to tidal and floodplain habitat. During the period of this study, an accidental breach occurred near the planned breach, allowing for flood flows through MWT along with intertidal habitat in non-flooding periods.

Just west of the MWT are the Delta Cross Channel Gates, which are a major feature of the Delta, controlling diversion of freshwater flows from the Sacramento River to the Southern Deltas major pumping plants for municipal, agricultural, and other export across California. North of the MWT are Middle, Lost, and Snodgrass Sloughs. Snodgrass Slough is the drainage for Morrison Creek and the Stone Lake National Wildlife Refuge, where the stream enters the Delta. Middle and Lost Sloughs are dead-end sloughs during non-flooding periods and convey Cosumnes overland flow during floods. The Cosumnes River is the only major river coming out of the Sierra Nevada Range without a major dam, allowing for a relatively natural hydrograph with natural overbank/floodplain flow [58]. Due to this hydrograph and a variety of restoration actions, the Cosumnes River provides floodplain rearing for a variety of native juvenile fishes and exports productivity downstream [6]. This relatively natural system dramatically differs from the other major stream source to the study areathe Mokelumne River. The Mokelumne River is a 5550 km2 watershed and has its headwaters in the Sierra Nevada Range extending down to the San Joaquin River in the Delta. River flow in the lower 55 km is regulated by Camanche Reservoir and conveyed to the confluence of the San Joaquin River through a leveed channel.

For this study, we developed two types of modeling methods to investigate the SWF of Mokelumne River water and Cosumnes River Water (locations shown in Figure 2.2).

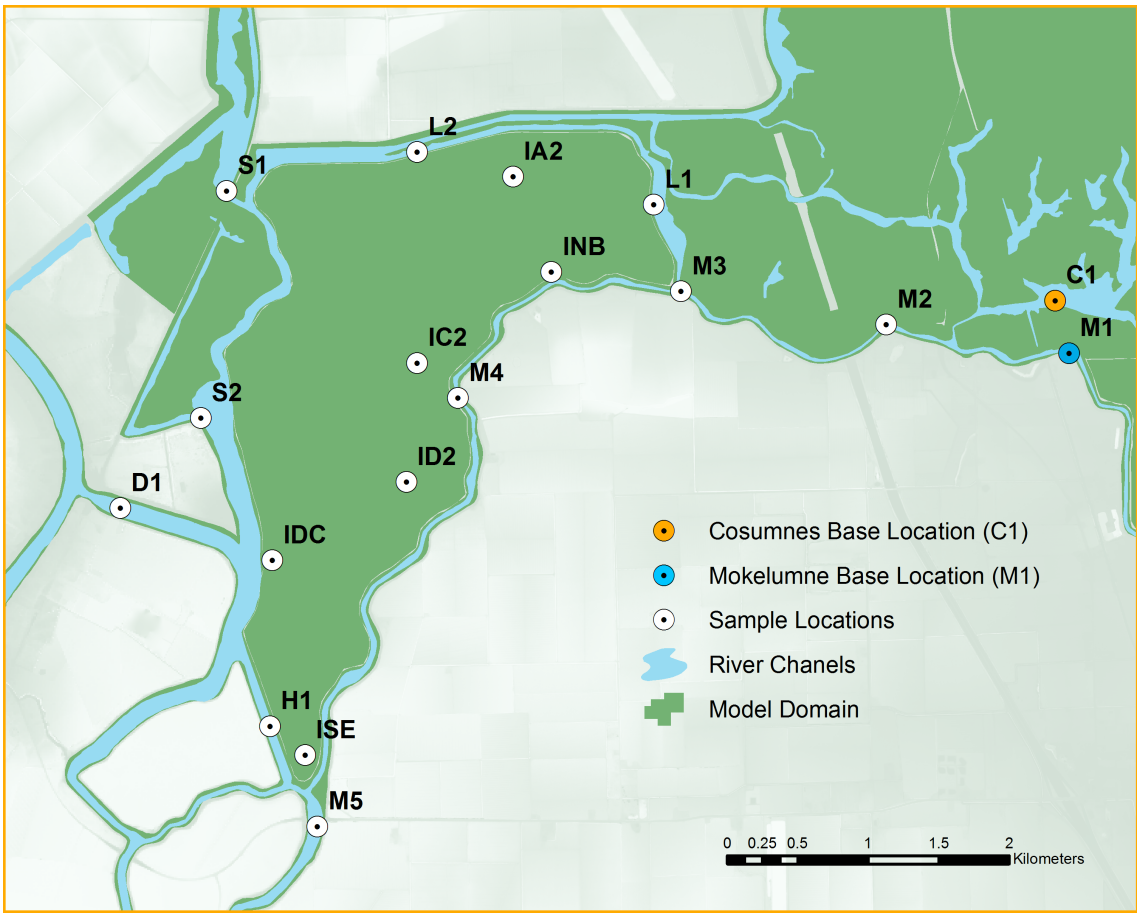

Figure 2.2: Study area showing isotope sample locations in white, with the Cosumnes and Mokelumne Base locations shown in orange and blue, respectively.

2.2.2 SWF Method I: Isotope Mixing Model

2.2.2.1 Mixing Model Theory

Figure 2.3: Schematic river system with single confluence.

Following Gibson et al. [42], a mass balance approach was used to estimate the volumetric fraction of two tributary waters at downstream sample site (Figure 2.3). The mixing model asserts that the isotopic composition at the sample site is a volume-weighted average of tributary isotopic composition.

$$f_A \cdot \delta X_A + f_B \cdot \delta X_B = f_{Site} \cdot \delta X_{Site} = \delta X_{Site} \tag{2.1}$$

Where f_A, f_B, and f_{Site} are the volumetric fraction of River "A", River "B", and whichever site was being analyzed, respectively. The isotopic composition, in delta notation, of each location is denoted as δX, where X is either ^2H or ^{18}O. After assuming that $f_{Site} = 1$ and $f_A + f_B = 1$, the SWF for River "A" or "B" at any given site is:

$$f_A = \frac{\delta X_{Site} - \delta X_B}{\delta X_A - \delta X_B} \tag{2.2}$$

$$f_B = \frac{\delta X_{Site} - \delta X_A}{\delta X_B - \delta X_A} \tag{2.3}$$

This mixing model applies to samples with $\delta X_A < \delta X_{Site} < \delta X_B$ or $\delta X_B < \delta X_{Site} < \delta X_A$. In the event that this condition was not met the sample was not included in the analysis. In addition, the mixing model assumes that the isotopic composition of rivers A and B are stationary, that local effects on $\delta^2 H$ (e.g., isotopic fractionation via evaporation) are negligible [59], and that the sampled water is comprised entirely of contributions from the two tributaries.

2.2.2.2 Field Data - Collecting Isotope Samples

The field campaign at the MWT sampled the water biweekly from August 2016 to June 2019 at 18 locations (Figure 2). Not all locations were sampled throughout the entire period, due to a variety of reasons. The MWT locations (those that start with "I") were only sampled during the MWT's breach from February 2017 to June 2017. At each location, a grab sample of water was taken from the top 0.25 m of water, filtered through glass fiber (GF/F) filters (nominal pore size: 0.7 microns) and stored refrigerated until isotopic analysis was performed.

2.2.2.3 Isotope Processing

We used delta notation ($\delta^{18}O$ and $\delta^2 H$) to characterize our samples. $\delta^{18}O$ and $\delta^2 H$ values change with precipitation elevation, evaporation, and other hydrologic factors, often making them dif-

fer significantly between watersheds. Delta notation describes the relative composition of stable isotopes in the sample through the formula: $\delta^n X = \_\_‰ = (R_{sample}/R_{standard}$ - 1) $\cdot 1000$; where n is the atomic number of the heavy isotope in question and R_{sample} and $R_{standard}$ represent the ratio of the heavy isotope (here, ^2H and ^{18}O) to the light isotope (here, ^1H and ^{16}O) in the sample and the international standard, respectively. We determined ^{18}O and ^2H via off-axis integrated cavity output spectroscopy (Los Gatos Research (LGR), Liquid Water Isotope Analyzer) at the University of California Merced. Working standards from LGR, calibrated against National Institute of Standards and Technology (U.S. Department of Commerce) reference materials (Vienna Standard Mean Ocean Water (VSMOW), Greenland Ice Sheet Precipitation (GISP), and Standard Light Antarctic Precipitation (SLAP)), were analyzed throughout and used to correct measured isotope ratios, so they could be expressed relative to the international standard: VSMOW. Four different standards ranging from $\delta^2H = 9.2‰$; $\delta^{18}O = 2.7‰$ to ($^2H = 154.0‰$; $\delta^{18}O = 19.5‰$ were used as internal standards. Raw data was processed using LWIA post-analysis software (LGR).

Each time we determined the isotopic ratio of a water sample or standard, it was analyzed via repeated injections. The standard deviation of our measured values ($n = 89$) for standards was $0.3 \pm 0.1‰$ and $0.06 \pm 0.01‰$ for δ^2H and $\delta^{18}O$, respectively. Averaging multiple injections per sample was effective at reducing uncertainty originating from small injection-to-injection differences, indicating high precision. Furthermore, our mean measured values differed from known standard values by only $0.03‰$ and $0.01‰$ for δ^2H and $\delta^{18}O$ respectively; indicating high accuracy, even when the above uncertainties are considered. Propagation of uncertainty into our model is addressed in section 2.3.1.

2.2.2.4 Application of Mixing Model

Addressing the C1 and M1 sites (Figure 2.2) as equivalent to the River "A" and River "B" hypothetical diagram (Figure 2.3), we modified Equations (2.2) and (2.3) to find the fraction of Cosumnes and Mokelumne water at any given site.

$$f_{Cos} = \frac{\delta X_{Site} - \delta X_{Moke}}{\delta X_{Cos} - \delta X_{Moke}} \tag{2.4}$$

$$f_{Moke} = \frac{\delta X_{Site} - \delta X_{Cos}}{\delta X_{Moke} - \delta X_{Cos}} \tag{2.5}$$

2.2.3 SWF Method II: Hydrodynamic Model

The second method of finding SWF in a natural system uses a two-dimensional hydrodynamic model coupled with a transport model that can transport a contaminant tracer with advection and diffusion. In this approach, the transport model releases conservative tracers in the tributaries of interest (Rivers "A" and "B" in Figure 2.3), which are tracked throughout the model domain in time. The summation of all tracer fractions at any given location is 1.0, allowing for a simple numerically based volumetric fraction of the tributary source waters.

2.2.3.1 Hydrodynamic Model Development

A two-dimensional hydrodynamic model was built and calibrated using UnTRIM [60]. The two-dimensional version of UnTRIM uses a semi-implicit algorithm for the depth-averaged shallow water equations under a hydrostatic assumption [61]. The mesh was generated using Preprocessor Janet (http://www.smileconsult.de) and contains quadrilateral and triangular elements, Figure 2.1) with a total of 109,129 elements. The average edge length was around 30 m with the smallest element being 3 m and the largest being over 200 m in an area insignificant to this study.

The three stage boundaries at the downstream end were set using observed gages. On the Sacramento River the boundary was set within 3 km of the United States Geological Survey (USGS) gage SRV-Sacramento River at Rio Vista-11455420 and the gage data was used directly. The other two downstream boundaries gages (USGS gages MOK-Mokelumne R A Andrus Island NR Terminous CA-11336930 and LPS-Little Potato Slough at Terminous-11336790) were located at the model boundary directly, but did not use a known datum, so the reported time series were adjusted using calibration offsets from a larger Delta-wide model.

2.2.3.2 Boundary Condition Development

The seven upstream flow boundaries used either gaged data or were calculated. The USGS discharge gages SDC-Sacramento R Above Delta Cross Channel-11447890 and WBR-Mokelumne R A Woodbridge CA-11325500 were used at the upstream ends of the Sacramento and Mokelumne Rivers, respectively. The discharge boundary at Snodgrass Slough was calculated using lagged discharge data from USGS MFR-Morrison C NR Sacramento CA-1136580. The boundaries at the Cosumnes River, Upper Laguna Creek, Lower Laguna Creek, and Dry Creek were all estimated using the results from a hydrologic study performed on the area by David Ford Consulting Engineers (DFCE) [62]. In order to estimate flows for the four unknown flow boundaries,

a lag and amplitude relationship was taken from the DFCE study and then the flow was routed using a simple Muskingum Routing method in order to attenuate flows to the model boundary locations based on stream lengths from the study locations to the boundary locations. The estimated flow magnitudes were calibrated against combined tidally-filtered North Fork Mokelumne and South Fork Mokelumne flow gages, since these two gages are the only outlets to the system during flood flows they account for all flow derived from the estimated boundaries as well as the Mokelumne River.

2.2.3.3 Model Calibration

For the hydrodynamic model calibration, we deployed 10 Solinst LevelLogger pressure sensors, which were RTK surveyed and barometrically compensated using a nearby Solinst BaroLogger.

The model was run for a period of December 2016June 2017 and was calibrated using USGS and California Department of Water Resources (DWR) gages, as well as the LevelLoggers (Figure 2.1). The performance of the model is demonstrated with Table 1. The model metrics used are the correlation coefficient R^2 and the Willmott Skill Index of agreement [63] (skill). The skill demonstrates a metric for comparing observed and computed time series data and ranges between 0 and 1, with 1 being perfect agreement.

$$Skill = 1 - \frac{\sum_{i=1}^{n} |P_i - O_i|^2}{\sum_{i=1}^{n} \left(|P_i - \overline{O}| + |O_i - \overline{O}| \right)^2} \tag{2.6}$$

Table 2.1: Model calibration metrics for the gages shown in Figure 2.1

	Gage Name	Gage ID	R^2	Skill	Date Range
Stage	Mokelumne R @ Benson's Ferry NR Thornton	BEN[C]	0.976	0.991	12/01/2016 - 07/01/2017
	Delta Cross Channel BTW Sac R & Snodgrass	DLC[U]	0.963	0.989	12/01/2016 - 07/01/2017
	Sacramento River Below Georgiana Slough	GES[U]	0.977	0.990	12/01/2016 - 07/01/2017
	Georgiana Slough at Sacramento River	GSS[U]	0.976	0.989	12/01/2016 - 07/01/2017
	Middle Slough	MSL[L]	0.959	0.986	01/20/2017 - 07/01/2017
	McCormack-Williamson Tract - Inlet	MTI[L]	0.932	0.974	02/16/2017 - 05/31/2017
	McCormack-Williamson Tract - Lower	MTL[L]	0.914	0.976	02/16/2017 - 05/31/2017
	South Mokelumne R at W Walnut Grove Rd	SMR[U]	0.969	0.990	12/01/2016 - 07/01/2017
	Snodgrass Slough Upstream of Meadow	SUM[L]	0.922	0.979	01/20/2017 - 07/01/2017
Flow	Sacramento River Below Georgiana Slough	GES[U]	0.993	0.997	12/01/2016 - 07/01/2017
	Georgiana Slough at Sacramento River	GSS[U]	0.974	0.973	12/01/2016 - 07/01/2017
	South Mokelumne R at W Walnut Grove Rd	SMR[U]	0.914	0.965	12/01/2016 - 07/01/2017

* Gage data sources are denoted as [C] - DWR, [U] - USGS, [L] - LevelLogger sensor deployed for this study.

A 72-hour model spin-up period was eliminated from the calibration metrics and plots due to the initial uniform water surface elevation being very low to ensure no water was initialized within the MWT ring levee. Figure 2.4 demonstrates model agreement with observations over time, along with a tidally dominant period in the inset to show resolution of the tidal regime.

2.2.3.4 Model Tracers

The UnTRIM modeling platform has the capacity to solve for the distribution of tracers with a transport scheme allowing for advection, diffusion, and source/sink terms. Conservative tracers were released within the model mesh and tracked across the domain with a horizontal diffusion coefficient of 0.0, considering only transport via advection using UnTRIM's built-in transport solver [64]. The tracers act similarly to an inert dye and allow the model to follow the traced water throughout the model domain, allowing for tracking of SWF in space and time.

The vertically integrated transport equation for the tracers used is:

$$\frac{\partial CH}{\partial t}+\frac{\partial UCH}{\partial x}+\frac{\partial VCH}{\partial y} = \frac{\partial}{\partial x}(HK_{xx}\frac{\partial C}{\partial x}+HK_{xy}\frac{\partial C}{\partial y})+\frac{\partial}{\partial y}(HK_{yx}\frac{\partial C}{\partial x}+HK_{yy}\frac{\partial C}{\partial y}) \quad (2.7)$$

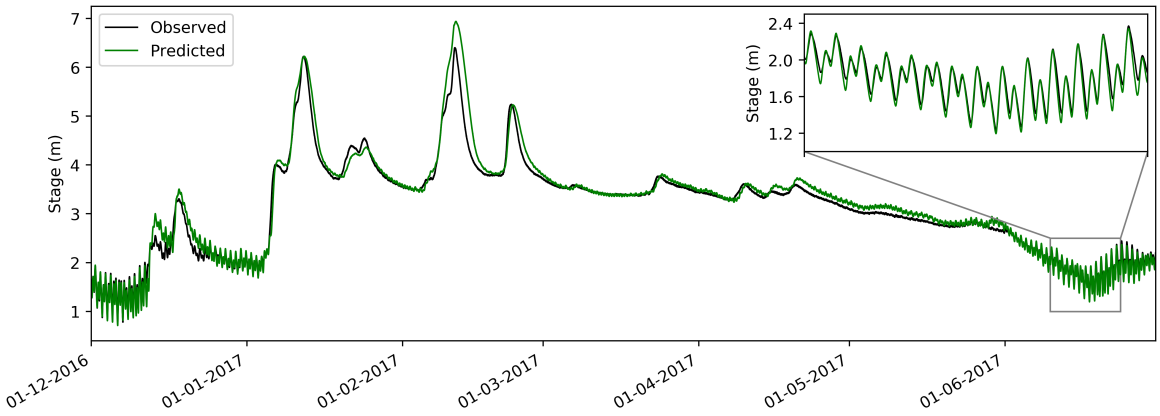

(a)

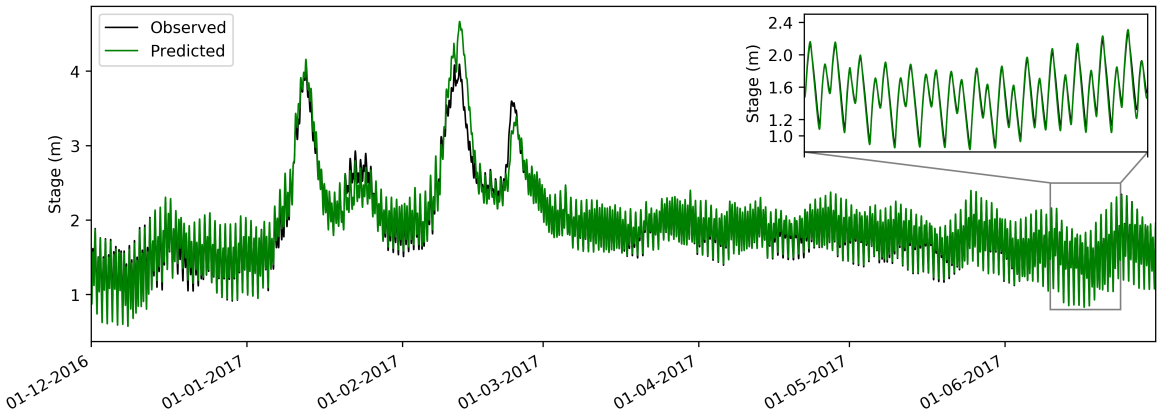

(b)

Figure 2.4: Calibration plot for the BEN (a), and SMR (b) gages (Table **??**) showing the observed (black) and modeled (green) water surface elevation for the period simulated. The inset shows the comparison of observed versus modeled during a tidally dominated period.

where C is the concentration of the conservative scalar tracer. In this study we considered the numerical diffusion introduced by the model to be on the same order as that of physical diffusion processes and set the right hand side of Equation (2.7) was set to zero by using horizontal diffusion coefficients (K_{xx}, etc.) of 0.0.

Throughout the simulation, tracers were released at the Cosumnes and Mokelumne Rivers with "Cosumnes" and "Mokelumne" tracers, corresponding to the C1 and M1 site locations, respectively. The tracers were released in all cells that spanned the rivers laterally at the locations where isotopes were collected for both rivers. An "Other" tracer was released at all flow boundaries and for all initial water. Upon passing through the Cosumnes release cells, the Mokelumne and Other tracers were set to zero. Similarly, for the Mokelumne release cells, the Other and Cosumnes tracers were set to zero. After the simulation ran, the volumetric fractions of each individual tracer (Cosumnes, Mokelumne, and Other) were queried for each sample location (Figure 2.2) and checked to ensure that the sum of all three tracers was 1.0 over time, confirming mass balance in the transport model.

In this study, there was no field validation of the transport mechanisms. This is a limitation of the confidence in accuracy of the hydrodynamic approach, despite good hydraulic calibration.

2.3 Results

2.3.1 Isotope Mixing Model Results

At each sample location and time, a mixing model was performed for both δ^2H and $\delta^{18}O$ (Figure 2.5). With an instrument uncertainty of 0.3 ± 0.1‰ and 0.02 ± 0.01‰ for δ^2H and $\delta^{18}O$, respectively, 95% confidence intervals were calculated from each mixing model result. The error bars were then calculated using the minimum and maximum error on each isotope value used in Equations 2.4. This calculation of instrument-derived error is the only measurable quantity of error that we addressed in this study due to the limitations associated with quantifying the error from breaking assumptions inherent in the mixing

model. These assumptions include stationarity in the tributaries, local effects assumed to be negligible, and the sampled water was composed of only the two tributaries. At the time of sampling, only one water grab sample was taken for each site and date, meaning we were unable to compute a standard deviation in space or time of isotope composition at each site to accompany instrument error.

In evaluating the data, differences between the C1 and M1 isotope values ranged from 7.47‰ and 22.45‰ for $\delta^2 H$, and from 0.79‰ and 2.96‰ for $\delta^{18} O$. Given that the instrument error could account for anywhere from 5% to 51% of that range, the mixing model uncertainty ended up being quite significant (Figure 2.5).

Any isotopic values which did not lie between the C1 and M1 (Cosumnes and Mokelumne sample locations, respectively), were discarded as they would produce fractions larger than 1.0. Out of the 312 $\delta^2 H$ and $\delta^{18} O$ mixing model results, only 13 were outside of the bounds set by the C1 and M1 values for those sample dates. After eliminating invalid data points, a total of 299 mixing model results were produced across 156 unique sample dates and times.

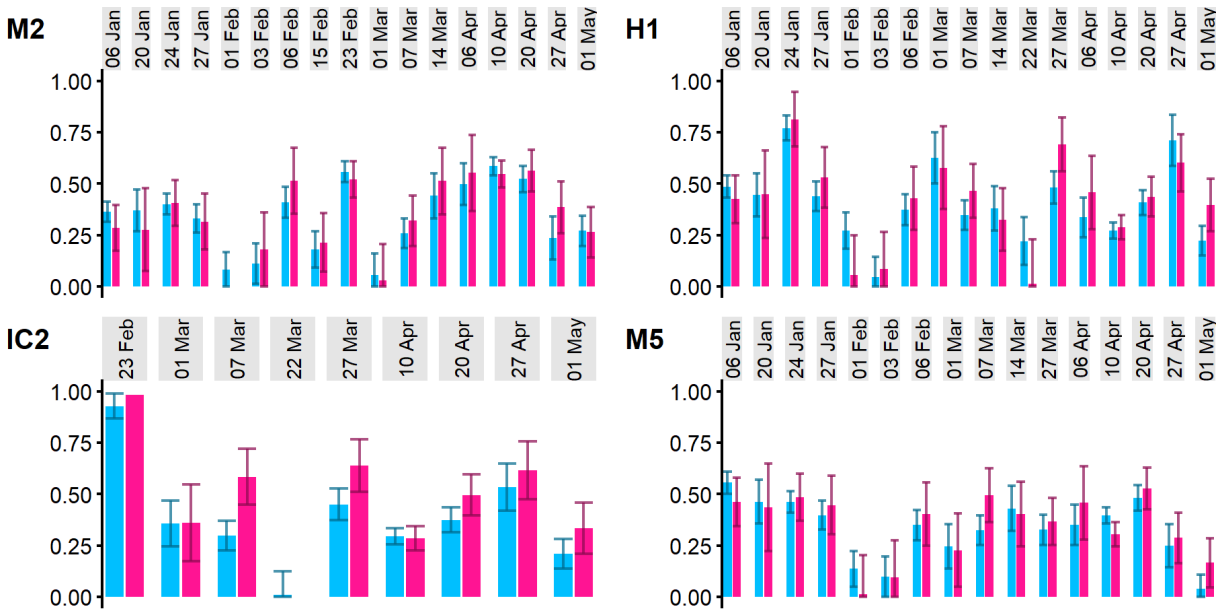

Figure 2.5: Isotope mixing model results showing fraction of Cosumnes on the y-axis for δ^2H (blue) and $\delta^{18}O$ (pink), along with instrument error bars at four example locations (depicted in Figure 2.2) in 2017. M2 Downstream of confluence. H1: Dead Horse Cut. IC2: Island site C2. M5: South Fork Mokelumne.

2.3.2 Hydrodynamic Tracer Results

The model tracer simulation predicts the proportion of Cosumnes, Mokelumne, and Other tracers at the sample locations (Figure 2.6). The modeled distribution of tracers can also be displayed spatially for any moment in time during the simulation (Figure 2.7). The model produced time-varying SWF time series, where all tracers summed to one at all points in time, confirming mass conservation across all tracers. The time series demonstrate that over time, there is a trade-off of the three tracers, and that certain periods are dominated by a single tracer.

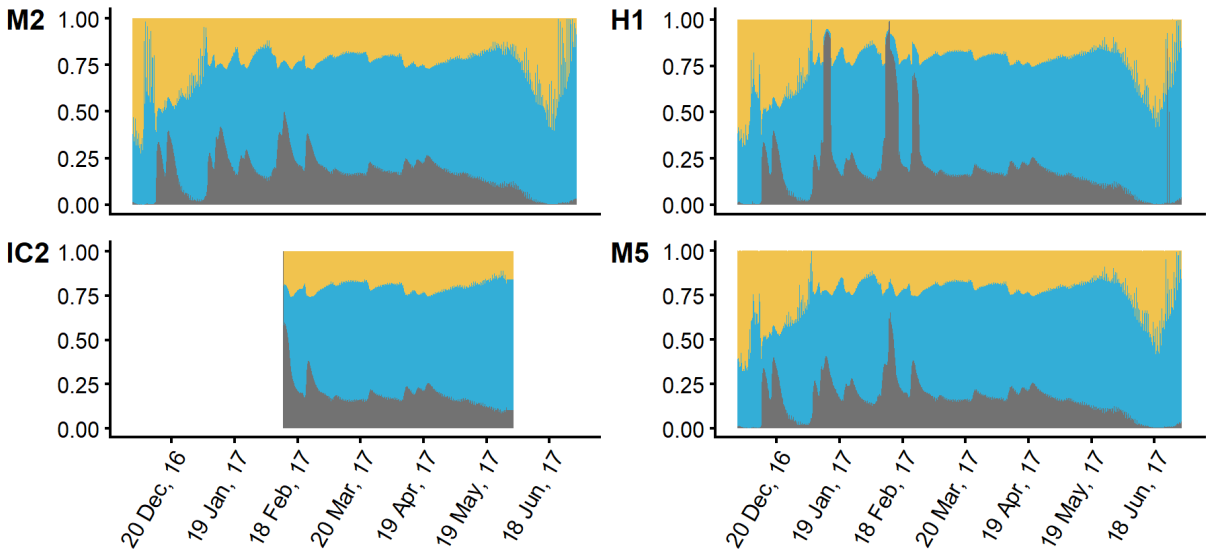

Figure 2.6: Source water fraction time series at four example locations (depicted in Figure 2.2) where all fractions add to 1.0. The yellow portion represents the Cosumnes tracer, the blue portion represents the Mokelumne tracer, and the grey represents the Other tracer. M2: Downstream of confluence. H1: Dead Horse Cut. IC2: Island site C2. M5: South Fork Mokelumne.

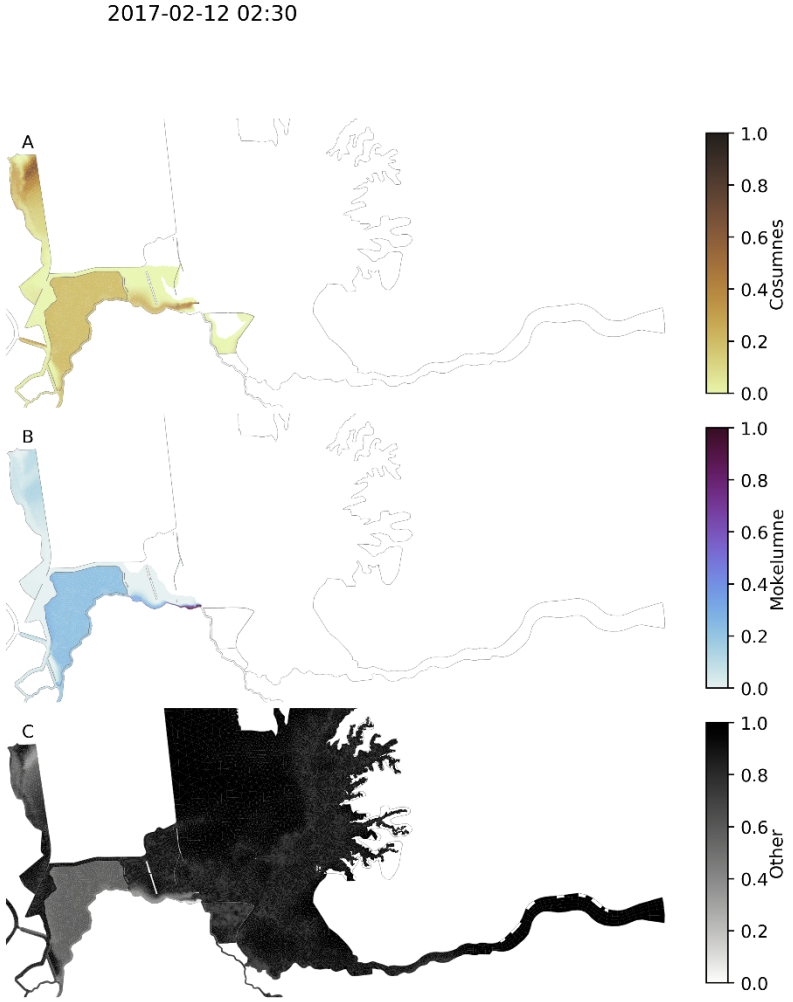

Figure 2.7: Mapping of the distribution of the three numerical tracers within the model domain. The Cosumnes tracer is shown in orange (A), the Mokelumne tracer is blue (B), and the Other tracer is shown in black/grey (C). The snapshot is at 12 February, 2017 02:30, and demonstrates how the Cosumnes and Mokelumne tracers are released and transported downstream (leftwards).

2.3.2.1 Mixing Model and Hydrodynamic Model Comparison

In comparing the difference between the model tracer-based estimation of source water versus the isotope mixing model approach (Figure 2.8), we assume the Other tracer would have a similar isotopic signature to the sample taken at the Cosumnes (C1, Figure 2.2) sample location. This is potentially due to the fact that the Cosumnes and its nearby tributaries (Deer Creek, Upper and Lower Laguna Creek, and Dry Creek) all have watersheds at similar elevations and inland extents to the Cosumnes watershed; presumably,

these waterways would receive precipitation of a similar isotopic composition. Furthermore, the water within the channel at the Cosumnes sample location is a continuation of the larger pulses of floodwaters coming through the Cosumnes River Floodplain following rain events, that would be considered Other by the hydrodynamic approach. Because of this assumption, we use the combined Other and Cosumnes tracer results to make a comparison with the averaged δ^2H and $\delta^{18}O$ mixing model results. Interestingly, this pattern of apparent isotopic similarity between the Cosumnes sample location and Other water is consistent at the S1 and S2 sites (Figure 2.2), which have a significant amount of Snodgrass Slough water. That Snodgrass water was tagged as Other in the model, as it is one of the flow boundaries where all water is tagged as Other. Where the isotope mixing model predicts Cosumnes water, the hydrodynamic model output presents that fraction as a combination of Other and Cosumnes water. This could be due to the source water for Snodgrass Slough (Morrison Creek) having similar watershed characteristics that lead to the isotope signature for the Cosumnes and its tributaries.

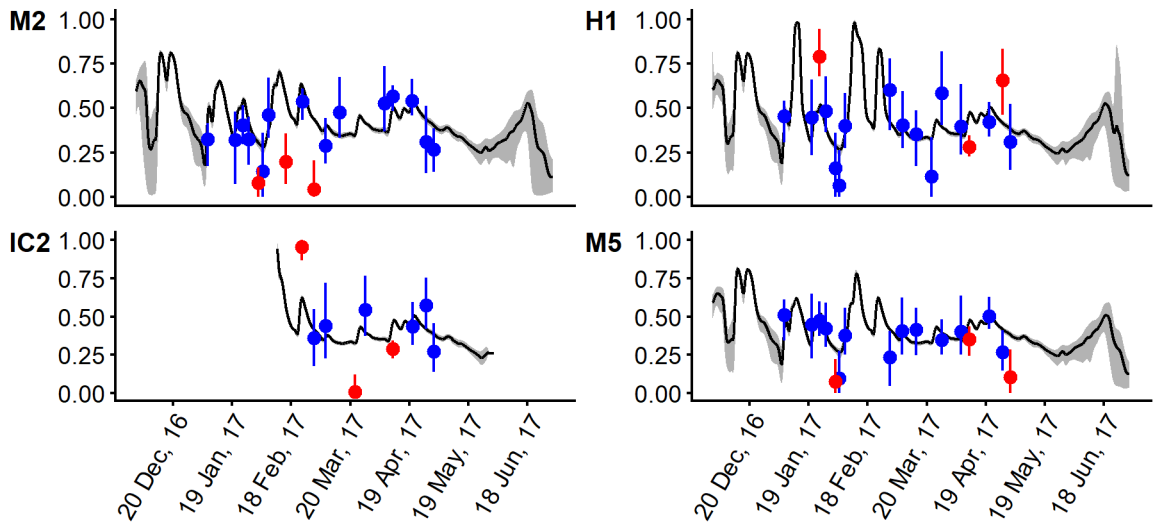

Figure 2.8: Time series at four locations showing the modeled Cosumnes and Other concentrations with the tidal average (black line) and tidal envelope (grey ribbon). The isotope mixing model values are shown as points with the isotope instrument 95% confidence intervals extending from the mixing model value. Blue points are those whose isotopic confidence intervals overlap with the modeled tidal envelope, while red points do not.

The hydrodynamic "Other" and "Cosumnes" tracers were combined into an instantaneous time series for each site, then the 12-hour running mean, minima, and maxima were tidally averaged using a Godin filter to produce a tidal envelope to compare to the isotope mixing model results (Figure 2.8). At each site, there were varying degrees of overlap (Table 2), with only two sites (ISE and L1) (Figure 2.1) under 60%.

Table 2.2: Summary statistics for each site (Figure 2.2) showing the percentage of points overlapping as well as the count.

Site	**Overlapping Samples**	**Total Samples**	**Percentage Overlapping Samples**
D1	5	8	82.4%
H1	14	17	62.5%
IA2	9	11	81.8%
IC2	6	9	66.7%
ID2	1	1	100.0%
IDC	8	11	72.7%
INB	1	2	50.0%
ISE	4	10	40.0%
L1	10	11	90.9%
L2	8	9	88.9%
M2	14	17	82.4%
M3	16	17	94.1%
M4	6	8	75.0%
M5	13	16	81.3%
S1	5	6	83.3%

An overwhelming majority of the sites were considered overlapping in uncertainty, implying that both methods produced similar results within the bounds of their uncertainty (Figure 2.9). In total, 123 out of the 156 samples compared were considered overlapping (78.9% overall). Although the methods largely agreed, the isotopic results alone produced

a good estimate with a lot of uncertainty from instrument error, while the hydrodynamic results provided improved accuracy, as well as finer spatiotemporal resolution.

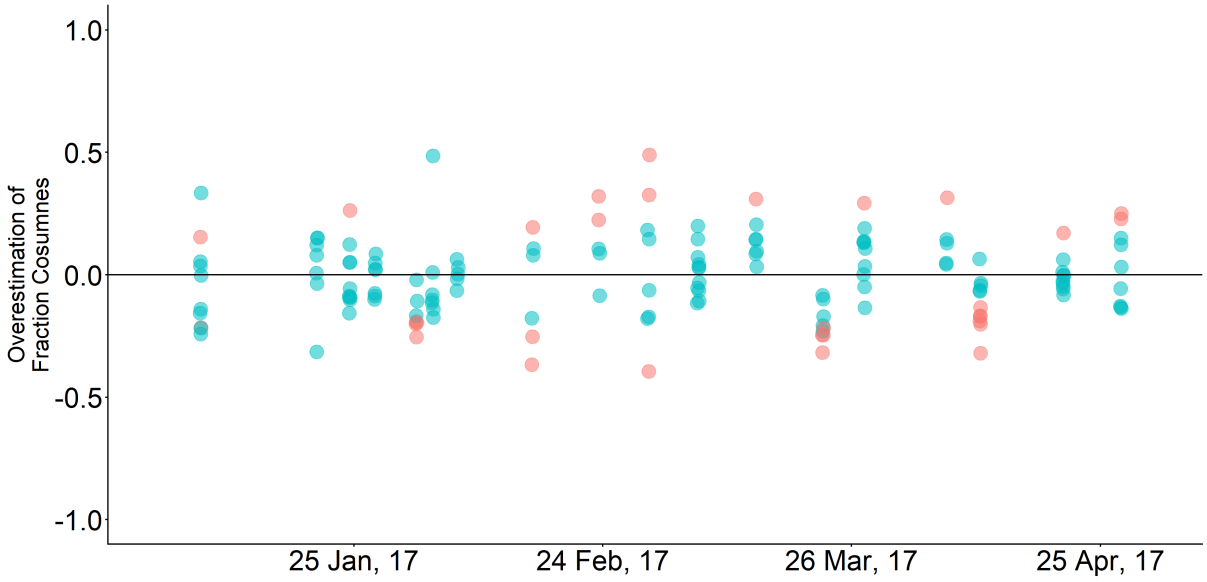

Figure 2.9: Time series of all locations with overestimation of the fraction Cosumnes found in the isotope method versus the hydrodynamic model method. The blue dots represent sample points whose uncertainty overlapped with the tidal envelope of the model results, and the red dots did not overlap (as in Figure 2.8).

2.4 Discussion and Conclusion

This study compared two techniques from two fields of study in order to arrive at estimates of source water fraction (SWF) within a natural system. The hydrodynamic model provided estimated flows and mixing patterns to complement a field-based isotope approach that would otherwise be unsubstantiated (as opposed to previous field-based studies [49], [50]). Similarly, the isotope findings act as a field-validation for a numerically-based method of finding SWF in surface-water systems. Both methodologies can be applied to other riverine systems. In order to confidently use the isotope mixing model approach, one would want to ensure that the system is fluvially dominated, that each source tributary has a distinct isotopic signature, and that some stationarity exists in the isotope composition of those source waters [59]. Both methods provide insight to the larger issue of tracing the composition of water in a system in order to better understand the larger

mixing processes and patterns in a complex river network. Inherent in the methods are a few assumptions.

Throughout the course of the 2017 sampling done for this paper, our river system was dominated by fluvial processes, unlike typical conditions in which the study area experiences a tidal signal. To compare to 2017, which was a wet year, we briefly compared the two SWF methods in 2018 and 2019 floods, which were below normal years, and found there was little agreement, likely because of the flows not being strong or persistent enough to maintain a fluvial character to the study site. During the 2017 period of this study, the two methods outlined produced similar results, despite the major assumption in the isotope mixing model ($f_A + f_B = f_{Site} = 1$) being imprecise due to widespread overland flow and the high Other fractions modeled at the sample sites. Presumably, an increased spatial extent for isotopic sampling could partially alleviate this limitation, although when the number of sources exceeds two, solutions to an expanded Equations 2.1, 2.2 and 2.3 become non-unique. There are additional limitations to the methodologies that may affect the validity of results.

The assumption that endpoint (C1 and M1) samples are representative of cross-sectional averaged isotopic composition may also be imprecise. At each of these locations one sample was collected at one location in the cross-section per sampling date. To evaluate the impacts of this limitation in single-sample field locations, we evaluated model output for all cells across the channel for sites M2, M3, and IA2 and found that the Cosumnes and Mokelumne River waters were well-mixed laterally at the time of sampling, indicating that the lack of replicate samples in the lateral did not necessarily present errors when compared to the model results. However, because this study was performed using a depth-averaged model we cannot investigate sensitivity to the water sample being taken near the top of the water column, but we can assume that the vertical mixing past the confluence is thorough [41]. Although the model accurately predicts cross-sectional flows and stage, the same issue arises as in the study on the model watershed by Peter et

al. [50]: the exact flow and mixing patterns are unknown.

The calibrated hydrodynamic model coupled with a transport model provides more spatiotemporally specific output that has proven to be reliable within the bounds of the field data approach this study used. Additionally, the number of water sources traced is unlimited, unlike the isotope-based approach that is limited to two source tributaries. Another advantage of the hydrodynamic model approach over the isotope mixing model is there is no necessity for the source waters to be isotopically distinct. Lastly, the hydrodynamic model predicts additional variables such as depth and velocity that could provide habitat characteristic values (e.g., Pasternack et al. 2004 [65], Whipple 2018 [18]) to be combined with SWF results to further evaluate restoration potential.

Before exploring the significance of applications to other systems, let us explore the significance to the McCormack-Williamson Tract (MWT). There have been a few examples of multiple restoration sites along a river having cumulative benefits as one moves downstream. These have been demonstrated in gravel restoration sites along rivers in the SacramentoSan Joaquin River system [65]–[67], and the multitude of restoration sites across freshwater tributaries of the Chesapeake Bay [68] where restored sites along a river continuum act as a string of pearls of aquatic habitat. Ultimately, as water moves through rehabilitated habitat its ecological value or potential cumulatively improves [68], [69] It follows that the restoration-laden Cosumnes River carries with it the potential to boost restoration value within the MWT restoration: the last pearl in the string. Understanding the spatiotemporal patterns of SWF allows us to identify regions that retain source waters from the Cosumnes, and thus water that has a higher likelihood to contain nutrients or productivity from upstream restoration sites [58], [70], [71]. Being downstream of completed and ongoing restoration projects is not a unique trait of the MWT within the Delta. Many restoration sites are slated or under construction in the Delta [72]. Understanding how these sites are connected and how they can be synergistic may help to better understand how a single site can have regional ecosystem benefits.

Given that the hydrodynamic method of finding SWF discussed in this paper could be applied to any river network, insights on riverine restoration potential can be gained in any system. For simple fluvial systems that satisfy the assumptions of the isotope mixing model method of finding SWF, isotope samples could suffice in place of developing hydrodynamic models. With careful regard for the limitations discussed, the implications for understanding SWF distribution can be further explored in any river network, and perhaps other connections to aquatic ecology or water quality processes can be found. For instance, Farly et al. used an isotope mixing model to investigate fish diet composition in terms of floodplain-produced or channel-produced resources [73]. This could be coupled with hydrodynamic models to investigate possible effects of drift versus autochthonous production. These methods (hydrodynamic tracers and isotope mixing models) can also be used to investigate habitat quality and its linkages to SWF, using a number of biological or water quality data.

Chapter 3

Zooplankton Response to Water Age

Abstract: In floodplains throughout the Delta there have been numerous ecological studies which suggest that waters with higher residence time make for more abundant lower-trophic-level biota. However, in most of these studies the higher residence time is difficult to observe. Many studies have been performed to assess the relationship between phytoplankton abundance and a quantified transport timescale (such as residence time). When it comes to zooplankton, few quantitative analyses were performed to evaluate effects of water age on zooplankton community and abundance. In our study we evaluate field data from an active floodplain and water age derived from a hydrodynamic model of the study area to find a numerically-based relationship between zooplankton and water age on a floodplain in the Sacramento-San Joaquin Delta.

Keywords— water age, zooplankton, floodplain, hydrodynamic model

3.1 Introduction

For many years researchers have been addressing physical drivers that determine the health of ecosystems. Some physical forcings are more direct, such as meteorological effects affecting surface-mixing layer depth, altering phytoplanktons light and nutrient availability, and therefore driving algal growth rates [74]. But also more broadly, morphological characteristics of estuaries such as tidal amplitude and wave height have been shown to impact food web activity [75]. These physical drivers, whether directly, or incidentally impacting an ecosystem, are driven by proven theories and laws of physics. Although complex, modeling equations in physics is often

more predictable and less empirical than biological processes, enabling the accurate prediction of physical phenomena.

Models of the physical environment in numerous study areas have produced predictions of events commensurate with observed data. Across ecosystems, models have demonstrated that an estimation of a physical environment can predict outcomes in ecology. For instance, numerical models following reservoir releases through riverine habitat have predicted cottonwood tree seedling recruitment spatial patterns [76] based on very specific water table requirements for successful recruitment of cottonwood dictated by flow peak magnitude and timing [3]. Climate models focused on the Kaibab Plateau (located north of the Grand Canyon in Arizona, USA) have allowed researchers to see how the changing climate has driven tree species composition and biomass accumulation in response to fire regime shifts [77] following major changes in fire suppression since settlement in the area. In avian science, numerical weather forecast models have predicted Golden Eagle migration behavior in British Columbia, Canada, which has allowed for the investigation of physical influences on these flight patterns [78]. In aquatic ecosystems, studies have linked the modeling of physical connectivity between shallow and deep water habitats and the resulting auto- and hetero-trophic balances [79]. These studies demonstrate the utility of modeling the physical environment in order to make useful predictions of ecological outcomes and how modeling can aid in understanding what environmental factors are critical to the success of an organism or ecosystem.

This study aims to use the approach of modeling physical forces in the aquatic environment, specifically off-channel habitat in order to understand ecological outcomes. Floodplain or off-channel waters are shallower, meaning a much greater percentage of the water column is penetrated by light allowing for higher rates of phytoplankton growth [79] both by more available light for photosynthesis and warmer conditions for optimizing growth rates [80]. The more time that phytoplankton has to take advantage of these shallow-water conditions, the more biomass they can produce barring predation or other loss terms [81]. Accordingly, organisms such as zooplankton that feed off phytoplankton would tend to thrive in habitats with an abundance of that food source. There are a number of zooplankton species that also have the ability to adapt to feeding on bacteria that are decomposing the organic matter that flushes in to off-channel

habitat during flood pulses [82], [83], providing yet another resource for zooplankton to capitalize on in floodplains and off-channel habitats [84]–[86]. Zooplankton are a vital component of riverine ecology, providing a valuable food source to juvenile and larval fish [87].

Before human intervention, rivers across the globe would have intermittent access to their over-banks or floodplains, providing a landscape of shallow and slower moving water. It has been shown repeatedly that floodplains are of great importance to the vitality of riverine ecosystems [6], [71], [88], [89], with some of the importance attributed to the lentic nature of the water [7], [90]. However, much of the worlds rivers have been altered and disconnected from their floodplains [91], eliminating the boost in productivity during floodplain connection and sparking an interest in restoring floodplain function [92]. In the Central Valley of California particularly, we see such dramatic channelization of the Sacramento and San Joaquin Rivers and their tributaries [29], [93]. All in all, 95% of floodplain and inter-tidal habitat were disconnected from the rivers in the Central Valley [56], resulting in a devastating loss of shallow water habitat that is especially significant for juvenile out-migrating fish (namely salmon). Within the Central Valley, the Sacramento-San Joaquin Delta (Delta), juvenile salmon would use floodplains as nurseries to provide refuge and nourishment via zooplankton [6], [8]. In order to benefit all the fauna that have adapted to use floodplains during their life cycle, major efforts have gone underway to re-institute floodplains in the Central Valley and Delta [94].

In accordance with those efforts to re-institute floodplains, studies have linked the physical environment of a shallow connected riverine habitat to coupled ecological field data to gain an understanding of the dynamics and distribution of ecological productivity. The physical environment being surface water flow, which can be simulated directly with hydrodynamic models. The reliability of hydrodynamic models lies in their ability to reproduce flood events in bodies of water at varying resolutions by following equations of fluid mechanics. Building on these simulated events, the flexibility of the models allows for the introduction of numerical tracers to be implemented, following parcels of water and their properties through the simulated domain. These tracers can be passive and inert for tracking source water or they can implement spatially-dependent aging processes to produce transport timescales such as residence time, exposure time, or age (e.g. Camacho and Martin 2013 [95]; Delhez et al. 2014 [25]; Delhez,

Heemink, and Deleersnijder 2004 [96]; Monsen et al. 2002 [22]). Floodplains or off-channel habitat have been a focus of hydrodynamic transport timescale studies because of coupled nature of biological productivity and time. Transport timescales can be an amalgamation of the several complex competing and interacting physical, chemical, and biological processes such as nutrient cycles, light availability, heat exchange, and predator-prey interactions that dictate the aquatic environment. Baranyi et al. [31] found that numerically-derived water age was positively related to overall zooplankton biomass and determined zooplankton community composition in a study of the Danube River floodplains. In field studies, study sites with qualitatively longer transport timescales (such as increased residence time) have been linked with increased phytoplankton biomass [97], [98]. These qualitative observations of longer timescales leading to more productivity indicates that a more explicit, spatially variable timescale brought by hydrodynamic modeling could be useful in determining the distribution of aquatic productivity.

In this study a calibrated hydrodynamic model was used to compare zooplankton abundance and community composition to a numerically-derived transport timescale. Our study allows for a nuanced approach that produces spatially explicit transport timescale values throughout the study region allowing for an investigation into the conditions that produce more secondary productivity in the form of zooplankton. During the field collection portion of this study, it was anecdotally noticed an increased presence and abundance of Daphnia pulex in areas with warmer and slower moving water. This observation suggests that a quantified timescale value would correlate positively with zooplankton abundance and D. pulex presence. The increased abundance of D. pulex is of particular importance because of the high caloric value it provides feeding juvenile fish. This opportunistic experiment was fueled by the idea that a floodplain system with a higher water age might have boosted primary and secondary productivity and therefore offer higher nutritional than a river channel with lower water age.

3.2 Materials and Methods

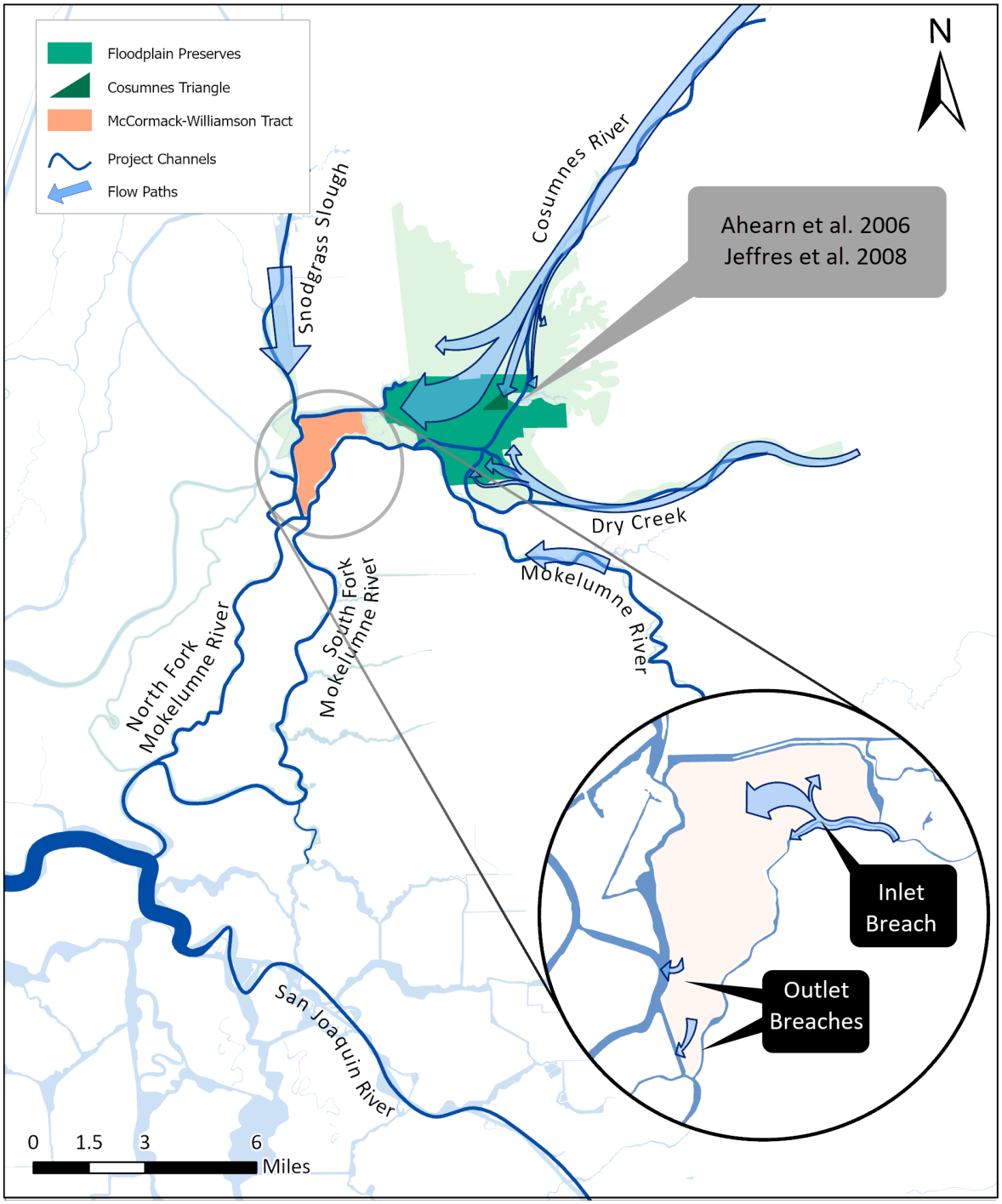

Figure 3.1: A landscape view of the study area showing the flow paths of the incoming tributary waters. The inset shows the breach locations and nature of flow through the Tract. Noted in dark green and annotated in grey is the location of two studies investigating productivity in the Cosumnes River floodplain: Ahearn et al. 2006 [7] and Jeffres et al. 2008 [6].

3.2.1 Study Area

In the Sacramento-San Joaquin Delta of California (Figure 1.2) there are over fifty islands or tracts that are essentially plots of land that are surrounded by levees and have undergone subsidence due to agricultural practices, making the elevations of many of the islands below the mean water level of the channels that surround them. This is contrary to the pre-settlement or historic Delta, where the system boasted an interconnected network of channels but was allowed floodplain access in times of high flows. The region is characterised as freshwater-tidal in low flows, with water surface elevations fluctuating with the sea tides despite having no salinity. This freshwater-tidal system would historically have sub-tidal and inter-tidal wetland and marsh habitat as well. Settlement has removed over 95% of shallow-water habitat from the Delta [56], making these now-seperated islands prime locations for restoration efforts to restore that lost habitat.

The McCormack-Williamson Tract (MWT) is a plot of agricultural land protected from surrounding river channels by a ring levee in the northeastern extent of the Delta (Figure 1.2). The MWT is the study area for this paper located just below the confluence of the Mokelumne and Cosumnes Rivers. The Cosumnes River is the only remaining major river off of the Sierra Nevada mountain range to the East that has no major dams, and thus has the opportunity to overflow and create floodplain habitat. Previous restoration efforts have gone underway along the Cosumnes River, creating floodplain preserves where the land is managed with habitat quality in mind (Figure 3.1). The MWT itself was slated for restoration as this study began, with the intention to connect shallow, fresh-water habitat to the surrounding channels. In the winter months this would allow floodwaters to inundate the floodplain, and for the rest of the year the freshwater-tidal system would have access to inter-tidal wetland habitat.

In the winter of 2017 (the first year of the study period) the levee protecting the MWT from flooding breached in multiple locations (Figure 3.1), offering a restoration preview and the ability to evaluate conditions for ideal off-channel habitat. Following the flood event, the levees were repaired and the disconnected nature of the MWT was returned. This study is an opportunistic experiment offered by this flood event, that allowed us to test the hypothesis that there is a positive relationship between zooplankton abundance and a quantified timescale. Along with

water quality and zooplankton sampling in the field (Figure 3.2,) a hydrodynamic model was developed to provide numerically derived parameters that could help explain the biological data. The hydrodynamic model was the platform for quantifying a transport timescale to characterize the water at the time of sampling and compare to zooplankton abundance providing data for the experiment.

3.2.2 Field Data

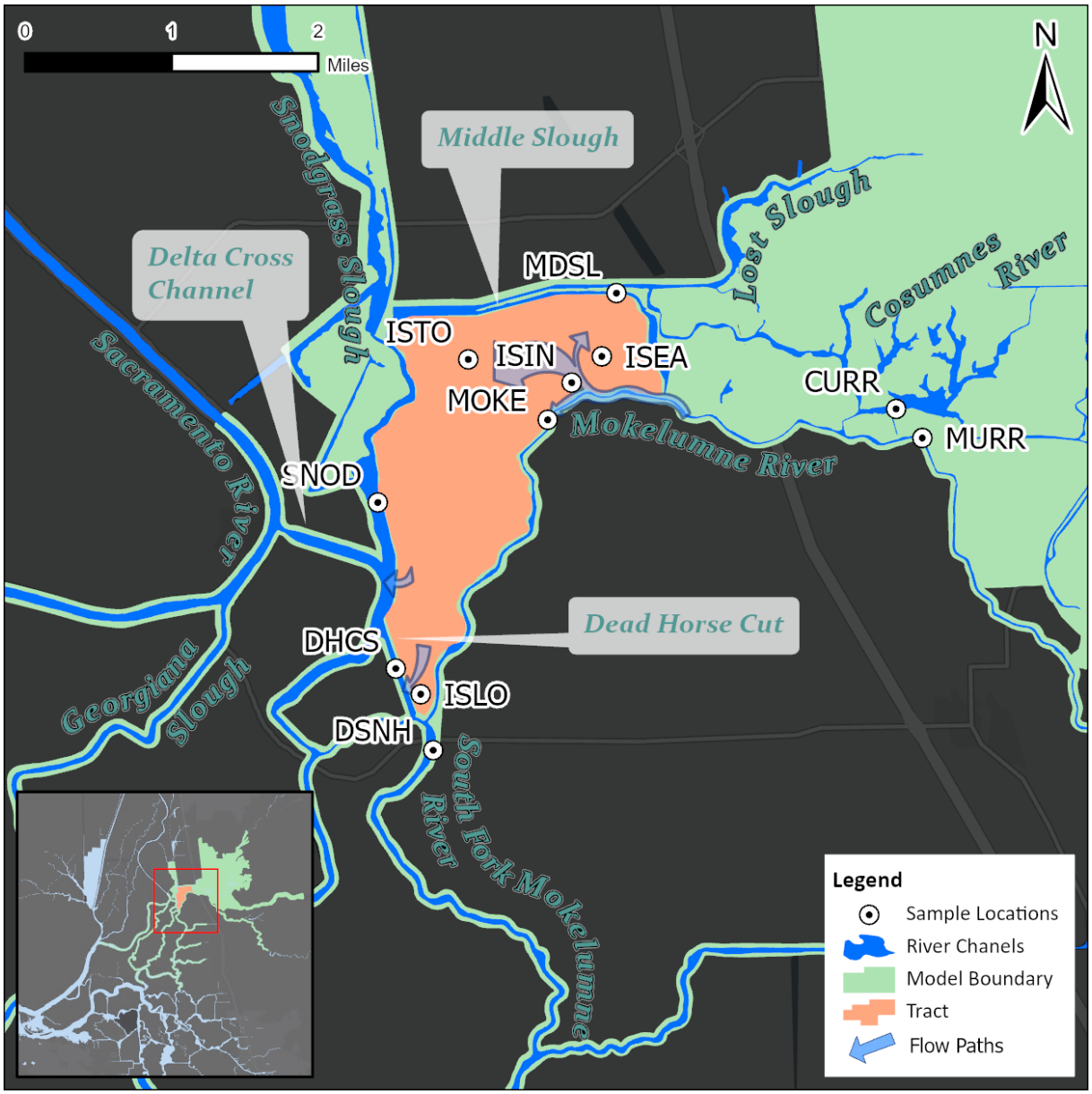

Figure 3.2: Zooplankton and water quality sample sites (shown in white/black target circles) with the model domain and river channels shown in green and blue, respectively.

The field data was gathered from a jet boat biweekly and weekly during flood events, when conditions allowed. Zooplankton and water samples were taken at 11 sample locations (Figure 1) along with recorded measurements from a Yellow Springs Instruments Sonde (YSI), the parameters recorded are listed in Table 1.

3.2.2.1 Water Quality

At each location, a grab sample was taken to quantify suspended chlorophyll a and water chemistry (pH, NO2- + NO3- [NO3-N], and soluble reactive PO43- [SR- PO43-]). SR- PO43- was measured using ammonium molybdate spectrophotometric method (limit of detection [LOD approximately 0.0005 mg/L]) and NO3-N using vanadium chloride spectrophotometric method (LOD = 0.01 mg/L) [99]. Suspended chlorophyll is sampled by field filtering 1 liter of water through a pre-combusted glass-fiber filter (GF/F) and freeze dried in the laboratory. Chlorophyll was measured by soaking filters in 90% ethanol for 24 hours prior to quantification by fluorometry and converted to pigment concentration (chlorophyll a [chl a] and pheophytin) [100].

In addition to the grab sample we also took spot measurements from a Yellow Springs Instruments Sonde (YSI) at each sample location. The YSI sonde was calibrated weekly for electrical conductivity and chlorophyll.

Table 3.1: Water quality parameters measured from grab samples and from the Yellow Springs Instruments Sonde (YSI) at each sample location.

Water Quality Parameter	Grab Sample	YSI Sonde
Electrical Conductivity(EC)	✓	✓
pH	✓	✓
Total Nitrogen	✓	✓
NH4 N	✓	
NO3 N	✓	
Total Phosphorous	✓	
PO4 P	✓	
Chlorophyll a	✓	✓
Pheophytin a	✓	
Pre-HCl/Post-HCl	✓	
Temperature		✓
Specific Conductance (SPC)		✓
Total Dissolved Solids (TDS)		✓
Dissolved Oxygen (DO)		✓
Blue-Green Algae (BGA)		✓

3.2.2.2 Zooplankton

Because of the unplanned nature of the breaches, ecological sampling was opportunistic - the highest trophic group the project could acquire permits for and legally sample was zooplankton, leaving fish out of the analysis. As a result, zooplankton became the main character of the ecological portion of this study.

Zooplankton Sampling

At the time of water quality sampling, a zooplankton sample was also taken using a $153\mu m$ zooplankton net attached to a rod with a flow-meter. Tow volumes were quantified with a General Oceanics flow meter using the reading before and after each sample. This was used to

determine the zooplankton abundance per volume. All samples were placed in Whirlpak bags (Nasco, USA) and preserved in a solution of 95% ethyl alcohol with rose bengal dye.

Zooplankton Sorting

Due to the high abundance of zooplankton, a sub-sampling protocol was used. Samples were rinsed through a $150\mu m$ mesh screen and emptied into a beaker filled to the desired volume and then sub-sampled with a 1-2 mL large bore pipette. If invertebrate densities were too great for enumeration, the sample was split using a Wildco Folsom Sample Splitter (Wildco, Yulee, FL, USA) prior to sub-sampling. Zooplankton samples were enumerated until greater than 100 individuals of the most common species were counted. Zooplankton were identified to the lowest taxonomic level possible using keys from pertinent ecological literature [101]–[103]. Due to the difficulties in identifying Copepods and nauplii, family level assignment of Copepods was used for analysis except for Acanthocyclops sp. and Psuedodiaptomus sp. Terrestrial and aquatic macroinvertebrates were rare and not included in final counts. Only zooplankton were used for analysis. All samples were standardized to individuals per cubic meter for abundance and biomass calculations.

3.2.3 Stage Observations

Solinst LevelLogger pressure and temperature sensors were deployed at nine locations in the study area, with one barometric logger nearby in order to compensate for atmospheric pressure. These sensors were surveyed with real-time kinematic (RTK) positioning devices and water surface elevations were able to be calculated from the deployments. Additionally, HOBO dissolved oxygen (DO) monitors were deployed at six locations to record DO levels at 15-minute intervals.

3.3 Hydrodynamic Model

This study uses a model developed in Tomkovic et al 2020 [30]. The model was developed to evaluate hydrodynamically-derived parameters such as source water fraction, or transport timescale in the study area. The model was two-dimensional and developed using UnTRIM [60], semi-implicit algorithm for the depth-averaged shallow water equations under a hydrostatic assumption [61]. The grid was generated using Preprocessor Janet (http://www.smileconsult.de) and contains quadrilateral and triangular elements. The model was calibrated using the same

procedures in the previous study. This study applies a three-dimensional model and evaluates the built-in age transport solver [64], outlined in Section 3.3.2.

3.3.1 Modifications to the Model

Since the development and calibration of the model used in Tomkovic et al 2020 [30], a few modifications to the model were made. One was to use a three-dimensional model instead of two-dimensions. This allowed for an apt comparison of zooplankton collected at the water surface to the modeled age in the surface layer of the three-dimensional model. The other was the addition of a temporally-varying wind field in order to increase accuracy in the mixing patterns observed within the Tract. This was derived from a nearby California Irrigation Management Information System (CIMIS) station from California Department of Water Resources (DWR). The reported wind data was collected 2.0 meters above ground at station 242 - Staten Island (Figure 3.3).

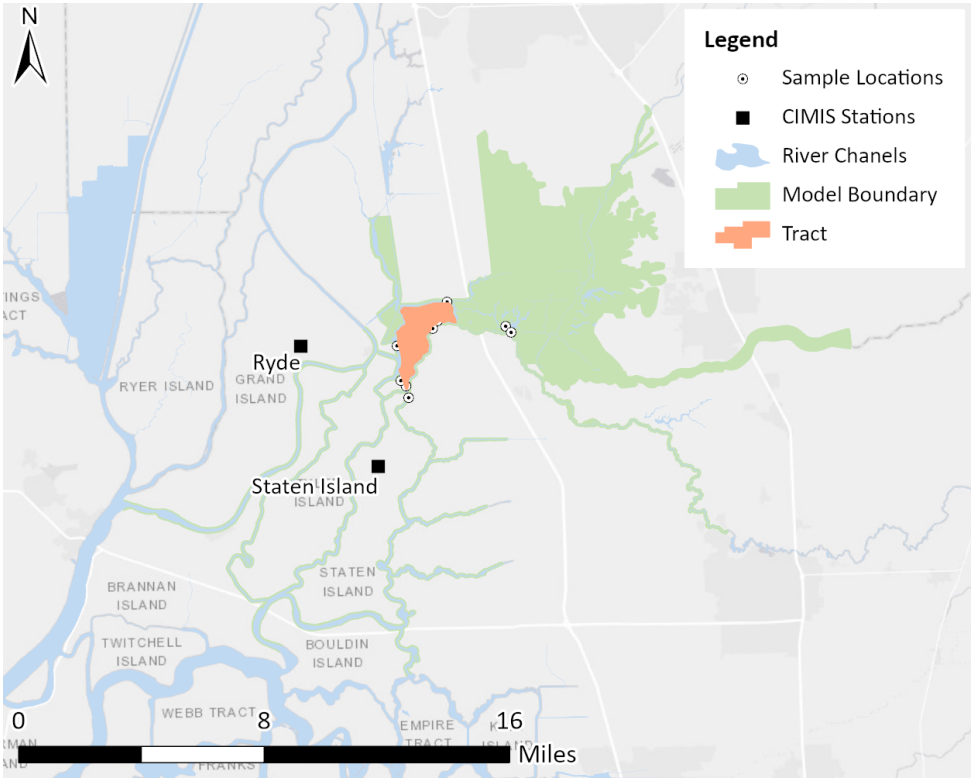

Figure 3.3: CIMIS stations near the study area. The station used in the model is the Staten Island station (CIMIS station ID 242).

3.3.2 Numerically-Derived Transport Timescale

For this study, we chose the transport timescale of water age due to the fact that it is simple to conceptualize, it is largely independent of the start time of the simulation, and it produces a continuous timescale for the duration of the hydrodynamic simulation. In essence, as water enters the model domain it starts with an age of 0 days and accumulates age proportionally with time, meaning if a water parcel has been in the model domain for 2 simulated days then it has an age of 2 days. Of course water is a constantly mixing medium, so age is advected and diffused just like any other constituent would.

Once the hydrodynamic model was calibrated against both agency gages existing in the model domain and four LevelLoggers deployed during the flow event, the hydrodynamic solution could be used to calculate age at the time of sampling for each site location. The method used in this study to calculate age was tracer-based as opposed to particle-based methods (e.g. Defne and Ganju 2015 [23]; Lemagie and Lerczak 2015 [104]; Rayson et al. 2016 [105]). To find age, this study employs two tracers when combined yield age, similar to Gross et al 2019 [27]. First, a conservative tracer, C, enters at each upstream model boundary with a concentration of 1. All other water in the model domain had an initial concentration of 0 at the beginning of the simulation. The concentration of tracer, C, is calculated using Equation 3.1, where $\mathbf{u}$ is a three-dimensional velocity vector, and K_T and K_{zz} are the horizontal and vertical eddy diffusivity, respectively. Equation 3.1 is implemented by the model with a conservative finite volume approach, with the horizontal and vertical diffusion coefficients (K_T and K_{zz}) set to zero, resulting in a right-hand-side of zero. Equation 3.1 is discretized as Equation 3.2, where $\mathcal{A}$ is the discrete advection-diffusion operator.

$$\frac{\partial C}{\partial t} + \nabla \cdot (\mathbf{u}C) = \frac{\partial}{\partial x}(K_T \frac{\partial C}{\partial x}) + \frac{\partial}{\partial y}(K_T \frac{\partial C}{\partial y}) + \frac{\partial}{\partial z}(K_{zz} \frac{\partial C}{\partial z}) \tag{3.1}$$

$$C^{n+1} = \mathcal{A}(C^n) \tag{3.2}$$

In addition to the conservative tracer at the upstream boundaries, an age-concentration tracer (α, Equation 3.3) is calculated at each cell which accumulates age proportionally to the concentration of the conservative tracer, C, in the cell. The age-concentration tracer, α, has

units of time-mass per volume. Similar to Equation 3.2, Equation 3.4 is the discretized form of Equation 3.3, where Δt is the model time-step.

$$\frac{\partial \alpha}{\partial t} + \nabla \cdot (\mathbf{u}\alpha) = \frac{\partial}{\partial x}(K_T \frac{\partial \alpha}{\partial x}) + \frac{\partial}{\partial y}(K_T \frac{\partial \alpha}{\partial y}) + \frac{\partial}{\partial z}(K_{zz} \frac{\partial \alpha}{\partial z}) + C \tag{3.3}$$

$$\alpha^{n+1} = \mathcal{A}(\alpha^n) + \Delta t C^n \tag{3.4}$$

To derive age, a, from these two tracers the age-concentration is divided by the tracer concentration (Equation 3.5) and results in units of time.

$$a = \frac{\alpha}{C} \tag{3.5}$$

The tracer-based age ultimately provides a geometric mean of the age within a cell. In order to relate the model results to the field data, the way-point stored in the boat GPS was used to specify the GPS coordinates of the cell. The depth-averaged age was used to compare to the field zooplankton data.

One could define the boundary where age begins to accumulate closer to the area being studied - i.e. within the MWT itself - but in this system the Cosumnes River, Upper and Lower Laguna Creek, and Dry Creek inflows (Figure 2.1) make up over 65% of the inflow volume that passes through the study area and all of these tributaries have ample access to their floodplains (Figure 3.1). Because of this floodplain connection upstream of the study area, the incoming water from these boundaries are going to have a different character than that of the Mokelumne River water which enters the system from the bottom of Comanche Reservoir and arrives at the study area in less than two days. It is for these reasons that this study uses the model domain as the region with which to define age accumulation.

3.3.3 Boundary and Initial Conditions

The model used a mixture of gaged and estimated flows (shown in Figure 2.1). The downstream stage boundaries were assigned with observed stage data (SRV, MOK, and LPS), and only two of the seven upstream boundaries were assigned flow with observed gage data (SDC and WBR). The remaining five upstream boundaries (Snodgrass, Cosumnes, Lower Laguna Creek, Upper

Laguna Creek, and Dry Creek) were estimated using an adapted method from Whipple 2018 [18]. The initial water surface elevation of the model was set to just below the lowest elevation of the Tract in order to ensure no water was initialized within the Tract boundaries before the modeled breaches occurred. Because no bathymetric survey was conducted for any of the breaches while they were open, breach geometry was inferred from two DEMs collected after the breach had been re-sealed with a levee. One was bathymetry data on the river-side of the breaches and the other was a DEM created from drone-collected photogrammetry. The breaches were modeled as gates that opened consistent with the breach timing and closed upon the repair of the levees.

3.3.4 Evaluation Criteria

In evaluating model results, skill (Equation 2.6) and R^2 (Equation 4.7) are used to determine the model's performance in accurately recreating a flood event. Typically this would be evaluated in both a calibration and validation simulation period, however since the MWT was only flooded once, the model was calibrated to the event and data coming from the model was used to test the relationship between zooplankton and water age. To test the strength of correlation between the two variables the data is evaluated with a Spearman correlation test which produces the Spearman rank correlation coefficient, rho (Equation 3.6). The Spearman rank correlation determines to what degree the data are correlated with a monotonically increasing relationship. The Spearman rank coefficient has a range of outcomes of -1 to $+1$, where $+1$ is a strong positive correlation and -1 is a strong negative correlation, and 0 or near-zero is no correlation. With the equation for the coefficient of:

$$rho = \frac{\sum(a' - \bar{z}')(z' - \bar{a}')}{\sqrt{\sum(a' - \bar{a}')^2 \sum(z' - \bar{z}')^2}} \tag{3.6}$$

where a' and z' are age rank and zooplankton abundance rank, respectively, and where $\bar{a}'$ and $\bar{z}'$ are average age rank and average zooplankton abundance rank, respectively. If the hypothesized relationship holds, the Spearman rank correlation coefficient would be positive and close to 1.0 (Table 3.2), and the $p - value$ of the analysis would be below 0.05.

Table 3.2: The meaning of the outcome of a Spearman rank correlation coefficient analysis [106]

rho **(positive or negative)**	**Meaning**
0.00 to 0.19	A very weak correlation
0.20 to 0.39	A weak correlation
0.40 to 0.69	A modest correlation
0.70 to 0.89	A strong correlation
0.90 to 1.00	A very strong correlation

3.4 Results

3.4.1 Hydrodynamic Model Age Results

Table 3.3: Model calibration metrics for the gages shown in Figure 2.1

	Gage Name	**Gage ID**	$\mathbf{R^2}$	**Skill**	**Date Range**
Stage	Mokelumne R @ Benson's Ferry NR Thornton	BEN^{C}	0.946	0.986	2/1/2017 - 07/01/2017
	Delta Cross Channel BTW Sac R & Snodgrass	DLC^{U}	0.955	0.975	2/1/2017 - 07/01/2017
	Sacramento River Below Georgiana Slough	GES^{U}	0.976	0.993	2/1/2017 - 07/01/2017
	Georgiana Slough at Sacramento River	GSS^{U}	0.975	0.992	2/1/2017 - 07/01/2017
	Middle Slough	MSL^{L}	0.945	0.986	01/20/2017 - 07/01/2017
	McCormack-Williamson Tract - Inlet	MTI^{L}	0.871	0.965	02/16/2017 - 05/31/2017
	McCormack-Williamson Tract - Lower	MTL^{L}	0.891	0.971	02/16/2017 - 05/31/2017
	South Mokelumne R at W Walnut Grove Rd	SMR^{U}	0.951	0.969	2/1/2017 - 07/01/2017
	Snodgrass Slough Upstream of Meadow	SUM^{L}	0.910	0.989	01/20/2017 - 07/01/2017
Flow	Sacramento River Below Georgiana Slough	GES^{U}	0.989	0.996	2/1/2017 - 07/01/2017
	Georgiana Slough at Sacramento River	GSS^{U}	0.974	0.989	2/1/2017 - 07/01/2017
	South Mokelumne R at W Walnut Grove Rd	SMR^{U}	0.935	0.980	2/1/2017 - 07/01/2017

* Gage data sources are denoted as ^{C} - DWR, ^{U} - USGS, ^{L} - LevelLogger sensor deployed for this study.

Similar to the analysis in Chapter 2, a 72-hour model spin-up period was eliminated from the time-series before computing calibration metrics. Figure 3.4 shows the model agreement for the 3D and wind-inclusive iteration of the model. Given the hydrodynamic agreement confirmed in the model metrics (Table 3.3), and the field confirmation of numerical tracers in this same model domain [30], the modeled produced a three-dimensional representation of age for the en-

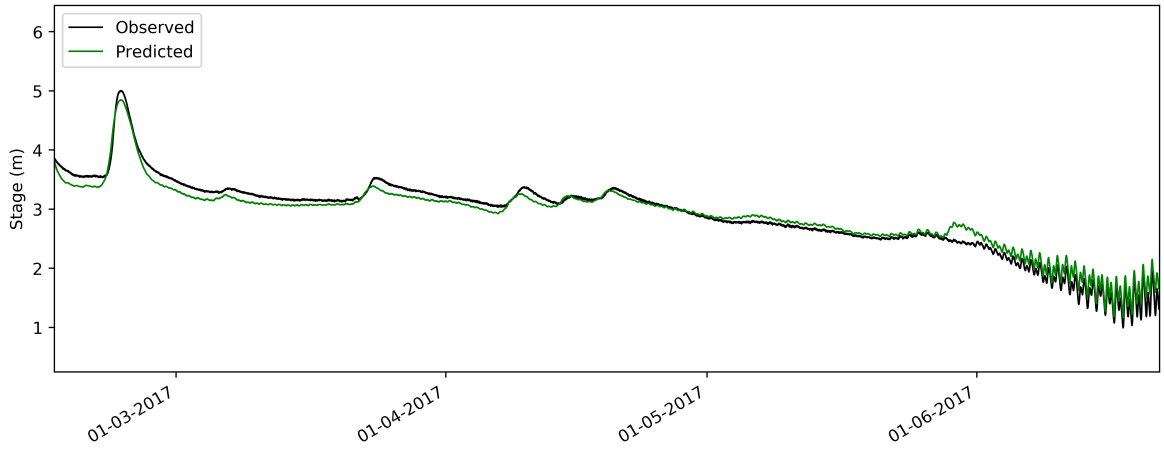

(a)

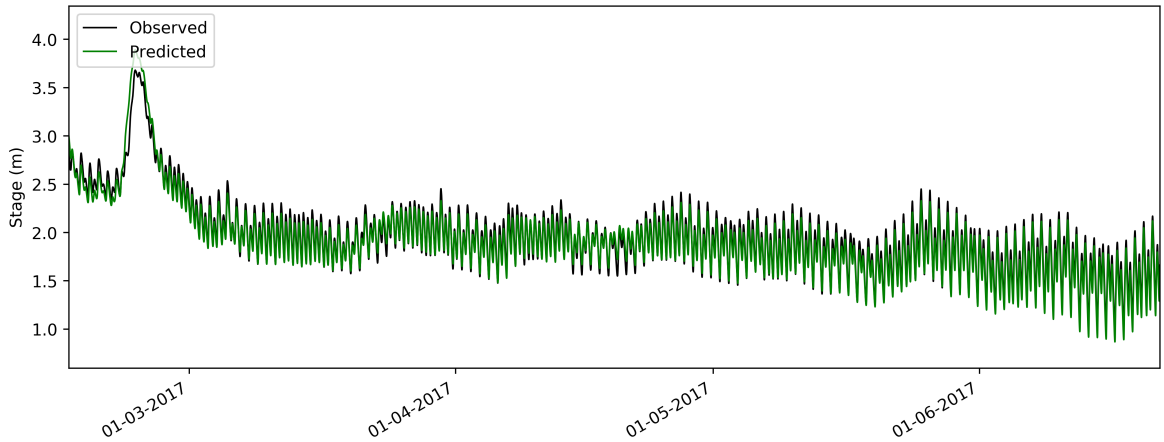

(b)

Figure 3.4: Calibration plot for the BEN (a), and SMR (b) gages (Table 3.3) showing the observed (black) and modeled (green) water surface elevation for the period simulated.

tire model domain at all times within the simulation period (Figure 3.5). The age results from the surface layer of the 3D model are to be used to compare to the zooplankton field data. At each site a time-series is produced which depicts the age as a function of time, demonstrating flushing and ponding periods (Figure 3.6).

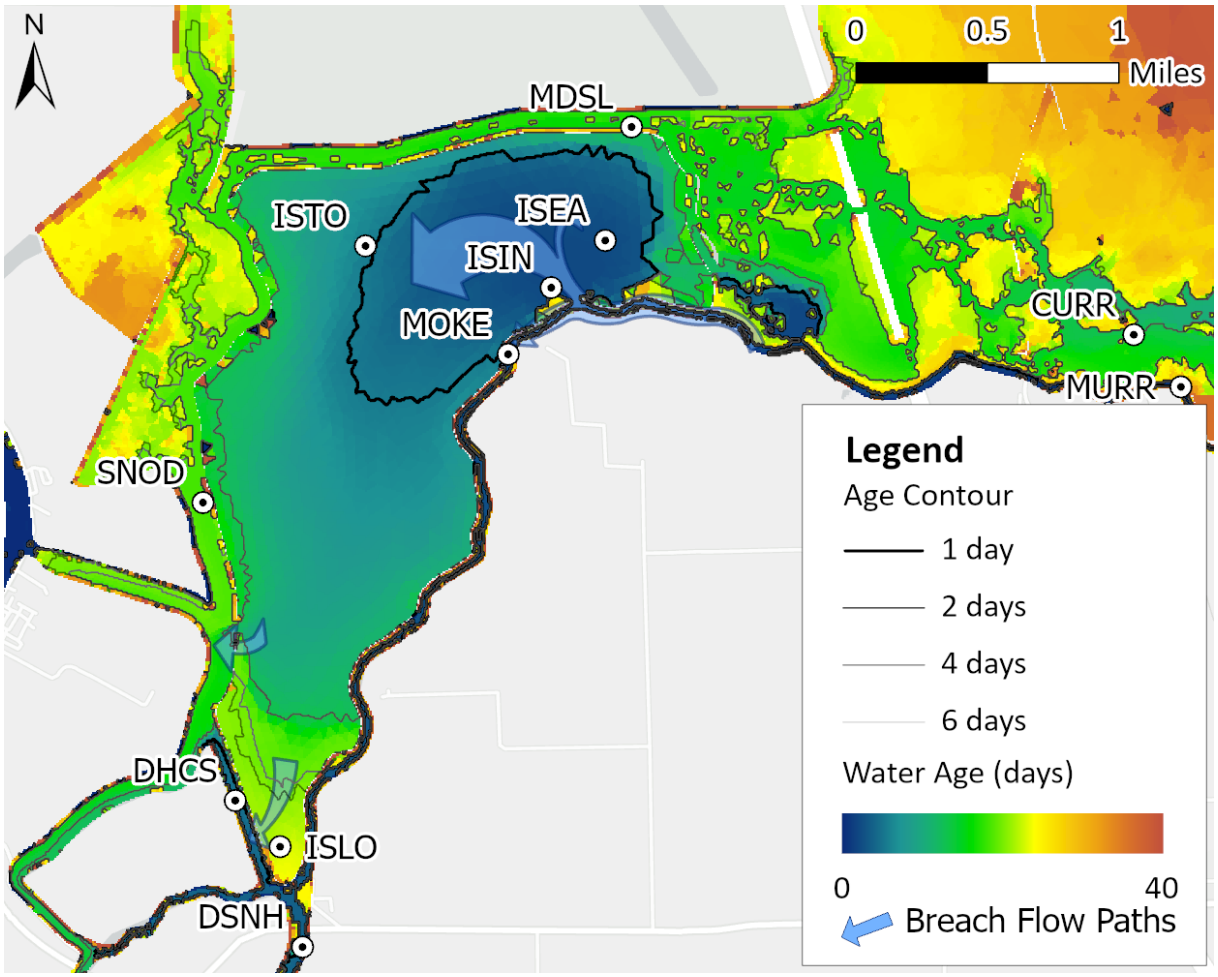

Figure 3.5: Modeled age distribution at the water surface on March 20, 2017.

The modeled age differences have a range of magnitudes (Figure 3.6), where the variation in ISEA and MOKE are small and less than 5 days as opposed to the SNOD site which reaches ages over 15 days. This difference in magnitude is due to the shallow inter-tidal area north of the SNOD site that allowed for accumulation of water age versus the more swift-moving water passing through the MOKE site (Figures 3.2 & 3.5). DHCS shows an intermediate age time series magnitude owing to its location in a channelized system that is also downstream of high age accumulation regions (Figures 3.2 & 3.5), allowing for advection of higher ages that are transported out of the region swiftly. Although the results for the ISEA site suggest a low age, discussion in Section 3.5 addresses this unexpected result.

As evidenced in Figure 3.6, age within the channels increases upon the closure of the Tract

on May 28, 2017 (denoted as a vertical dotted line in Figure 3.6). This closure coincided with less overall boundary flows coming into the system, which meant lower velocities and thus increased age. The other factor which increased age at that time is that the Tract was draining into the system and advecting its higher age waters with it.

3.4.2 Zooplankton

After collecting and sorting the zooplankton samples at each site for each date, a time series of zooplankton abundance was produced for each site (Figure 3.6).

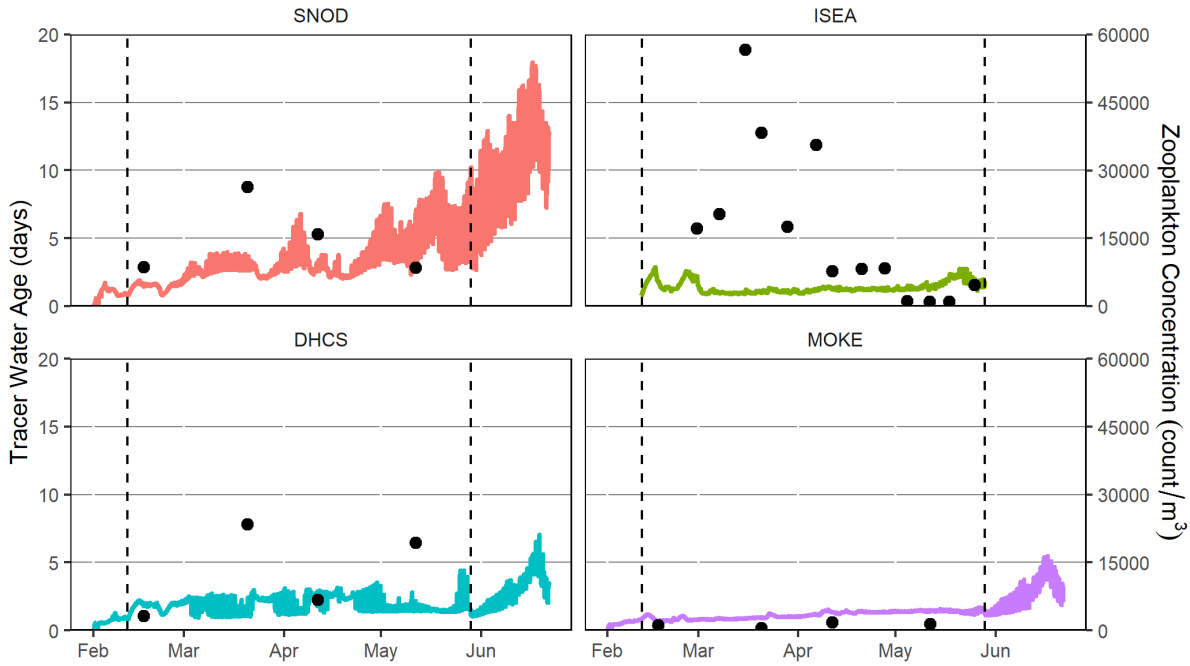

Figure 3.6: Water age and zooplankton abundance time series for Snodgrass Slough (SNOD, red), MWT East (ISEA, green), Dead Horse Cut (DHCS, blue), and Mokelumne at MWT (MOKE, purple). Water age is shown as lines against the left axis and zooplankton abundance is shown as points against the right axis. See Figure 3.5 for sites.

3.4.3 Zooplankton v. Age Comparison

Using the exact time of zooplankton collection at each site, water age results were extracted from the model tracer output to be compared to the field values of zooplankton abundance. Figure 3.7 shows the resulting relationship between zooplankton and modeled age with the Tract sites shown as triangle points and the channel sites shown as circles.

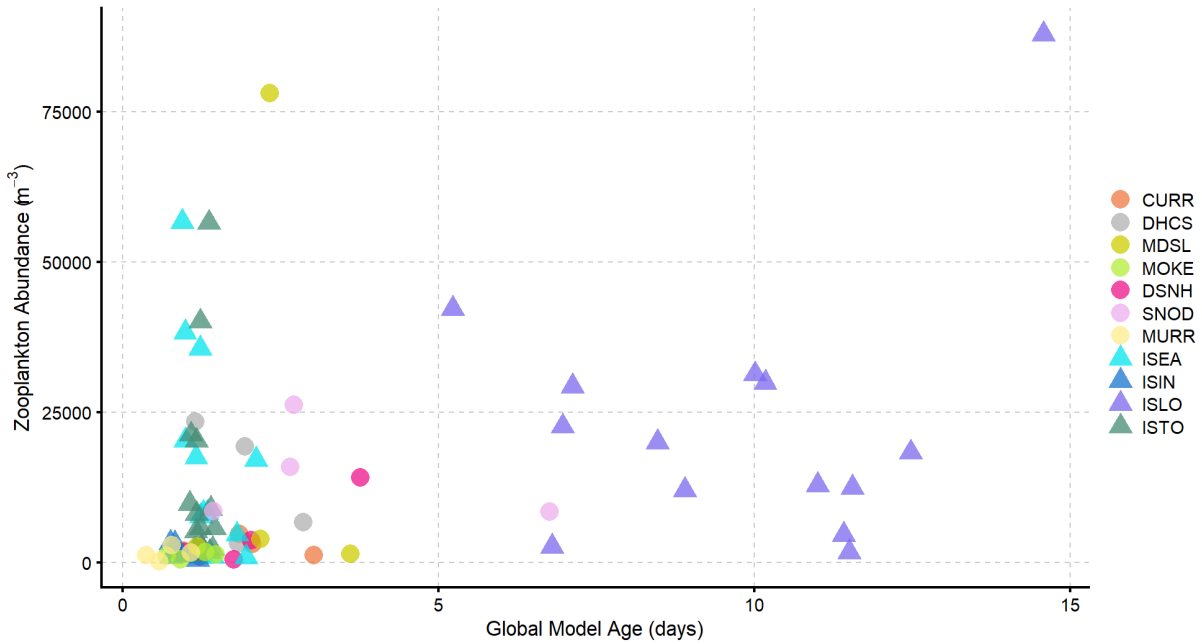

Figure 3.7: Zooplankton abundance versus modeled age for all sites during the study period with sites within the Tract shown as triangles and sites outside of the tract shown as circles.

The relationship shown in Figure 3.7 was tested with a Spearman correlation test (Equation 3.6) and a significance level $\alpha = 0.05$ the data suggests there's a positive relationship between age and zooplankton with a correlation coefficient of 0.37 and a p-value of 0.00064. Although this confirms the positive relationship, the correlation value of $rho = 0.37$ means the correlation is weak (Table 3.2).

3.5 Discussion

In performing this analysis, a positive relationship between zooplankton and age was expected due to several studies suggesting that there was a relationship between primary/secondary productivity and the transport time that the biological samples were taken in [7], [22], [25], [31], [90], [95]–[98]. In addition, a parallel study found that the floodplain habitat provided by the MWT did in fact subsidize zooplankton communities in the channels downstream [107]. However, the study found a weak correlation, with $rho = 0.37$. The weakness in correlation could be attributed to a lack of true correlation, going against what previous studies suggest, or the weak correlation could be due to errors in either measurement of zooplankton or quantification of water age. For the former, that would imply that a simple zooplankton-versus-age relationship

does not exist. If that were the case, it could be that there are also several other water quality variables that contribute to zooplankton abundance [108]. In the interest of investigating sources of error in this analysis, the study will look to weaknesses in the study design, zooplankton sampling, and modeling of water age.

Unlike the Baranyi et al. study [31] where a positive relationship was found between zooplankton productivity and a quantified transport time scale, our study did not evaluate zooplankton biomass against a reach-scale modeled water age. This study had two major differences: it used zooplankton abundance instead of biomass, and it used a fully discretized model domain in which the computed water age was reported at a point location instead of a more coarse reach-scale analysis. Prior studies comment on the ability of lentic systems such as floodplains to support the rapid growth of juvenile fish [6], [7], [90], and simple abundance doesn't indicate the caloric value of the observed zooplankton as prey in the same way that biomass would. Perhaps the absence of a strong correlation could be attributed to using the wrong quantitative variable to describe zooplankton productivity. So far we treat the sampling method as an accurate means to quantify zooplankton abundance in an area, however there are limitations to the temporal frequency and spatial sampling method that were utilized in this study. The fleeting nature of the breach event and the high-water conditions of this study period meant that a more consistent and frequent sampling schedule could not be followed safely. This allows for gaps between sampling periods reaching up to 27 days with an average of 10.1 days between samples. Many zooplankton in this system have a lifespan of around two weeks [109], meaning that the sampling periods could've missed the temporal scales of variability inherent in zooplankton. Additionally we took very spatially discrete samples, which in more lotic sample regions like the channels would be sufficient since zooplankton would have very little choice as to where to be in the reach but in the more lentic regions such as the shallow slow-moving waters within the Tract zooplankton would have a bit more agency and would be more spatially distributed both in the water column and laterally. Without making deliberate efforts as to where to sample specifically in order to get a true "apples-to-apples" comparison between the observed and modeled, a point-based comparison of zooplankton to modeled age sets the study up for missing spatio-temporal variability in a natural system that is quite complicated to replicate. The study now evaluates the modeling component as a source of error in the opportunistic experiment, although proven

to be capable of reproducing mixing patterns to some degree of accuracy (Chapter 2), there may be room for improvement in the next effort to test the relationship between zooplankton productivity and water age.

Table 3.4: Modeling parameters changed to get to the final modeling iteration, with the parameter being changed on the left and the outcome in attempting to replicate the observed mixing patterns in the Tract (Figure 3.8). The first iteration was the model used in Chapter 2 and only a condensed version of the many iterations are shown here.

Iteration	**Parameter Changed**	**Outcome relative to previous iteration**
0	2D no wind	No water age gradient and very little accumulation of water age w/in Tract
1	3D	Very diffused water age gradient with more accumulation of water age along the edges of the Tract
2	changed inlet breach geometry	Location of the diffuse gradient shifted according to the inlet geometry*
3	pre-processed wind data from Staten Island station[1]	Less diffused water age gradient within the Tract
4	wind applied directly from the Staten Island station[1]	Different but still seemingly inaccurate water age distribution within the Tract
5	wind applied directly from the Ryde station[1]	Different water age distribution within the Tract, seemingly more inaccurate distribution
6	wind applied directly from the Staten Island station using a different wind friction method	Different water age distribution within the Tract, location of diffuse mixing line significantly shifted

* Process repeated with different geometry estimations to find best mixing pattern

[1] Refer to Figure 3.3 for CIMIS station location

During the modeling process it was observed that the modeled water age mixing patterns were sensitive to a few key modeling parameters. One particularly sensitive mixing feature was a distinct shear layer that had been observed between the ISIN and ISEA site (Figure 3.8), which was observed qualitatively upon collecting field data and was also seen near the ISTO site. Several different modeling techniques were deployed to attempt to better replicate the

mixing line that was observed in the field, with the final iteration being the one presented in this paper (Table 3.4).

The previously mentioned mixing line was observed from the field with colder, clearer, dilute water without many zooplankton on one side and on the other was warmer, more turbid, and much more zooplankton-rich water. The mixing line was set up around the eddy that formed in response to the plume formed by the MWT inlet breach (Figure 3.1), and would set up on either side of the ISEA and ISTO sample locations and vary in space and time, but would almost always be present. The difference in temperature on either side of the mixing line was quite exaggerated and the contrasted warm and cold temperatures could be felt over a difference of 10 meters or so, making it quite distinct despite being a largely qualitative observation. Given that solar heating was the dominant mechanism for increased temperature and that the depth around the ISEA and ISTO sites were more or less uniform, the warmer water must have been significantly older water than the fresh-water plume coming into the MWT from the Mokelumne River and it was therefore expected that the modeled age gradient would at least mimic the observed temperature gradient strength and location. After many iterations of modifying model parameters in order to better replicate the strength and spatial variability of the mixing line between the colder plume and the warmer eddy (Table 3.4), the study was concluded with the current representation of the spatio-temporally varying age distribution. The sensitivity of modeled age to wind data input and inlet breach geometry makes the replication of mixing patterns within the Tract less accurate for the shallow water sites, leading to a weakened relationship between zooplankton abundance and water age with the ISEA and ISTO sample locations. Notice the other sites have a more clear positive relationship between zooplankton and water age (Figure 3.9) as well as a clearer relationship between observed temperature and water age (Figure 3.10). These plots visually indicate that the exclusion of the ISEA and ISTO sites strengthen the relationship between zooplankton and modeled water age. Since there is a disparity between the observed and modeled mixing patterns surrounding the ISEA and ISTO sites, it is reasonable to suggest that the modeled age for those two sites was not as accurate as the rest of the sample locations in the study. Further, the statistical improvement of the zooplankton abundance versus water age relationship upon exclusion of the ISEA and ISTO sites will be discussed.

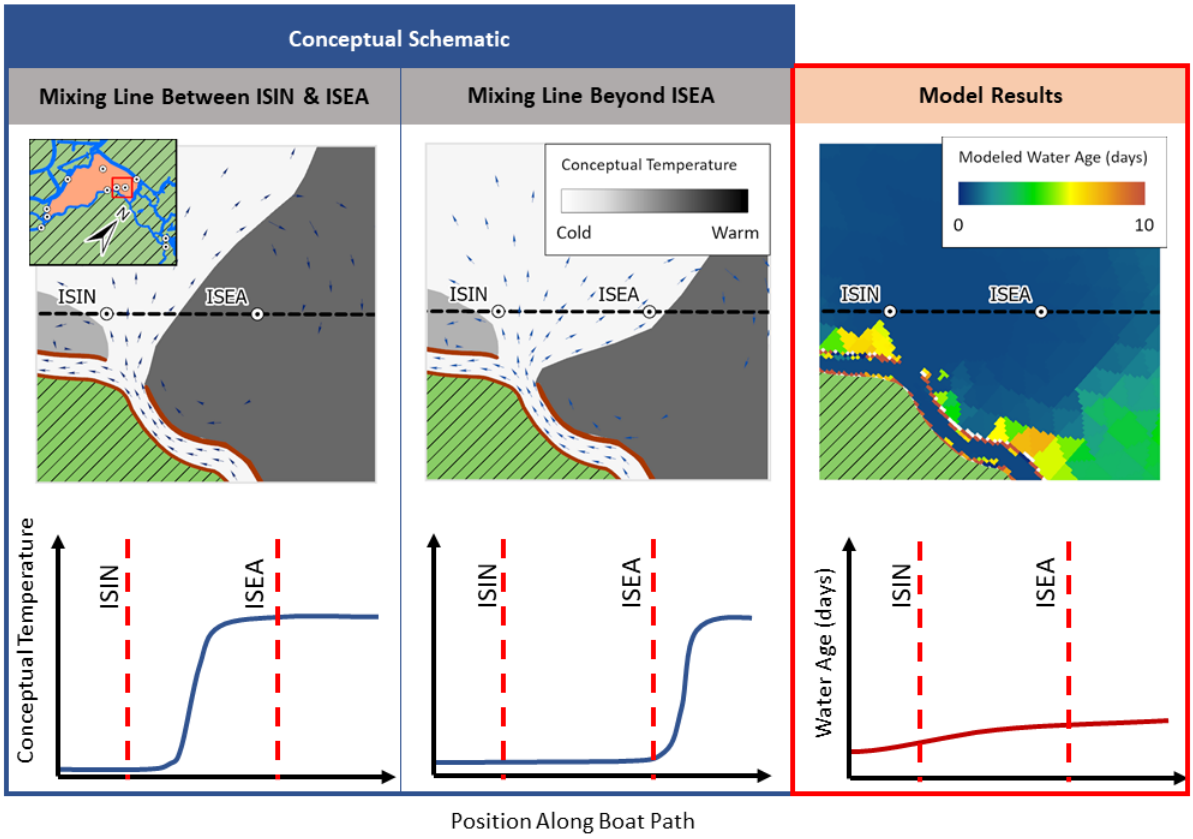

Figure 3.8: Conceptual mixing line dynamics within the McCormack-Williamson Tract for sites ISIN and ISEA. The top row shows conceptual plan-view schematics with the boat path taken from the ISIN site to the ISEA site (black dashed line), the sites (white and black points), and the conceptual age distribution (blue-to-red color gradient). The bottom row shows what the age would look like in profile view along the boat path shown above, with the ISIN and ISEA sites shown as red dashed lines. The left and center scenarios showing the observed mixing line that occurred either between the ISIN and ISEA sites or beyond the ISEA sample location (left and center, respectively). The right panel shows the what the modeled results looked like in either case.

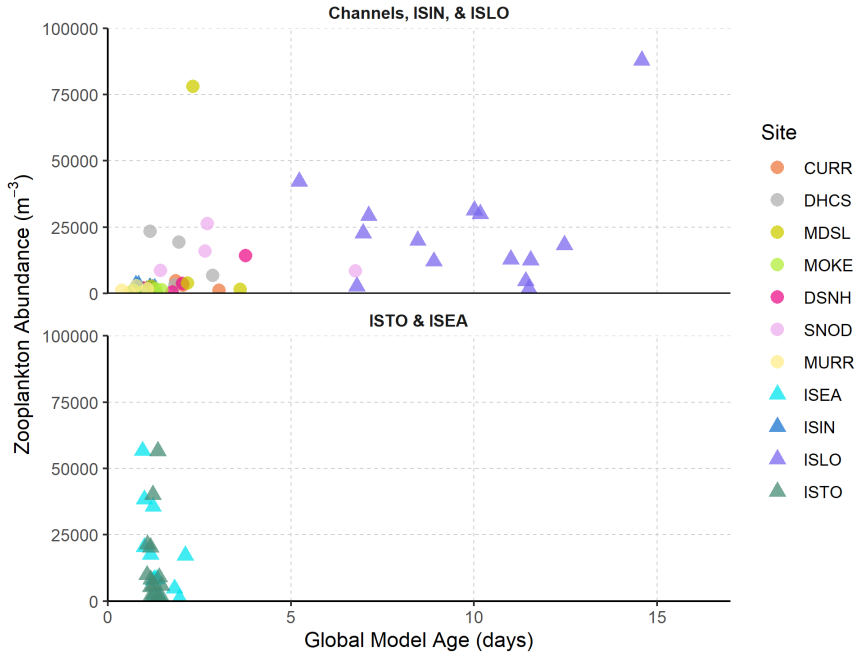

Figure 3.9: Zooplankton abundance versus modeled age for all sites except ISTO and ISEA (top) and zooplankton abundance versus modeled water age for ISTO and ISEA (bottom). See figure 3.2) for sample locations surveyed during the study period with sites within the Tract shown as triangles and sites outside of the tract shown as circles.

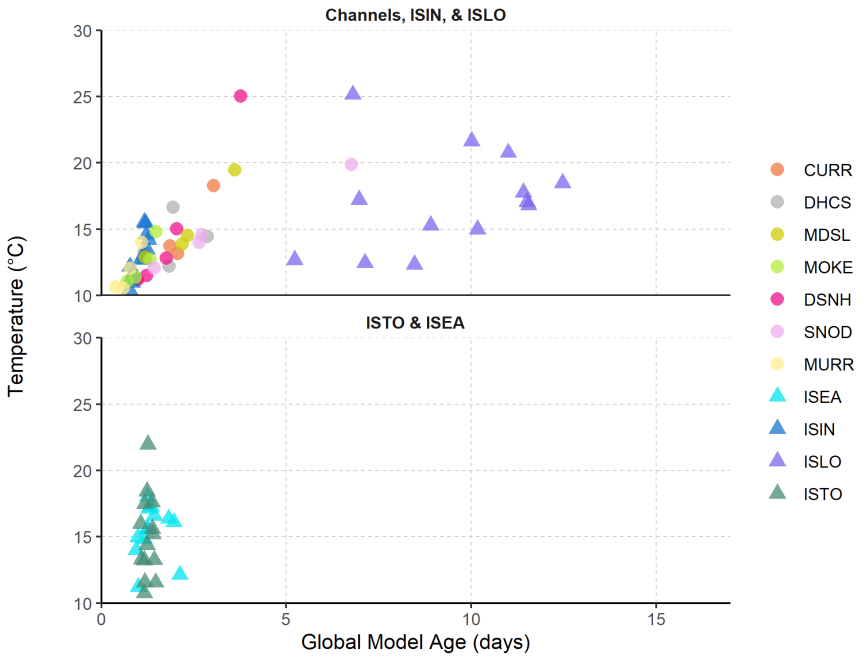

Figure 3.10: Observed temperature versus modeled water age at all sites except ISTO and ISEA (top) and observed temperature versus modeled water age for ISTO and ISEA (bottom). See figure 3.2) for sample locations surveyed during the study period with sites within the Tract shown as triangles and sites outside of the tract shown as circles.

Given the aforementioned shortcomings of the modeling performance for the shallow water MWT sites ISEA and ISTO, the visual disparity between the zooplankton-age relationship (Figure 3.9)for the remaining sites demands statistical inspection. When evaluating the Spearman rank correlation coefficients (Equation 3.6) for the modeled water age, zooplankton abundance, and observed water quality variables (Table 3.1), it is shown that the exclusion of the ISEA and ISTO sites improves not only the correlation between age and temperature, but also between age and zooplankton (Figure 3.11). Exclusion of the ISEA and ISTO sites brings *rho* from a weak correlation with a value of 0.35 to a modest correlation with a value of 0.63 (Table 3.2). This indicates that the zooplankton-age relationship would have been more strongly positive if the model had better depicted the water age mixing dynamics at the ISEA and ISTO sites. This also indicates that for the channelized sites as well as the ISLO and ISIN sites a spatio-temporally quantified transport time scale was perhaps simpler to develop.

The ease in producing modeled water age for the well-performing sites (all sites except ISEA and ISTO) could be attributed to a few factors. For the channelized sites this improved correlation is perhaps due to the more complete mixing experienced within channels that is simpler to model and replicate than the large-scale mixing patterns of shallow water in the Tract. That complete mixing is inferred from the three-dimensional model results which indicate that the quantified age is fairly uniformly mixed laterally and vertically in any given sample area. There are two sites, ISLO and ISIN, which are within the MWT but aren't near a strong age gradient so they are easier to replicate in the model, making the correlations stronger for those sites. Figure 3.12 shows modeled velocities in the Tract and the surrounding sites and one can see that all of the sites save for ISLO have velocities well over 1 cm/s which is beyond the swimming velocity of zooplankton. Although the vertical velocities and velocities near the bed are slower, the system is an advectively dominated system one wouldn't expect to observe anywhere near the magnitude of zooplankton that were collected at the ISEA and ISTO sites, strengthening the case that the model's ability to accurately depict the velocity and age results at those sites was a key issue in proving the positive relationship between zooplankton productivity and a transport time scale. The previous evidence from observed temperature gradients near the ISEA and ISTO sites as well as the correlation improvement upon exclusion of said sites (Figures 3.11b - 3.11c) is an indication that the study design and model development did not allow for a direct

comparison of modeled results to in-situ data in a broad shallow body of water and that there may be especially sensitive parameters to heed when attempting an experiment of this nature again.

This study identifies two major factors that affect the model results when it comes to the mixing patterns in the MWT and specifically the ISEA and ISTO sites. One is the application of wind data, and the other is the bathymetry of the breaches - particularly the inlet breach (Figure 3.1). Upon calibrating the three-dimensional version of this model and realizing that the model was not capturing the age gradient that was expected based on the observed temperature gradient when field sampling (Figure 3.8), many methods of incorporating wind into the model were evaluated (Table 3.4). It was noticed that even a slight difference in the input wind data produced dramatically different mixing patterns within the MWT itself. This is consistent with another study which demonstrated that wind fetch has a strong effect on water velocities and phytoplankton patchiness in a small shallow lake [110]. This means that although the hydrodynamics are accurate, the mixing patterns within the Tract may be less accurate. If one were to attempt this experiment again, it would be strongly encouraged that they acquire precise local meteorological data, and if possible generate a spatio-temporally varying wind field so as to most accurately capture the wind friction effects on mixing patterns within the system if there is a lot of fetch in the shallow water habitat of interest.

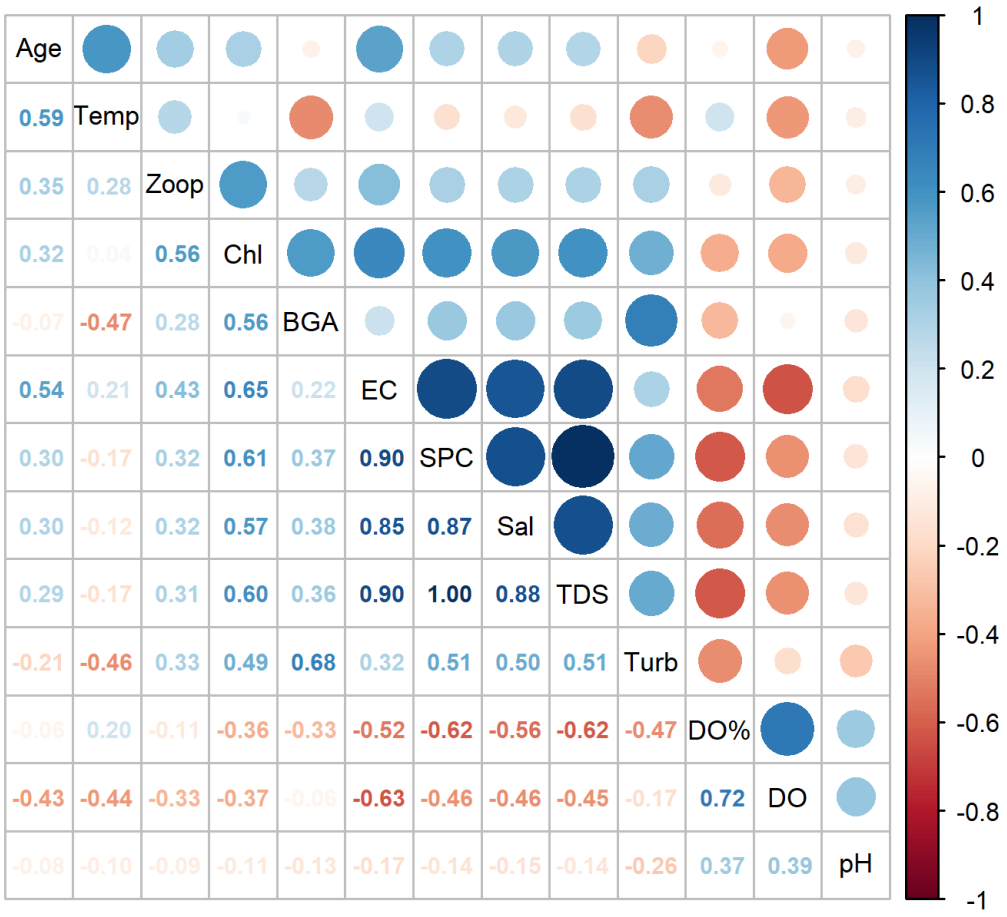

(a) Spearman rank correlation coefficients for all sites

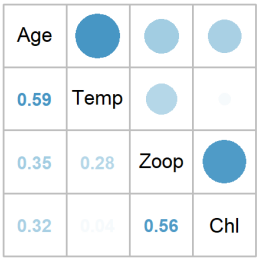

(b) Subset of correlation coefficients for all sites

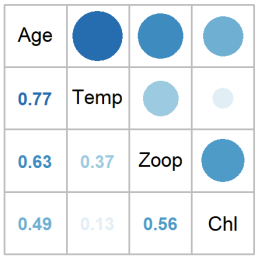

(c) Subset of correlation coefficients for all sites except ISEA and ISTO (Figure 3.2)

Figure 3.11: Spearman rank correlation coefficient matrices for modeled water age (Age), observed water temperature (Temp), zooplankton abundance (Zoop), chlorophyll a (Chl), blue-green algae (BGA), electrical conductivity (EC), specific conductance (SPC), salinity (Sal), total dissolved solids (TDS), turbidity (Turb), dissolved oxygen percentage (DO%), dissolved oxygen in milligrams (DO), and pH (pH). Positive correlations are shown in blue, negative correlations are shown in red. The upper triangle of the plots shows both color and size of circle to indicate correlation value, and the bottom triangle of the plots shows the numeric value with a color scale added.

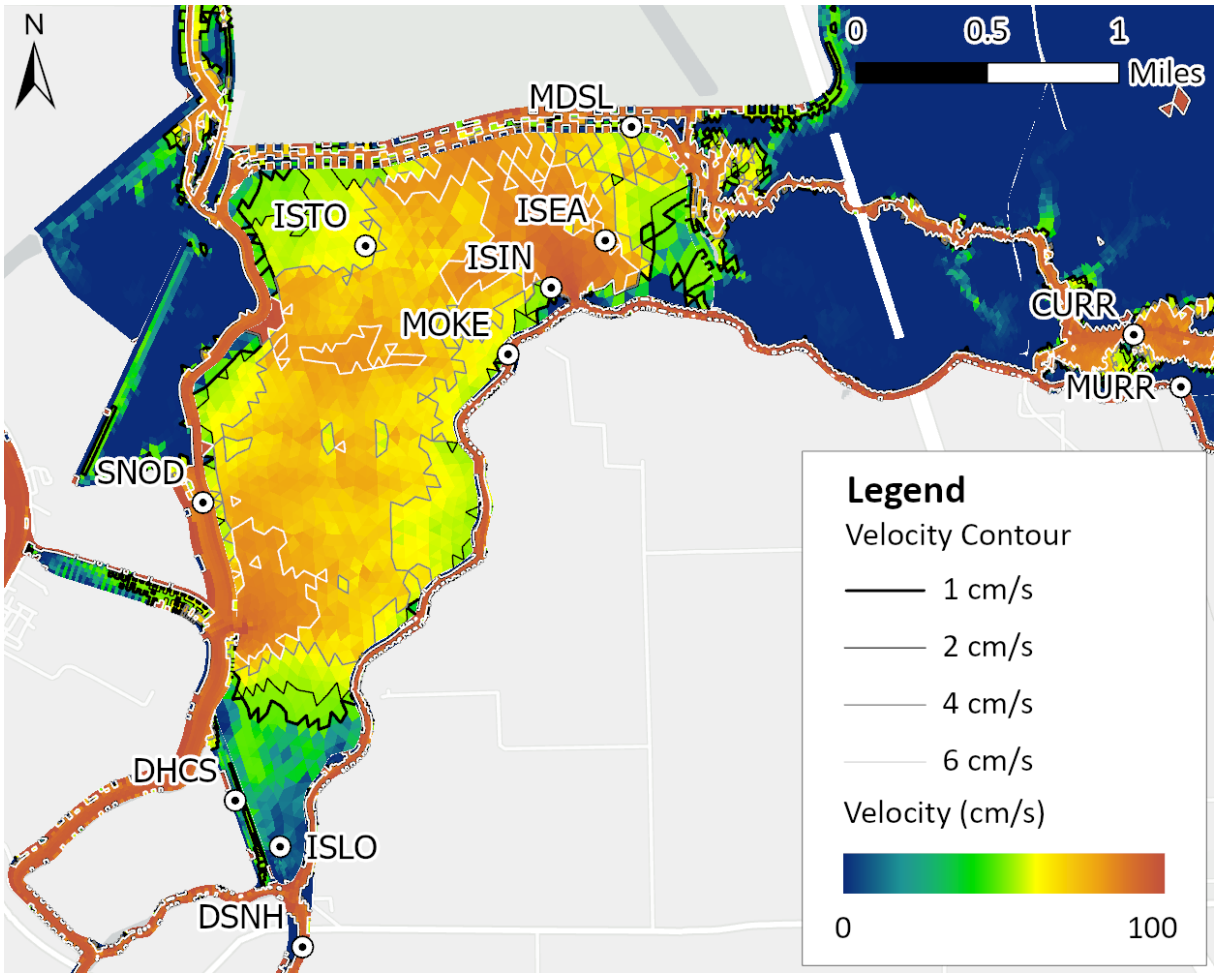

Figure 3.12: Modeled depth-averaged water velocity distribution on May 12, 2017.

The second major factor that affected the mixing patterns specific to the ISEA and ISTO sites was the bathymetry used for the MWT inlet breach (Figure 3.1). The exact bathymetry of the breaches into and out of the MWT is unknown as no survey on the breaches were performed while the Tract was open from the accidental breach. In addition to wind, the shape of the breach affects the specific nature of the incoming freshwater plume in the Tract. The direction and intensity of the plume affects the orientation and strength of the eddies that form in response to the incoming water. Those eddies recirculate water and allow water to accumulate age in them, and they form mixing lines between the younger colder plume and the older warmer eddy water. Therefore, better replicating the intensity and direction of the plume by accurately depicting the breach geometry would allow for increased accuracy in generating the spatial water age patterns observed in the field, and better capturing the observed mixing line. Because

this geometry was estimated, the modeled age distribution within the Tract could be suffering additional inaccuracies, and in turn affecting the experiments zooplankton-age relationship.

These potential shortcomings in the modeling of age could shed light on the limitations of Chapter 2. In Figure 2.8 it's clear that aside from the initial breach, the fraction of Cosumnes and Other water is relatively constant as compared to other sites. This is likely due to the fact that the Cosumnes and Mokelumne source waters were completely mixed past the confluence by the time the river entered the Tract and then that water has limited influence over the source water fraction (SWF) for the Tract sites. These dynamics lead the SWF to be more easily replicated than the complicated dynamics of water age within the Tract. With water age you see strong gradients in the Tract that do not appear when modeling SWF dynamics.

3.6 Conclusions

For a test of correlation between the two variables zooplankton abundance and modeled water age, this study did not find a strong significant correlation when evaluating all of the collected field data against the modeled data. However upon further inspection into the shortcomings of the modeled data, there was reason to believe that the modeled age of two of the sites was not reliable and consequently the exclusion of those sites made the correlation coefficient nearly double. This strengthened correlation is more in keeping with what the study expected to find.

As previously mentioned, the strength of the correlation found in the experiment could be affected by the actual relationship between zooplankton and age, the quality of the zooplankton data collected, or the ability of the model to replicate age mixing dynamics in the study system. Although the study found a moderate and significant correlation between zooplankton abundance and water age when excluding the ISEA and ISTO sites, the study finds a few areas of improvement in study design which would better test the relationship.

Were this study to be repeated on a natural floodplain system elsewhere, much more detailed data on the inflow geometry as well as appropriate wind proxies would be needed in order to better replicate the water age mixing patterns in the shallow water environment. Moreover, in

order to properly resolve the spatio-temporal scales of zooplankton fluctuations it would behoove future authors to sample the biological data more frequently and at varying depths to be able to discuss the behavioral dynamics of the taxa in the system. There is also a chance that biomass across taxa would be a better quantification metric than abundance since the impetus behind exploring this relationship is to test if longer residence time systems are more energetically productive systems than ones with smaller transport time scales, and more biomass means more available grazing supply to the next trophic level. With those warnings to heed when repeating an experiment like this on a natural system, there is reason to believe that the resultant relationship would be more strongly positive.

Alternatively to a study in a natural system, if one could repeat a similar study with a system that has discrete shallow water environments, such as flooded fields, that are allowed different flushing times perhaps the modeled age would more closely follow the zooplankton abundance within each discrete environment. It is the authors belief that a study that directly evaluates the relationship between zooplankton and water age by controlling random variables could more clearly test the relationship as well as investigate any other compounding variables that may contribute to the availability of zooplankton. For now, under this study as it stands, the zooplankton abundance versus modeled water age relationship holds as positively correlated with moderate strength.

Chapter 4

Hydrodynamic modeling for river restoration: The case of the Yolo Bypass

Abstract: In order to provide a tool for stakeholders to understand the effects of pending restoration, a hydrodynamic model was developed of the Yolo Bypass, a flood control feature of the Sacramento Valley that allows high winter flow events floodplain access to protect neighboring cities. The model was developed in response to one specific restoration alternative, but was intended to be used as a free publicly available tool for anyone interested to use. This chapter intends to walk through the development process of the model as well as outline some proposed applications of the model in order to better understand the utility of a tool like this.

Keywords— Yolo Bypass, hydrodynamic modeling, floodplains

4.1 Introduction

Through the years, both uninhabited and settled, the Sacramento Valley has taken many forms. Previous to settlement, it was at the mercy of the Sacramento and Feather River's whims. Naturally formed levees would collapse catastrophically as the persistent rivers would convulse and inundate the valley floor [111]. These avulsions would provide a huge boost in primary productivity for native fish both coming and going from their natal spawning grounds by connecting floodplains to the main stem of the River [7], [112]. Since early western settlers began to colonize

the area, engineering efforts were made to tame the Sacramento River via levees and dykes, but these efforts were in vain [28]. The Sacramento River watershed would overwhelm the fortified channel and inundate California's capital, Sacramento. The Yolo Bypass, established after the 1917 Congressional approval of the Sacramento River Flood Control Project [113], allowed the Sacramento River waters to mimic their pre-establishment behavior by taking advantage of the topography of the Yolo flood basin west of Sacramento, allowing floodwaters to naturally divert the main channel and fill the flood basin, which then rejoins the main channel downstream of vulnerable developed areas (Figure 4.1). The Bypass both diverts the flow from populated areas and attenuates flows so the downstream-most flow rates are within the capacity of the channel it rejoins. As floodwaters attenuate in the Bypass, water quality conditions become prime for algal productivity [7], and migrating fish can take advantage of the trophic effects of this boost in primary productivity [89], [114].

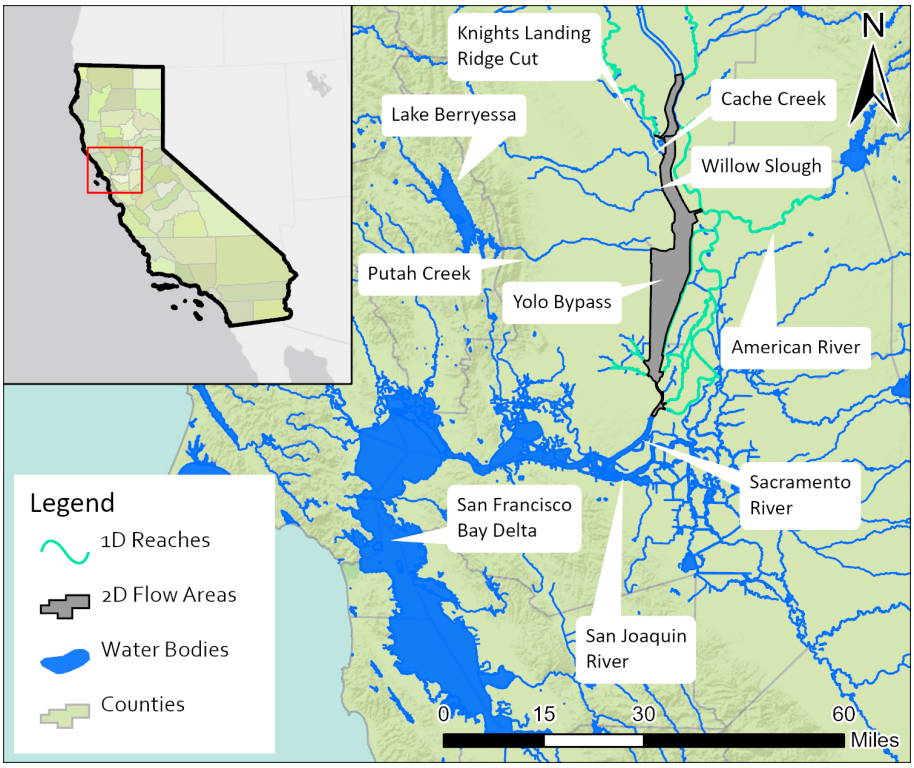

Figure 4.1: The geographic setting of the Yolo Bypass with the project's model domain.

In designing the Bypass, engineers lowered a one-mile stretch of the southern bank of the Sacramento River near Woodland and constructed the Fremont Weir in 1924 [113]. The de-

cision of what height the weir should be was made based off of the stage of the Sacramento River at a 20% return frequency, 33.5 ft allowing Sacramento River access to the Bypass only when a storm of that magnitude occurred. The design capacity of the Bypass and its flood control structures is intended to convey up to 80% of the flood system's flows. Although the biota in the Yolo Bypass fortuitously benefited from this intermittent re-connection of floodplain, the design was primarily to reduce flood risk for cities in the Sacramento Valley and not to mitigate the drastic reduction in shallow-water habitat undergone as colonizers settled in the Sacramento-San Joaquin Delta (Delta) [13]. Given the disparity in attention given to human benefit versus ecological benefit, it's unsurprising that in recent years more and more efforts have targeted improving habitat in the Yolo Bypass and understanding its potential [5], [53], [84], [112], [115]–[117].

California EcoRestore is an inter-agency initiative that has focused on restoration efforts in the Central Valley and particularly in the Delta (Figure 1.2). California's Department of Water Resources (DWR) is the lead on the EcoRestore initiative that began in 2015, and one particular area of interest was the Yolo Bypass and the Fremont Weir. The efforts focused on the Yolo Bypass necessitated quantitative analysis via a hydrodynamic model, which was developed using proprietary software, TUFLOW. The TUFLOW model was then used to develop an environmental impact report (EIR) for the proposed adult fish passage structure (AFP) improvements in the Fremont Weir. Much of the Yolo Bypass agricultural land is within Yolo County, and so the County wanted to provide a publicly available version of the TUFLOW model. This public model would be developed with the United States Army Corps of Engineers' (USACE) Hydrologic Engineering Centers River Analysis System (HEC-RAS) software and made available to whomever wanted to analyze alternatives on the Bypass. This study was in direct response to that need and developed a fully free model for the public. The model built off previous studies (Table 4.1) by implementing calculated hydrologic inputs as well as implementing surveyed data to inform the models geometry.

Table 4.1: Models developed in prior hydraulic studies focused on the Yolo Bypass

Dimension	Software	Description	Sponsor	Year
1-D	HEC-1 and HEC-2	Willow Slough, Dry Slough, Covell Drain & Yolo County Flood Control	Water Conservation District	1992
1-D	UNET	Steady state, 1-D model for the Upper and Lower Sacramento Valley	USACE	1995
1-D	HEC-2	Putah Creek	USACE	1995
1-D	HEC-2	Cache Creek	USACE	1995
2-D	RMA2	2-D hydrodynamic model for the Yolo Bypass. Steady state. Designed for high flow scenarios.	USACE	1995 - 2007(Updated)
1-D	HEC-RAS	Updated model for the Sacramento River.	USACE	2006
2-D	MIKE 21	2-D unsteady flow model for the Yolo Bypass. Boundary conditions for western tributaries based on estimates.	MWD, DWR, cbec eco-engineering	2007
1-D/2-D	HEC-RAS	Coarse-level HEC-RAS model of the Yolo Bypass from Fremont Weir to Liberty Island	CWS	2007
1-D/2-D	HEC-RAS 4.2	As part of the CVFED effort, an unsteady model was developed for the entire Sacramento Valley using the UNET model as the basis.	DWR	2010
2-D	RMA2	2-D unsteady flow model developed to examine low flow field-scale drainage	UC Davis	2012
1-D/2-D	TUFLOW	TUFLOW is a 1-D/2-D flood modeling software it was used to develop flooding extents in Cache Creek, Willow Slough and Putah Creek. Breach hydrographs from the HEC-RAS model were used as inputs.	Yolo County	2012
1-D/2-D	HEC-RAS 4.2	Coupled 1-D/2D for the Yolo Bypass.	UC Davis	2012/2013
1-D/2-D	HEC-RAS 5.0	Coupled 1-D/2D for the Yolo Bypass and part of the Sutter Bypass south of Tisdale Weir.	CWS	2013-2015

This chapter outlines the development of this publicly available useful tool and applies a simple environmental analysis to demonstrate the utility of the model in predicting outcomes. This study tests the use of a habitat suitability index (HSI) approach of estimating habitat quality for different species. Use of a habitat quantification metric has evolved from the Instream Flow Incremental Methodology (IFIM) approach of Bovee 1986 [118] to examine species-specific habitat requirements and preference. The approach looks at physical parameters and applies how well suited a particular species or taxa is to a range of values for each parameter to a set of curves. The curves are then used to interpolate the habitat quality of a physical system using

those physical parameters. In an aquatic environment those parameters are quite often depth- and velocity-centric [18]. There have been a range of applications in which a hydrodynamic model is used to evaluate habitat modifications and improvements or evaluate the suitability of a riverine system to specific taxa [18], [65], [119], [120]. These applications take the hydraulic output of a numerical model - such as depth, velocity, and inundation frequency - and can integrate with other observational data - such as substrate makeup or riparian coverage - to evaluate against known biological and physiological constraints of a species or set of species. This study demonstrates the utility of the calibrated and validated hydrodynamic model by applying an HSI technique on a dry year simulation and evaluating the inclusion of a fish passage structure in the Fremont Weir which was constructed in 2018 [121].

Although the Yolo Bypass was constructed to protect humanity from flood, and although this model was developed in order to benefit people who own land in the Bypass, focus can be shifted both in the use of this model and the use of the Bypass towards improvements of ecological habitat and this model provides a tool for that shift.

4.2 Methods and Materials

In order to provide all landowners, stakeholders, flood management, and environmental interests with a free and publicly available resource to evaluate the results of modifications to flows and structures within the Yolo Bypass, a hydrodynamic model was developed and calibrated. The primary impetus was to evaluate proposed modifications to the Fremont Weir, but the model serves other purposes in the Yolo Bypass hydroscape and that is further discussed in the Conclusion.

The hydrodynamic model was developed by a team at the University of California Davis' Center for Watershed Sciences and was built to mimic the domain and scope of a privately owned model developed with a proprietary model developed by a local consulting firm, cbec, for the California Department of Water Resources (DWR) (Table 4.1).

4.2.1 DWR and cbec: TUFLOW Model

Under a contract with DWR, cbec developed a hydrodynamic model of the region using TUFLOW, a proprietary software. The primary upstream extents of the model are the Sacramento River just below Tisdale Weir, the Sutter Bypass at the point where the Feather River overbanks meet it, the Feather River just downstream of the confluence of the Yuba River, and the American River just below Lake Natomas. The downstream extent is the Sacramento River at Rio Vista, with short representations of Georgiana Slough and the Delta Cross Channel (Figure 4.2).

At the time of development, the TUFLOW model had the capability of one- and two-dimensional coupling, structure representation in both 1D and 2D, and producing a full suite of hydrodynamic outputs. More recently, several advances have been made in TUFLOWs modeling capabilities, but at the time of the development of the publicly available model there were limitations.

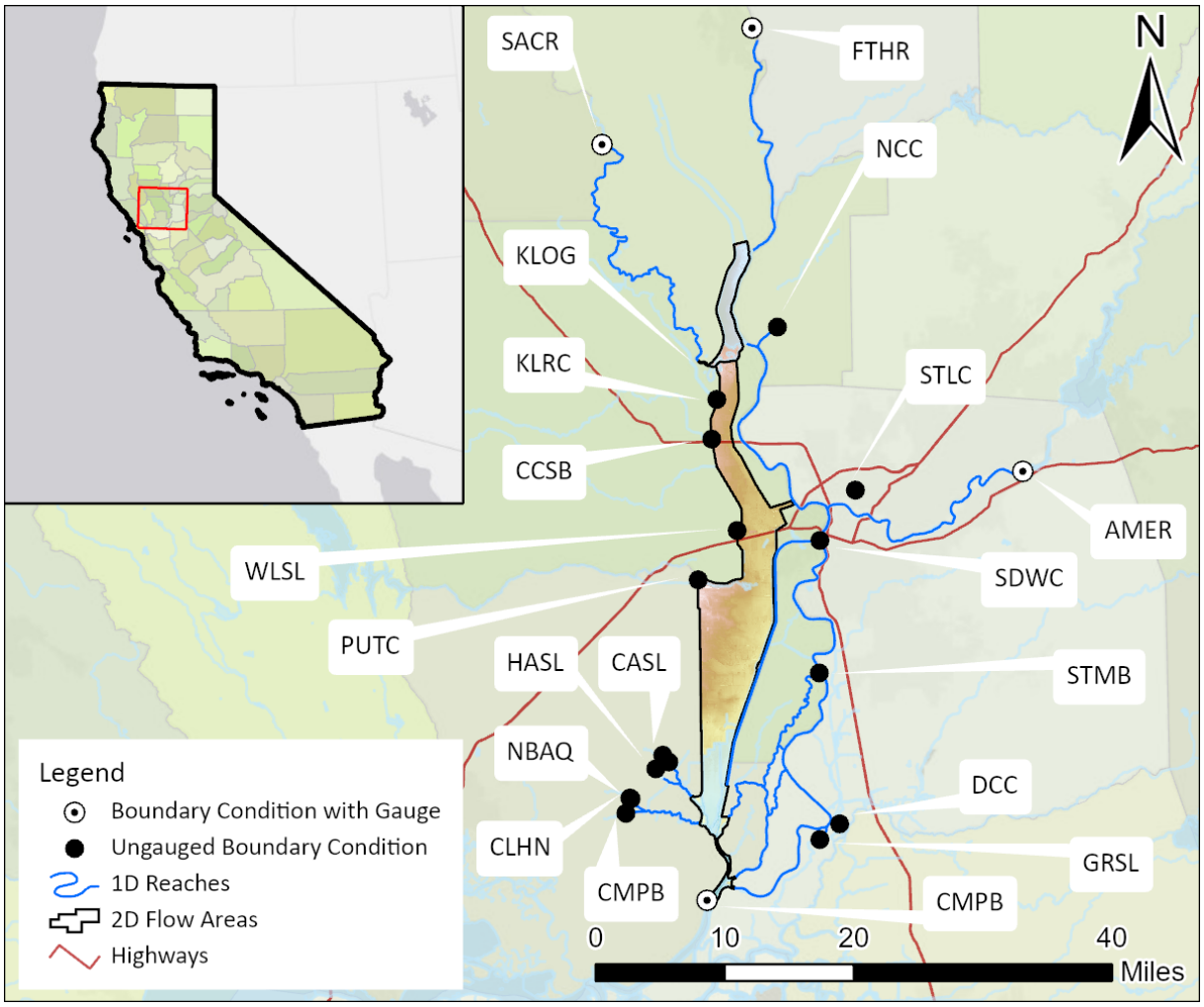

Figure 4.2: The domain of the CWS HEC-RAS model as well as the model boundary condition locations. Ungaged boundaries shown as filled black dots and gaged boundaries as white bulls-eyes.

4.2.2 CWS and HEC-RAS: Free Software as Tool for Public Use

The model used in this paper was created using River Analysis Systems (RAS) software developed by the United States Army Corps of Engineering's Hydrologic Engineering Center (HEC). The model domain is the same as the cbec TUFLOW model and uses the same flow data but uses terrain and land use data compiled by the Center for Watershed Sciences (CWS).

The model runs with both one- and two-dimensions simultaneously while incorporating a sub-grid bathymetry in the 2D regions. Sub-grid bathymetry is now available in TUFLOW, but at the time of the model development this was an advantage of RAS over TUFLOW. The 2D grid is unstructured and orthogonal and can align cell faces to specified 'breaklines' in order

to account for physical barriers or refined mesh regions. The model also allows for a spatially variable roughness representation corresponding to terrain type in the 2D mesh. HEC-RAS uses a semi-implicit, semi-Lagrangian Finite Volume scheme and solves full 2D shallow water equations (Equations 4.1-4.3).

$$\frac{\partial H}{\partial t} + \frac{\partial (hu)}{\partial x} + \frac{\partial (hv)}{\partial y} + q = 0 \tag{4.1}$$

$$\frac{\partial u}{\partial t} + u\frac{\partial u}{\partial x} + v\frac{\partial u}{\partial y} = -g\frac{\partial H}{\partial x} + \nu_t \left(\frac{\partial^2 u}{\partial x^2} + \frac{\partial^2 u}{\partial y^2} \right) - c_f u + fv \tag{4.2}$$

$$\frac{\partial v}{\partial t} + u\frac{\partial v}{\partial x} + v\frac{\partial v}{\partial y} = -g\frac{\partial H}{\partial y} + \nu_t \left(\frac{\partial^2 v}{\partial x^2} + \frac{\partial^2 v}{\partial y^2} \right) - c_f v + fu \tag{4.3}$$

where H is the water surface, h is the depth of water, u and v are velocities in the x- and y-direction, respectively, g is the gravitational term, ν_t is the horizontal eddy viscosity, c_f is the friction term, and f is the Coriolis factor.

4.2.3 Data Sources

Data for terrain, land use, and hydrologic inputs were gathered from multiple agencies in order to supplement the model inputs and create a more detailed simulation of the Bypass. These data were to upgrade the existing TUFLOW model as well as to adapt to the needs of the HEC-RAS platform.

4.2.3.1 Terrain

The terrain was compiled using multiple data sources in an effort by Andy Bell of CWS in 2010. Additional bathymetric surveys were taken by Thomas Handley of CWS in order to supplement missing or coarse bathymetry that had previously been represented in 1D reaches of the TUFLOW model. The terrain was then stitched together in ArcMap in order to create a singular continuous digital elevation model (DEM) to be applied to the HEC-RAS 2D areas (Figure 4.3).

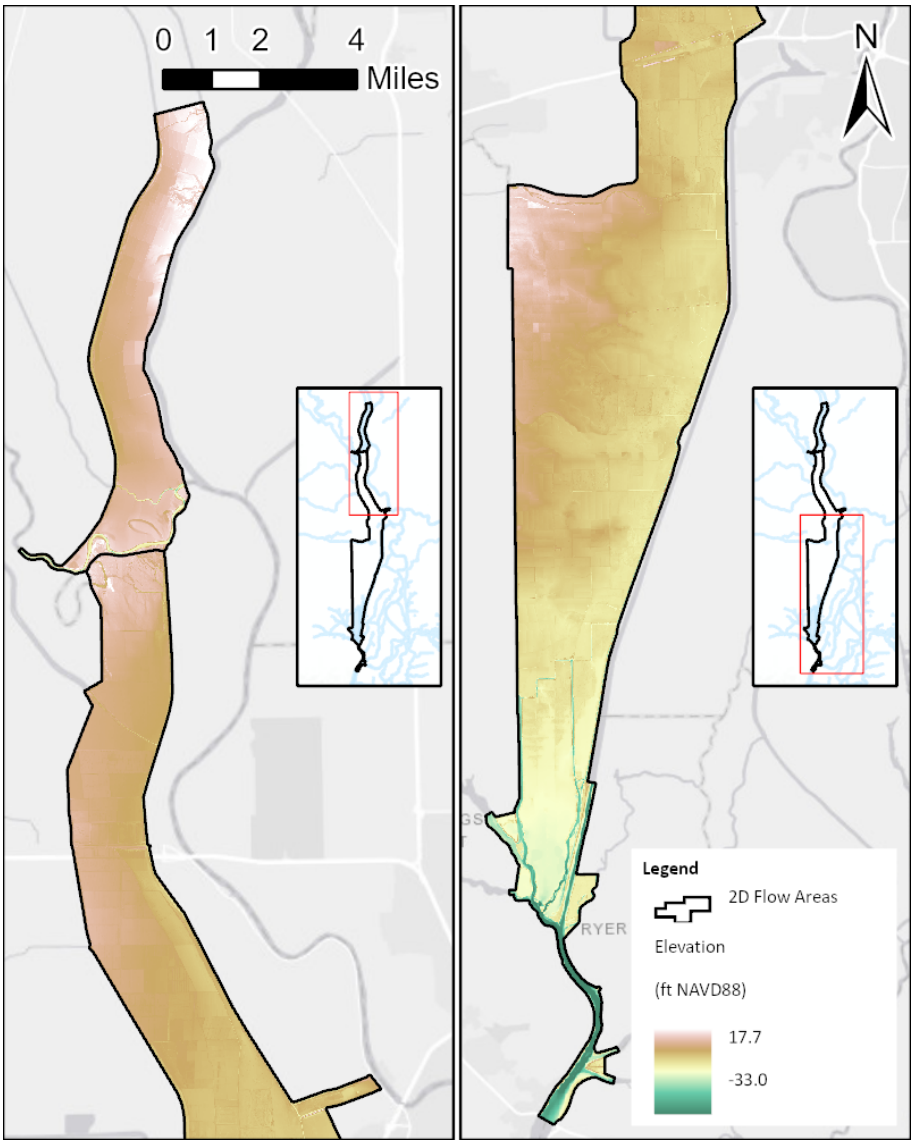

Figure 4.3: Digital elevation model (DEM) of the study area with an outline of the 2D model domain that uses the DEM for numerical computations.

4.2.3.2 Land Use/ Roughness

The spatially variable roughness mentioned in 4.2.2 was prescribed using land use classifications. The spatial classifications were taken from DWR land use surveys in Yolo, Sutter, Sacramento, and Solano Counties in 2008, 2004, 2000, and 2003, respectively. The classifications were then converted to roughness values (Figure 4.4) using a previous study in the same area, which outlined Manning's n values as they correspond to land use type such as walnut grove, tomato crop, etc [122]. The values range from 0.03 for smooth-bottomed channels and marshes and up to 0.082 for orchards and dense riparian canopy. The values were initially assigned based on the

DWR land use surveys and then was used as a calibration parameter in regions where the model results were inconsistent with the observed stage and flow values.

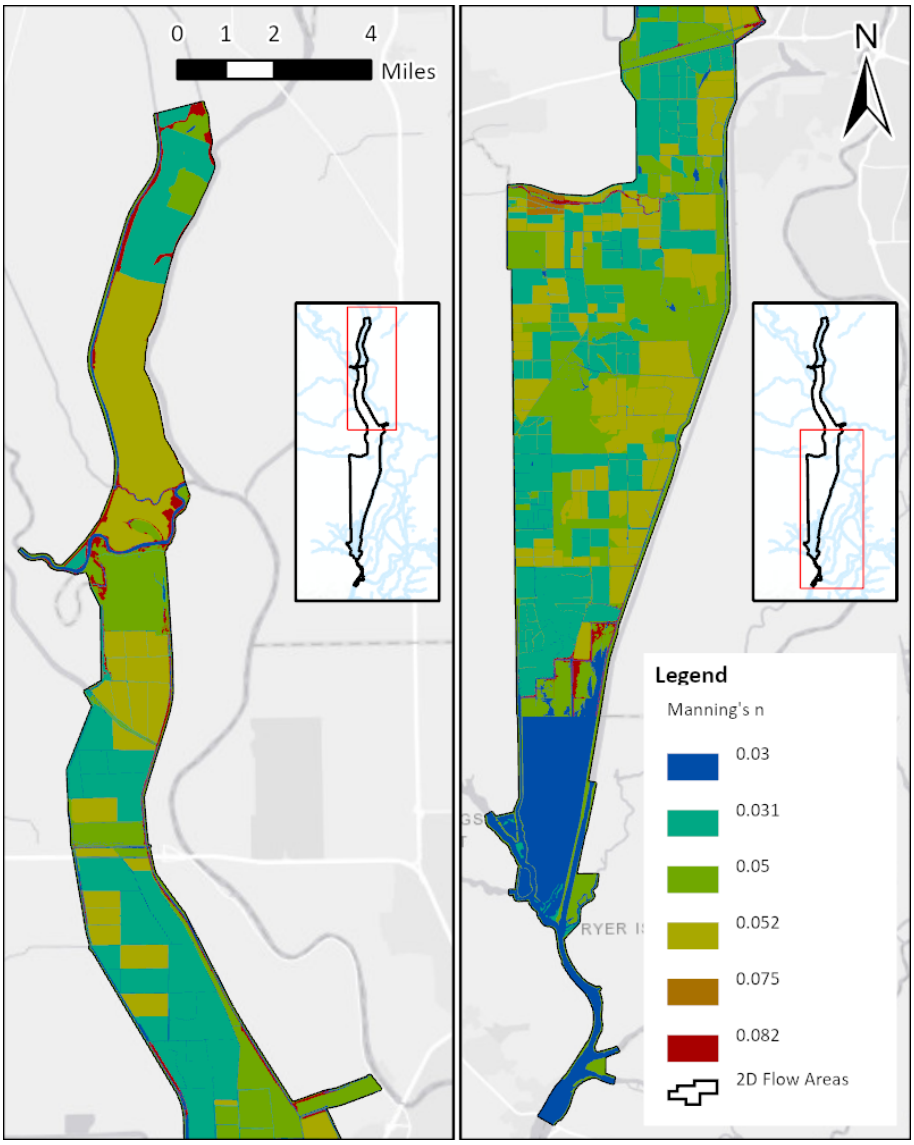

Figure 4.4: Spatially variable Manning's n values with an outline of the 2D model domain that uses these values for computations.

4.2.3.3 Hydrologic Inputs

Both flow and stage information are applied to the model boundaries in order to initiate and replicate a flood event (Figure 4.2). These data were acquired from cbec's delivery of the TUFLOW model inputs and were either taken directly from gaged data or estimated from neighboring gages (Table 4.2).

Table 4.2: Boundary conditions for the HEC-RAS Yolo Bypass model with Map IDs corresponding to Figure 4.2

Map ID	Boundary Condition	Source	Data Type
SACR	Sacramento River flow below Wilkins Slough	USGS 11390500	Gaged flow
KLOG	Knights Landing Outfall Gates Inflow	DWR A02945	Gaged flow
FTHR	Feather River and Sutter Bypass Flows	Based on USGS 11390500, 1142500; DWR A02930, A02945; Arcade Creek EMC02 gages	Calculated
NCC	Natomas Cross Canal Flow	Based on Arcade Creek EMC02 gage	Calculated
KLRC	Knights Landing Ridge Cut Flow	DWR A02930	Gaged and calculated from A02976, A02945, A02930 gages
CCSB	Cache Creek Settling Basin Inflow	USGS 11452500	Gaged flow
WLSL	Willow Slough Bypass Flow	Yolo Bypass Management Study	Calculated
PUTC	Putah Creek Flow	Yolo Bypass Management Study	Calculated
AMER	American River Flow	USGS 11446500	Gaged flow
STLC	Steelhead Creek Flow (Natomas East Main Drainage Canal)	Based on Arcade Creek EMC02 gage	Calculated
DCC/GRSL	Delta Cross Channel & Georgiana Slough flows	DWRs Dayflow program	From gages and estimates
NBAQ	North Bay Aqueduct	DWRs Dayflow program	From gages and estimates
RIOV	Rio Vista tidal stage	DWR B91212	Gaged stage
HASL	Hass Slough	cbec Study	Estimated flow
CLHN	Calhoun Cut	cbec Study	Estimated flow
CASL	Cache Slough	cbec Study	Estimated flow
CMPB	Campbell Lake	cbec Study	Estimated flow

4.2.4 Calibration Data

In order to test the model performance in simulating flood events, gages within the model domain were used to compare the observed stage or discharge versus the model output (Figure 4.5.

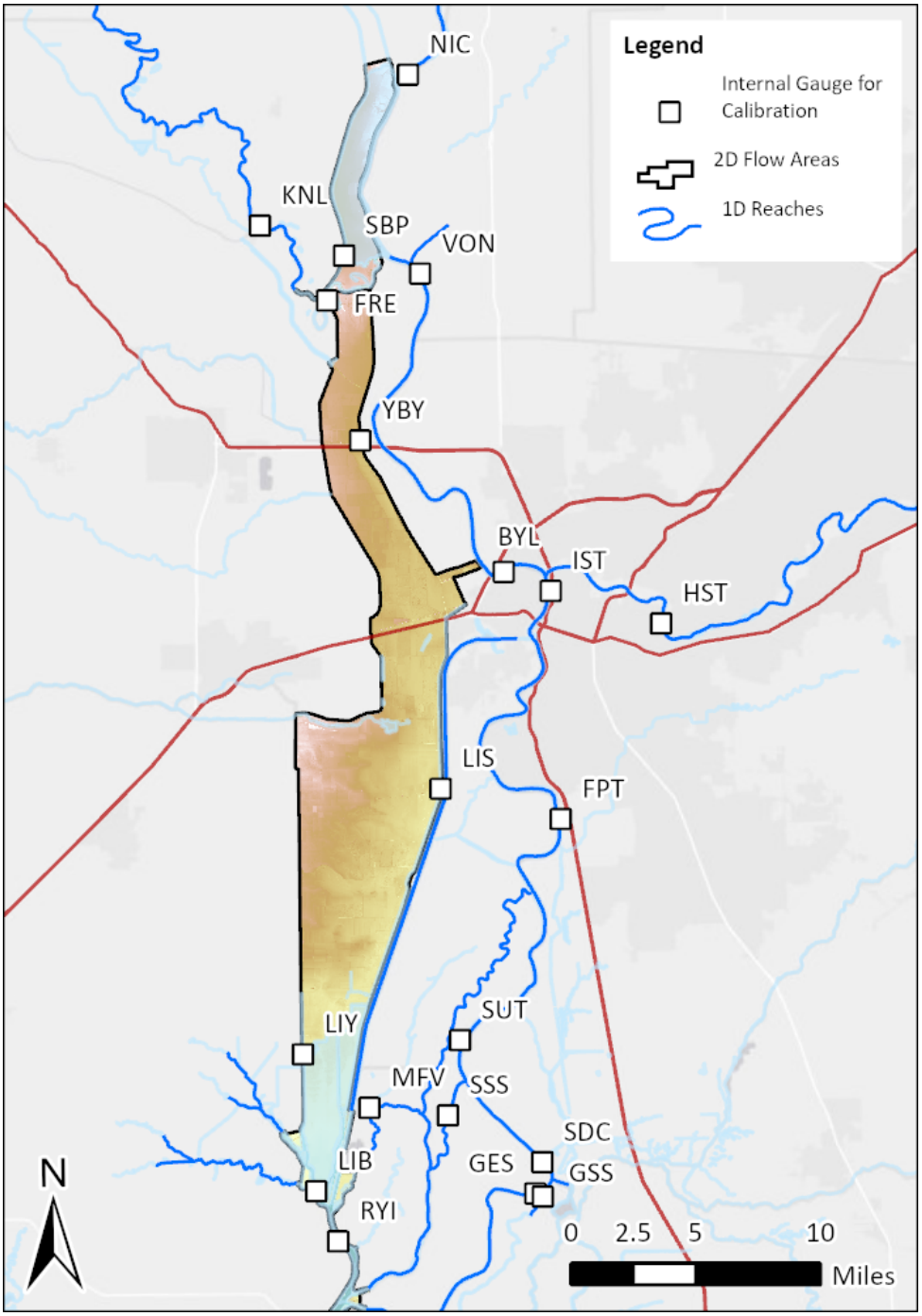

Figure 4.5: Calibration points for the model.

4.2.5 Application of Habitat Quality Quantification

This study uses the habitat suitability index (HSI) technique for quantifying habitat quality. The approach originates from the Instream Flow Incremental Methodology (IFIM) approach of Bovee 1986 [118] and has been simplified for this Chapter. This study's application uses only three parameters (depth, velocity, and timing) to describe habitat quality and many more can be implemented in order to create a robust analysis for a single species or multiple species [18], [123]. In an HSI analysis, curves are developed which describe the suitability on a scale from zero to one for a range of parameter values (Figure 4.6). Those curves are then applied to measured or observed parameters to determine the HSI for any particular region. In hydrodynamic modeling, the regions are often the computational cells and are used as such in this analysis. After determining the spatial distribution of HSI for one parameter one uses the combined suitability index values in order to determine the overall suitability index, and in this study that would be the HSI determined from the depth, velocity, and timing of the modeled inundation for any given time-step (Equation 4.4).

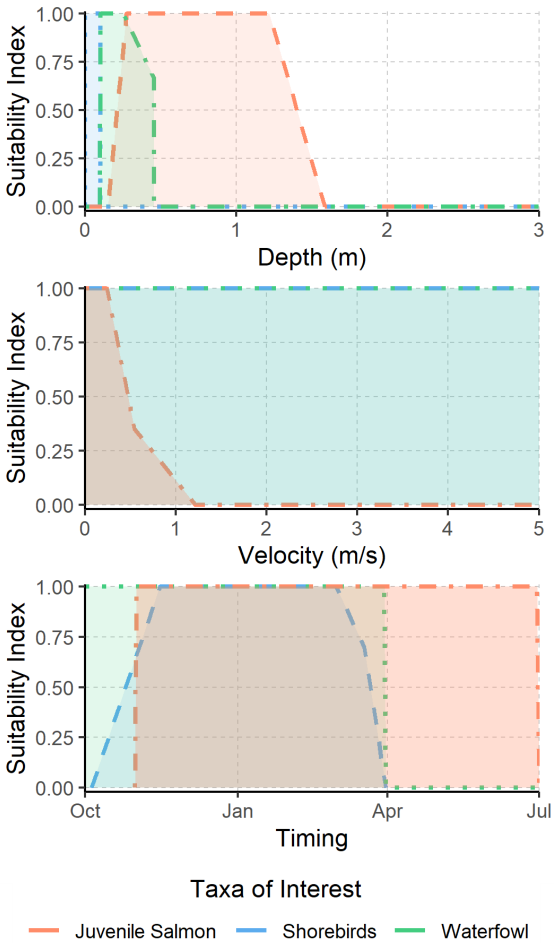

Figure 4.6: Habitat suitability curves developed for juvenile rearing salmon, shorebirds, and waterfowl for the Central Valley, adapted from cbec. X-axes show the parameters (depth, velocity, and timing), and y-axes show the suitability index for each value.

$$HSI_{overall} = HSI_{depth} \cdot HSI_{velocity} \cdot HSI_{timing} \tag{4.4}$$

This HSI analysis was performed on three taxa: juvenile rearing salmon, shorebirds, and waterfowl. As seen in Figure 4.6, juvenile rearing salmon prefer inundated terrain up to 1.2 m that is slow moving and will benefit from inundation most in the November to July time window. Because the rearing salmon is quite small, it requires refugia found in plants and natural debris

found in shallow water [124], and since they can't swim especially fast [125], they benefit from slower moving water so that they can choose their location. The timing window set for juvenile rearing salmon is in keeping with the timing of the major runs of salmon (winter-, fall-, and spring-run). These criteria are in contrast with shorebirds, which benefit from marsh-like conditions for foraging, meaning depths above 10 cm are unsuitable, and velocities are less impactful on shorebirds since depths below 10 cm often corresponds to the wetted fringe of an inundated footprint. For the Central Valley, shorebird populations are typically present in the October to April time frame [126]. Finally, waterfowl enjoy water deep enough to dabble in, which means depths above 10 cm, with peak preference between 10 and 25 cm and suitable up to 46 cm of depth [127], with little effect of velocities in that depth range, and a preference for the winter months of October to April.

Once the overall HSI has been determined from the combined depth-, velocity-, and timing-HSIs for each time-step in a model simulation, a summary metric known as the weighted usable area (WUA) can be calculated for the entire model domain, producing a single value corresponding to the area of suitable habitat:

$$WUA = (cell\ size)_n \cdot \sum_{n=1}^{n} HSI_{overall_n} \tag{4.5}$$

where n is the cell index, and the $cell\ size_n$ is the area of cell n with HSI output, and $HSI_{overall}$ is the overall HSI for a particular taxa. The WUA value for each time-step can then be aggregated over all time in the simulation to provide a single metric for each taxa in units of area-time. Alternatively one can aggregate over time instead of space and produce a spatial summary of the HSI in the model domain for each taxa in units of time by summing all HSI values in a cell over time (HSI_{t-ag}), leaving null cells equal to zero (Equation 4.6).

$$HSI_{t-ag_{cell}} = \sum_{t} HSI_{overall_{cell,t}} \tag{4.6}$$

where $HSI_{t-ag_{cell}}$ is the time-aggregated HSI for a particular cell, t is each time step of the simulation, and $HSI_{overall_{cell,t}}$ is the HSI value for a particular cell at time t.

After the model was calibrated and validated it was used to simulate the flood pulse of 2010, a dry year, from February to the end of March. This simulation was then repeated with the

inclusion of the Fremont Weir adult fish passage (AFP) structure renovation that was constructed in 2018. The AFP structure construction widened and lowered an existing notch in the Fremont Weir in order to improve adult fish passage for up-migrating fish moving northward through the Yolo Bypass and back into the Sacramento River. Although the efficacy of the AFP structure improvements were tested for adult salmon, and this analysis evaluates possible impacts on other taxa as well as for juvenile salmon - an all together separate life history stage - in order to demonstrate the utility of evaluating for a range of biota that inhabit the region.

4.3 Model Results

4.3.1 Evaluation Criteria & Model Metrics

The model metrics used were R^2 and the Willmott Skill Index of agreement [63]. These are calculated with Equations 4.7 - 4.8.

$$R^2 = 1 - \frac{\sum_i (P_i - \bar{O})^2}{\sum_i (O_i - \bar{O})^2} \tag{4.7}$$

$$Skill = 1 - \frac{\sum_{i=1}^{n} |P_i - O_i|^2}{\sum_{i=1}^{n} \left(|P_i - \overline{O}| + |O_i - \overline{O}| \right)^2} \tag{4.8}$$

where P is the predicted or modeled result and O is the observed record, both for a point in time, i.

Throughout the calibration period of the model development, adjustments were made to the Manning's n values (Figure 4.4) both in the 1D and 2D areas of the model domain (Figure 4.2). Adjustments were made until the modeled results produced the most ideal metrics as compared to observed data (Equations 4.7 - 4.8). The values were only adjusted within the bounds of reasonable Manning's n values.

4.3.2 Calibration & Validation Results

The model stage and flow results were pulled for the three simulated floods (2006, 2009, and 2011) at the gages with available data for each period. The periods were ran to capture just the flood pulses and the flows before and after the higher flows. A few calibration plots are shown

below (Figures 4.7 - 4.8), but all of the gage results from Figure 4.5 are summarized in Table 4.3.

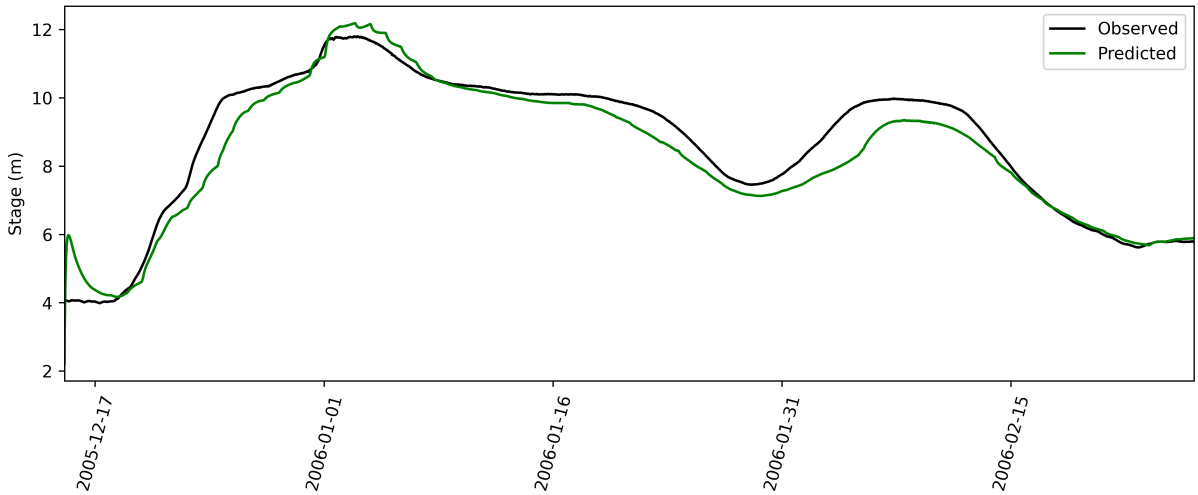

Figure 4.7: Comparison of observed (black) against modeled stage (green) at the Sacramento River at Verona (VON) Gage (Table 4.3, Figure 4.5)

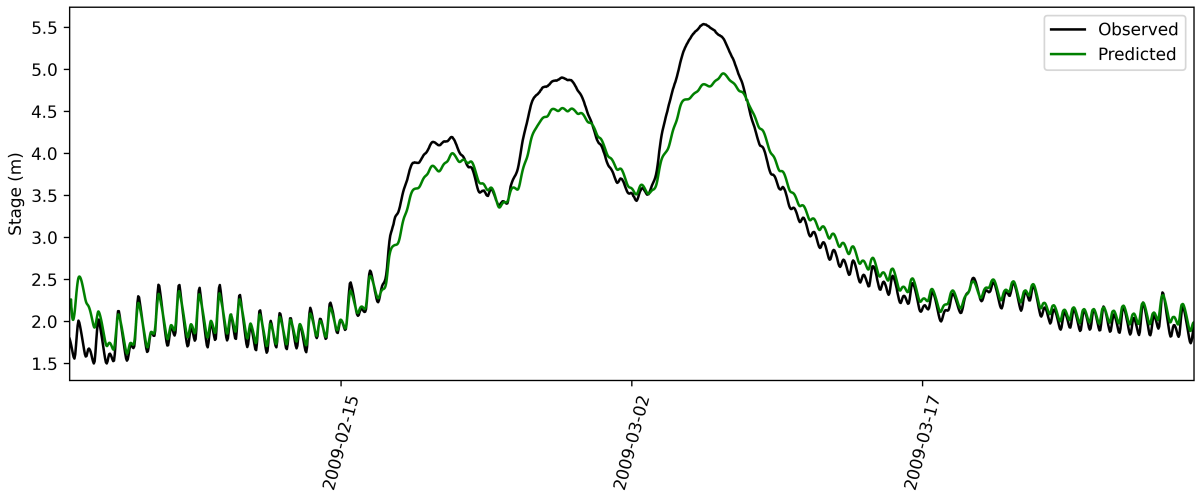

Figure 4.8: Comparison of observed (black) against modeled stage (green) at the Sacramento River at I St (IST) Gage (Table 4.3, Figure 4.5)

Table 4.3: Model calibration metrics for the gages shown in Figure 4.5.

			2006		2009		2011	
	Gage Name	**Gage ID**	**R^2**	**Skill**	**R^2**	**Skill**	**R^2**	**Skill**
Stage	Sacramento River at Fremont Weir	FRE[C]	0.98	0.91	0.98	0.97	0.97	0.97
	Sacramento River Below Georgiana Slough	GES[U]	0.76	0.85	0.97	0.98		
	Georgiana Slough at Sacramento River	GSS[U]	0.83	0.88	0.97	0.98		
	Liberty Island	LIB[U]			0.38	0.19		
	Yolo Bypass at Lisbon Weir	LIS[C]	0.60	0.46	0.94	0.87	0.96	0.97
	Liberty Island - Yolo Bypass	LIY[C]	0.89	0.94	0.98	0.99	0.99	0.98
	RD 1500 Pumping Station near Karnak	SBP[C]	0.94	0.79	0.96	0.98	0.95	0.96
	Sutter Slough at Courtland	SUT[U]	0.84	0.91	0.97	0.98		
Flow	Sacramento River Below Georgiana Slough	GES[U]	0.82	0.90	0.95	0.94		
	Sacramento River at I St	IST[C]	0.84	0.88	0.71	0.73		
	Steamboat Slough btwn Sac R and Sutter Sl	SSS[U]	0.87	0.89	0.97	0.77		

* Gage data sources are denoted as [C] - DWR, [U] - USGS

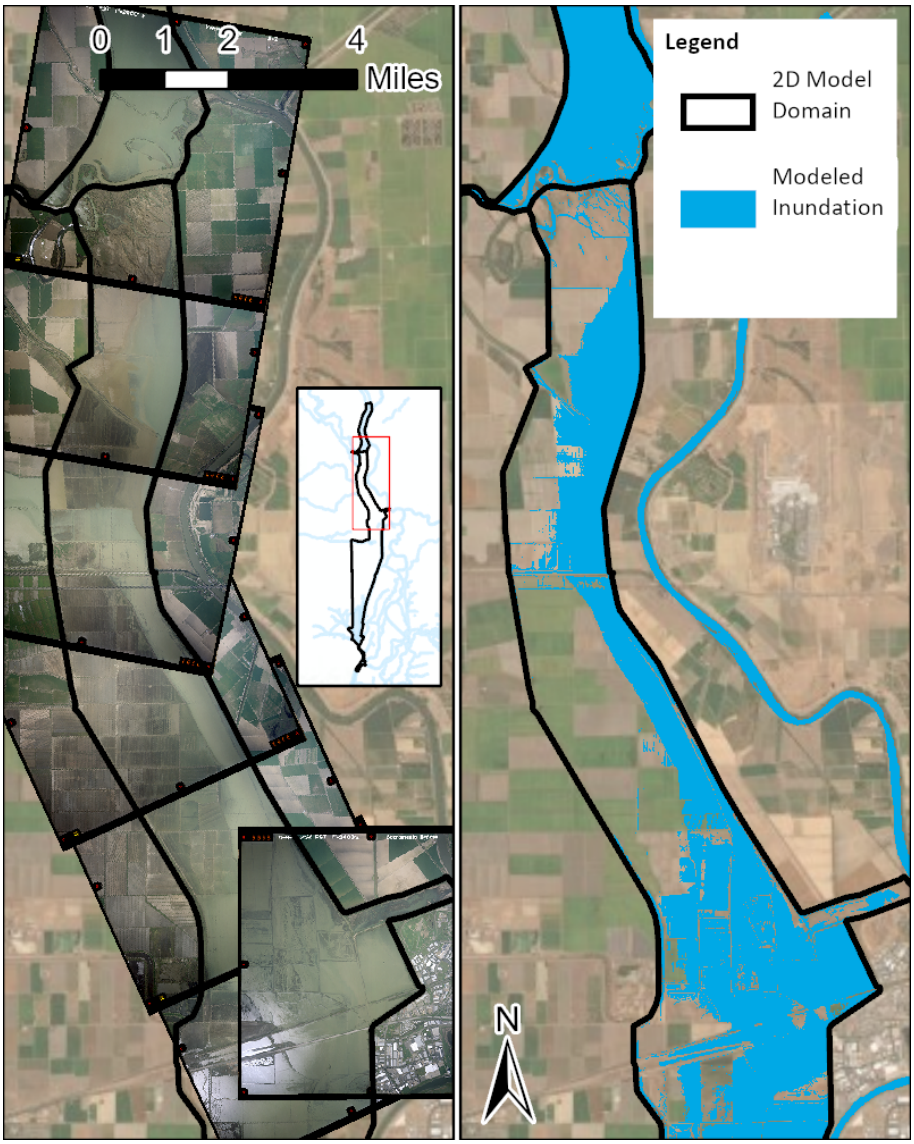

Figure 4.9: Aerial comparison of inundation extent on April 9, 2011 with aerial photos (left), and model output deeper than 0.5 ft (6 in) (right).

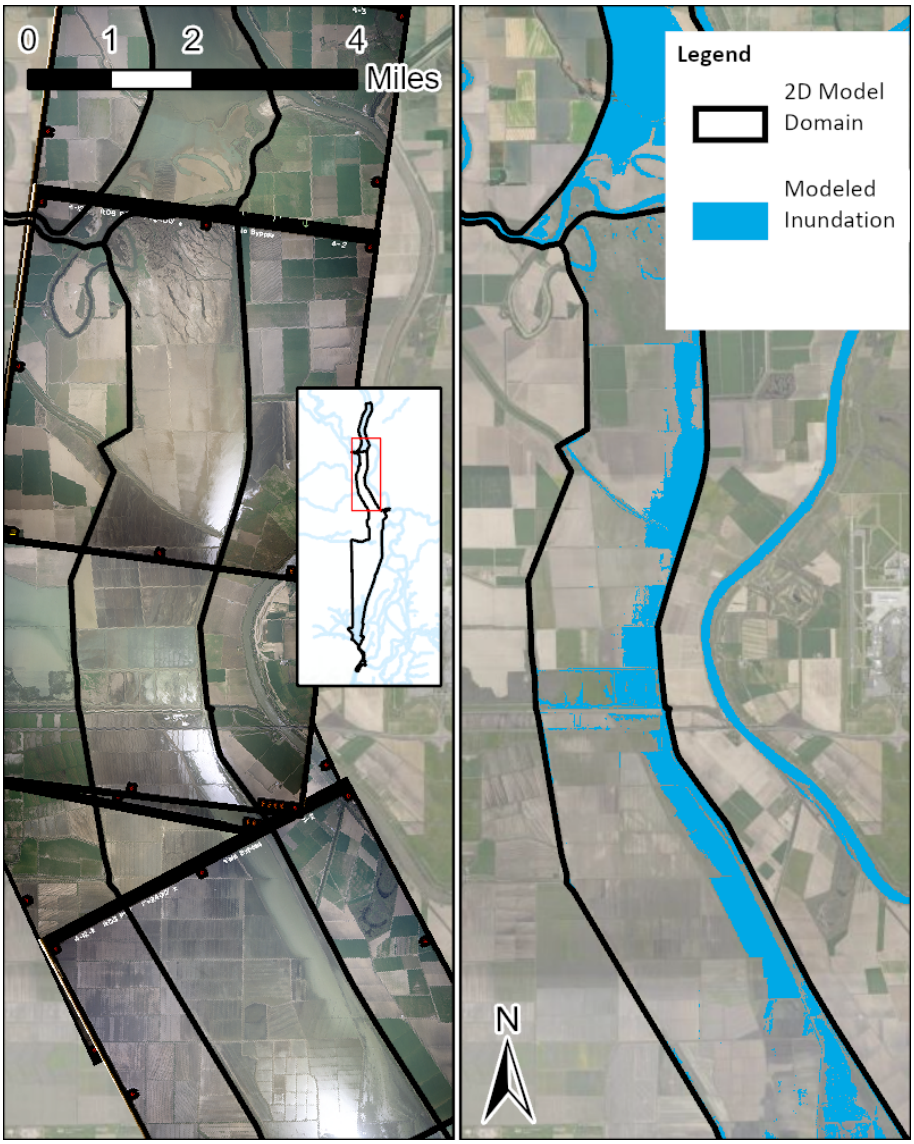

Figure 4.10: Aerial comparison of inundation extent of the Northern portion of the model extent on April 12, 2011 with aerial photos (left), and model output deeper than 0.5 ft (6 in) (right).

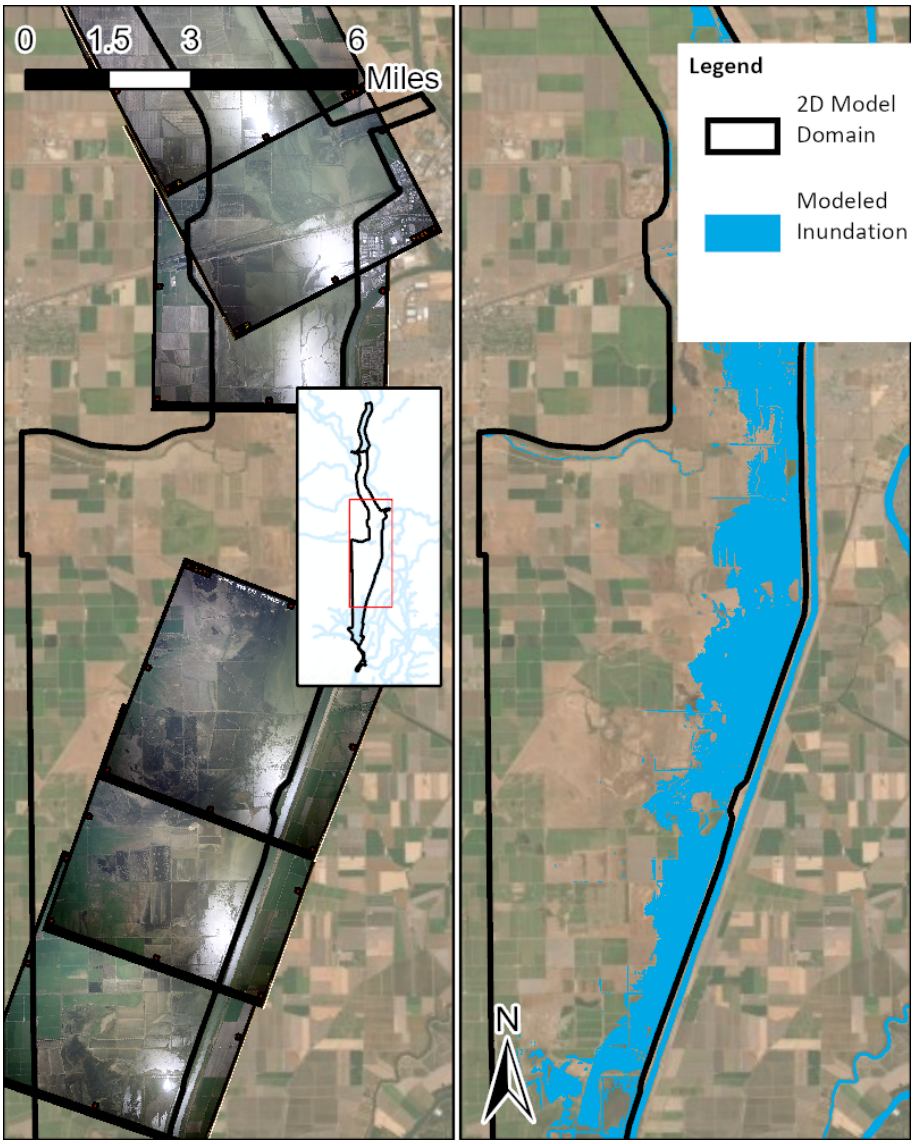

Figure 4.11: Aerial comparison of inundation extent of the Southern portion of the model extent on April 12, 2011 with aerial photos (left), and model output deeper than 0.5 ft (6 in) (right).

4.3.3 HSI Analysis

Presented here are three ways to evaluate the HSI-derived WUA for the taxa analyzed: a WUA time series comparison, a tabular analysis of WUA-days for the simulation period, and a spatial analysis of time-averaged HSI.

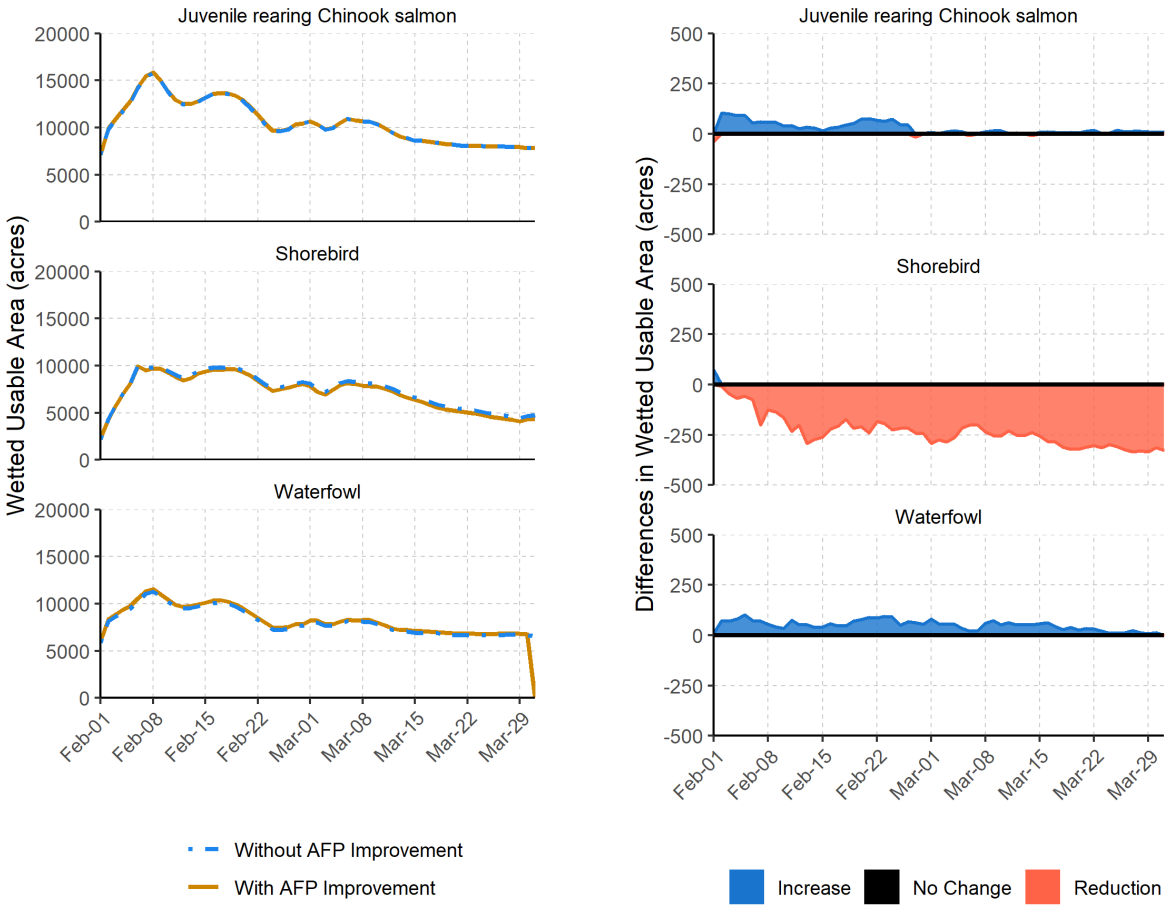

(a) WUA over time

(b) WUA difference with and without AFP construction

Figure 4.12: A time-series comparison of weighted usable area (WUA, Equation 4.5), with the left plot showing WUA over time for both with and without the adult fish passage (AFP) structure improvements, and the right plot showing difference in WUA between the with and without AFP condition

Table 4.4: The time-aggregated weighted usable area (WUA, Equation 4.5) values for the taxa analyzed with and without the inclusion of the Fremont Weir adult fish passage (AFP) structure improvements

Project condition	**Juvenile Rearing Salmon**	**Shorebirds**	**Waterfowl**
Without AFP Construction	10,200.79	7,154.96	7,854.98
With AFP Construction	10,228.57	6,924.91	7,904.46
Percent Difference	+0.27%	-3.22%	+0.63%

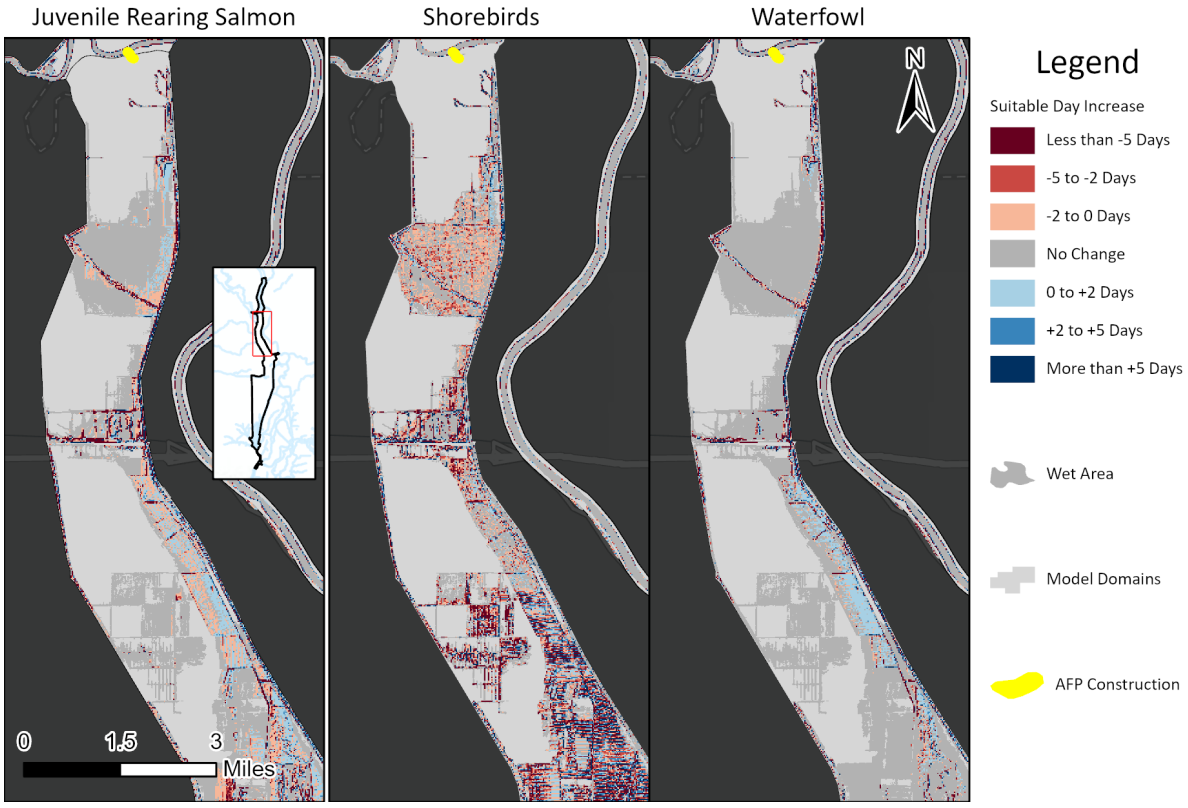

Figure 4.13: Difference maps of time-aggregatd HSI showing whether the time-aggregated HSI (units of suitable days) has improved (blue) or degraded (red) with the inclusion of the Fremont Weir adult fish passage (AFP) structure improvements. Each map pane corresponds to a different taxa being analyzed

As evidenced in Figures 4.12 and 4.13 and Table 4.4, the inclusion of the AFP structure improvements in the model did not have significant impacts on the habitat quality for juvenile rearing salmon, shorebirds, or waterfowl. Upon analyzing the HSI maps for individual time-steps

and parameters, the shorebirds experienced the modest decrease in suitability largely because depths exceeded the 10 cm threshold set in the HSI curves (Figure 4.6). Juvenile rearing salmon experienced modest increases in habitat quality due to the Sutter Bypass which is North and upstream of the Fremont Weir having slightly lower inundation depths and velocities along with the Yolo Bypass experiencing a slightly larger footprint that inundates for a longer period of time due to the improved AFP notch invert elevation being slightly lower. Waterfowl experienced similar benefits to the juvenile rearing salmon.

4.4 Discussion and Conclusions

As seen in Table 4.3 and Figures 4.7 - 4.8, the model generally captures the observed hydrographs within the model domain (Figure 4.5) at lower flows. Being that this model is mostly applied outside of peak flow events, the agreement is suitable. The model also demonstrated the ability to replicate the spatial inundation pattern against aerial imagery (Figures 4.9 - 4.11). During analysis of results, a few gages were eliminated from analysis for various reasons including unreliable observed data. Overall, this model has the ability to replicate an observed flood event and can thus be used to investigate proposed modifications to the systems topography, bathymetry, structures, or hydrologic inputs, which provides a valuable tool for various interested parties. There is still room for improvement in the peak flows and should be used for smaller flood events.

Additionally, the application of a HSI analysis demonstrates the relatively minor impacts that the construction of the adult fish passage structure improvements of 2018 had on other regional taxa with different habitat requirements. Although the model agreement shown in Figure 4.8 diverges by about a meter at higher flows, habitat is completely unsuitable for flows at that magnitude since velocities and depths are beyond the suitable ranges defined by the HSI curves (Figure 4.6).

The development of this model was funded by Yolo County with the intention of providing landowners a free and publicly available tool to evaluate impacts of a major modification to the Fremont Weir taken on by the California Department of Water Resources and the Bureau of Reclamation. Although the original impetus was to use the tool to evaluate flood risk, agricultural damages, and road access, the model can also be used to interrogate possible ecological improvements, as well as optimize economic performance in the region. Previous studies on the

Yolo Bypass can be combined with this modeling effort to fully understand the complexities of the ecology and economics of the system.

Given the sensitivity of several species in the Sacramento-San Joaquin Delta region, a study could use this model of the Yolo Bypass to evaluate current and projected habitat suitability in the Yolo Bypass as a result of changing climatological conditions or due to projected restoration projects affecting flows and inundation patterns. This model would provide insight to the sensitivity of the ecosystem to variables affecting the physical system such as flow magnitude, timing, and duration. Additionally knowing the targeted species HSI curves could allow for development and testing of restoration strategies that would amplify ideal conditions, such as berms or bladder dams to slow the draining of a flood pulse from leaving the system, allowing for a higher age of water for aquatic species to thrive. Effectively the coupling of the hydrodynamic model with known physical preferences of species of interest allows for a sandbox to experiment in before actually implementing strategies or rejecting construction and operational changes.

A similar "sandbox" approach could also be used to evaluate economic impacts of projected futures in the Yolo Bypass. Robyn Suddeth, who originally began the effort at the Center for Watershed Sciences at UC Davis to develop this Yolo Bypass model, did perform such an analysis before the model was finished being developed [128]. The economic analysis uses a similar approach to that of the habitat suitability approach in that there are parameterizations that are crop-dependent that are then combined cumulatively to determine the economic suitability - maximum profit ($Max\ P$):

$$Max\ P = \sum_{i} \left[\left(\sum_{j} \sum_{t=start}^{date} \left(A_{jti,d=0} - A_{j(t-1)i,d=0} \right) \cdot R_{jti} \right) \right] - \sum_{j} \Theta ije^{\Upsilon_{ij} A_j} \tag{4.9}$$

where i is the spatial zone, j is the land use type, d is depth, t is the time interval, $A_{jti,d=0}$ is the acres of land-use type j in zone i available for use at time t, and Θ_{ij} and Υij are cost parameters for operations. Essentially, the formula is revenues minus costs equal profit. Revenues are highly influenced by yield of the crop per year and yield is affected by the conditions during the growing season. The timing of post-flood drying in a field determines when a crop can be planted and then the onset of floods after planting can affect the yield of a crop and thus affect revenues, which in turn affects profit. The Suddeth et al. [128] study uses set zones and broader statistics to determine what the optimal conditions would be to maximize habitat quality while

not incurring significant crop losses, and as mentioned in the study, a hydrodynamic model would allow for further exploration of impacts due to specific construction or restoration efforts.

There are a range of applications for use of this model and given that it is developed in a free software, anyone who has an interest in outcomes on the Yolo Bypass would be able to access it and run different alternatives. With the frequently updated HEC-RAS software, practical availability of the model will require updates in order to guarantee compatibility with software versions. Because HEC-RAS is a highly popular hydrodynamic modeling software, interested parties wouldn't struggle to find a modeler acquainted with the software to be able to perform evaluations on whichever proposed future scenarios. It's ubiquity in the world of hydrodynamic modeling also means that online and peer support is readily available, making the development of this model a big step forward in providing the public with a tool to evaluate whatever impacts they desire.

This model of the Yolo Bypass presents a major stepping stone in providing a tool for the public to evaluate ecological and economic impacts of proposed restoration. This and the other models used in this thesis are examples of using numerical tools to interrogate the natural environment. These hydrodynamic models offer a sort of time traveling device in the investigation of flood event impacts. Once one can replicate an event via a calibrated model, they can pause at any moment in time and see how a system is behaving physically. At any point in time one can see where source waters are moving (Figure 2.7), they can understand the distribution of age within a system (Figure 3.5), and with these pieces of information they can construct a more complete narrative about the inner workings of the ecosystem. With a more thorough understanding of how various components of an aquatic ecosystem distribute spatially and temporally, linkages to the health of the ecosystem can be derived. Ultimately, this thesis aims to expand the suite of tools developed to link hydrodynamic models with biological data in order to better predict biological outcomes in a system by providing a spatio-temporal description of the physical components of that system.

Acknowledgement

The Habitat suitability index criteria as well as the code used to determine the weighted usable area was developed by Luke Tillmann at cbec under the guidance of Chris Campbell and was used with permission of the company. Thank you to Chris and Luke for aiding in the completion of this chapter.

References

[1] G. C. Nanson and J. C. Croke, "A genetic classification of floodplains," Tech. Rep., 1992, pp. 459–486.

[2] B. A. Gordon, O. Dorothy, and C. F. Lenhart, *Nutrient retention in ecologically functional floodplains: A review*, Oct. 2020. DOI: 10.3390/w12102762.

[3] J. M. Mahoney and S. B. Rood, "Streamflow requirements for cottonwood seedling recruitment-An integrative model," *Wetlands*, vol. 18, no. 4, pp. 634–645, 1998, ISSN: 02775212. DOI: 10.1007/BF03161678.

[4] G. H. Copp, "The habitat diversity and fish reproductive function of floodplain ecosystems," *Environmental Biology of Fishes*, vol. 26, no. 1, pp. 1–27, 1989, ISSN: 03781909. DOI: 10.1007/BF00002472.

[5] T Sommer, W. C. Harrell, M Nobriga, and R Kurth, "Floodplain as habitat for native fish: lessons from Californias Yolo Bypass," *California Riparian Systems: Processes and Floodplain Management, Ecology, and Restoration*, vol. 2001 Ripar, no. Photograph 1, pp. 81–87, 2003.

[6] C. A. Jeffres, J. J. Opperman, and P. B. Moyle, "Ephemeral floodplain habitats provide best growth conditions for juvenile Chinook salmon in a California river," *Environmental Biology of Fishes*, vol. 83, no. 4, pp. 449–458, 2008, ISSN: 03781909. DOI: 10.1007/s10641-008-9367-1.

[7] D. S. Ahearn, J. H. Viers, J. F. Mount, and R. A. Dahlgren, "Priming the productivity pump: Flood pulse driven trends in suspended algal biomass distribution across a restored floodplain," *Freshwater Biology*, vol. 51, no. 8, pp. 1417–1433, 2006, ISSN: 00465070. DOI: 10.1111/j.1365-2427.2006.01580.x.

[8] P. B. Moyle, P. K. Crain, and K. Whitener, "Patterns in the Use of a Restored California Floodplain by Native and Alien Fishes," *San Francisco Estuary and Watershed Science*, vol. 5, no. 3, pp. 1–29, 2007, ISSN: 1546-2366. DOI: 10.5811/westjem.2011.5.6700. arXiv: 0608246v3 [physics].

[9] K. E. Selwood, J. R. Thomson, R. H. Clarke, M. A. McGeoch, and R. Mac Nally, "Resistance and resilience of terrestrial birds in drying climates: do floodplains provide drought refugia?" *Global Ecology and Biogeography*, vol. 24, no. 7, Jul. 2015, ISSN: 1466822X. DOI: 10.1111/geb.12305.

[10] O. E. Wing, P. D. Bates, A. M. Smith, C. C. Sampson, K. A. Johnson, J. Fargione, and P. Morefield, "Estimates of present and future flood risk in the conterminous United States," *Environmental Research Letters*, vol. 13, no. 3, Mar. 2018, ISSN: 17489326. DOI: 10.1088/1748-9326/aaac65.

[11] S. M. Yarnell, G. E. Petts, J. C. Schmidt, A. A. Whipple, E. E. Beller, C. N. Dahm, P. Goodwin, and J. H. Viers, *Functional Flows in Modified Riverscapes: Hydrographs, Habitats and Opportunities*, Sep. 2015. DOI: 10.1093/biosci/biv102.

[12] J. Mount, B. Gray, C. Chappelle, G. Gartrell, T. Grantham, P. Moyle, N. Seavy, L. Szeptycki, B. Buzz, and. Thompson, "Managing California's Freshwater Ecosystems Lessons from the 2012-16 Drought," Public Policy Institute of California, Tech. Rep., 2017.

[13] A. A. Whipple, R. M. Grossinger, D Rankin, B Stanford, and R. A. Askevold, "Sacramento-San Joaquin Delta Historical Ecology Investigation: Exploring Pattern and Process.," *A Report of SFEI-ASC's Historical Ecology Program, Publication #672*, no. august, p. 408, 2012.

[14] T. E. Dahl and G. Allord, "Technical aspsects of wetlands: History of wetlands in the conterminous United States," U.S. Department of the Interior, Tech. Rep., 1996, pp. 19–26. [Online]. Available: https://www.fws.gov/Wetlands/Documents/History-of-Wetlands-in-the-Conterminous-United-States.pdf.

[15] P. K. Kundu, I. M. Cohen, and D. R. Dowling, *Fluid Mechanics*, Sixth. San Diego, CA: Elsevier Inc., 2016, ISBN: 978-0-12-405935-1.

[16] T. Tu, K. J. Carr, A. Ercan, M. L. Kavvas, and J. Nosacka, "Two-dimensional Sediment Transport Modeling in Cache Creek Settling Basin, California," in *World*

Environmental and Water Resources Congress - Floods, Droughts, and Ecosystems, 2015, pp. 1851–1858.

[17] A. J. Bever and M. L. MacWilliams, "Simulating sediment transport processes in San Pablo Bay using coupled hydrodynamic, wave, and sediment transport models," *Marine Geology*, vol. 345, pp. 235–253, Nov. 2013, ISSN: 00253227. DOI: 10.1016/j.margeo.2013.06.012.

[18] A. A. Whipple, "Managing Flow Regimes and Landscapes Together: Hydrospatial Analysis for Evaluating Spatiotemporal Floodplain Inundation Patterns with Restoration and Climate Change Implications," PhD thesis, University of California Davis, 2018. [Online]. Available: https://watershed.ucdavis.edu/files/biblio/Whipple_Dissertation_2018_0.pdf.

[19] M Bormans and I. T. Webster, "Dynamics of Temperature Stratification in Lowland Rivers," *Journal of Hydraulic Engineering*, vol. 124, no. October, pp. 1059–1063, 1998, ISSN: 0733-9429. DOI: 10.1061/(ASCE)0733-9429(1998)124:10(1059).

[20] R. C. Martyr-Koller, H. W. Kernkamp, A. van Dam, M. van der Wegen, L. V. Lucas, N. Knowles, B. Jaffe, and T. A. Fregoso, "Application of an unstructured 3D finite volume numerical model to flows and salinity dynamics in the San Francisco Bay-Delta," *Estuarine, Coastal and Shelf Science*, vol. 192, pp. 86–107, 2017, ISSN: 02727714. DOI: 10.1016/j.ecss.2017.04.024. [Online]. Available: http://dx.doi.org/10.1016/j.ecss.2017.04.024.

[21] J. L. Largier, "Considerations in estimating larval dispersal distances from oceanographic data," Tech. Rep. 1, 2003, pp. 71–89.

[22] N. E. Monsen, J. E. Cloern, L. V. Lucas, and S. G. Monismith, "A comment on the use of flushing time, residence time, and age as transport time scales," *Limnology and Oceanography*, vol. 47, no. 5, pp. 1545–1553, 2002, ISSN: 00243590. DOI: 10.4319/lo.2002.47.5.1545.

[23] Z. Defne and N. K. Ganju, "Quantifying the Residence Time and Flushing Characteristics of a Shallow , Back-Barrier Estuary : Application of Hydrodynamic and Particle Tracking Models," pp. 1719–1734, 2015. DOI: 10.1007/s12237-014-9885-3.

[24] . J. Delhez and E. Deleersnijder, "Residence and exposure times : When diffusion does not matter," *Ocean Dynamics*, vol. 62, no. 10-12, pp. 1399–1407, 2012, ISSN: 16167341. DOI: 10.1007/s10236-012-0568-y.

[25] . J. M. Delhez, B. de Brye, A. de Brauwere, and. Deleersnijder, "Residence time vs influence time," *Journal of Marine Systems*, vol. 132, pp. 185–195, 2014, ISSN: 09247963. DOI: 10.1016/j.jmarsys.2013.12.005.

[26] . J. Delhez, "On the concept of exposure time," *Continental Shelf Research*, vol. 71, pp. 27–36, 2013, ISSN: 02784343. DOI: 10.1016/j.csr.2013.09.026. [Online]. Available: http://dx.doi.org/10.1016/j.csr.2013.09.026.

[27] E. Gross, S. Andrews, B. Bergamaschi, B. Downing, R. Holleman, S. Burdick, and J. Durand, "The use of Stable Isotope-Based water age to evaluate a hydrodynamic model," *Water (Switzerland)*, vol. 11, no. 11, 2019, ISSN: 20734441. DOI: 10.3390/w11112207.

[28] L. Allan James and M. B. Singer, "Development of the Lower Sacramento Valley Flood-Control System: Historical Perspective," *Natural Hazards Review*, vol. 9, no. August, pp. 125–135, 2008, ISSN: 1527-6988. DOI: 10.1061/(ASCE)1527-6988(2008)9:3(125).

[29] R. Kelley, *Battling the Inland Sea: Floods, Public Policy, and the Sacramento Valley*. Berkeley and Los Angeles, CA: University of California Press, 1998, ISBN: 0520214285.

[30] L. A. Tomkovic, E. S. Gross, B. Nakamoto, M. L. Fogel, and C. Jeffres, "Source water apportionment of a river network: comparing field isotopes to hydrodynamically modeled tracers," *Water*, vol. 12, no. 4, 2020. [Online]. Available: https://doi.org/10.3390/w12041128.

[31] C Baranyi, T Hein, C Holarek, S Keckeis, and F Schiemer, "Zooplankton biomass and community structure in a Danube River floodplain system: effects of hydrology," *Freshwater Biology*, vol. 47, no. 3, pp. 473–482, 2002, ISSN: 0046-5070. DOI: 10.1046/j.1365-2427.2002.00822.x. [Online]. Available: isi:000174308400011.

[32] J. W. Day, C. A. Hall, W. M. Kemp, and A. Yanez-Arancibia, *Estuarine ecology*, 2nd, J. W. J. Day, B. C. Crump, W. M. Kemp, and A. Yanez-Arancibia, Eds. Hoboken, NJ, USA: John Wiley & Sons, Inc., 1988, ISBN: 0471062634. DOI: 10.2307/2937399. [Online]. Available: https://doi.org/10.2307/2937399.

[33] G. M. Ruiz, J. T. Carlton, E. D. Grosholz, and A. H. Hines, "Global invasions of marine and estuarine habitats by non-indigenous species: mechanisms, extent, and consequences," *American Zoologist*, vol. 37, no. 6, pp. 621–632, 1997, ISSN: 00031569. DOI: 10.1093/icb/37.6.621.

[34] B. Worm, E. B. Barbier, N. Beaumont, J. E. Duffy, C. Folke, B. S. Halpern, J. B. Jackson, H. K. Lotze, F. Micheli, S. R. Palumbi, E. Sala, K. A. Selkoe, J. J. Stachowicz, and R. Watson, "Impacts of biodiversity loss on ocean ecosystem services," *Science*, vol. 314, no. 5800, pp. 787–790, 2006, ISSN: 00368075. DOI: 10.1126/science.1132294.

[35] H. K. Lotze, H. S. Lenihan, B. J. Bourque, R. H. Bradbury, R. G. Cooke, M. C. Kay, S. M. Kidwell, M. X. Kirby, C. H. Peterson, and J. B. C. Jackson, "Depletion, Degradation, and Recovery Potential of Estuaries and Coastal Seas," *Science*, vol. 312, no. June, pp. 1806–1809, 2006.

[36] J. L. Bowen and I. Valiela, "The ecological effects of urbanization of coastal watersheds: historical increases in nitrogen loads and eutrophication of Waquoit Bay estuaries," *Canadian Journal of Fisheries and Aquatic Science*, vol. 58, pp. 1489–1500, 2001, ISSN: 1051-0761. DOI: 10.1139/cjfas-58-8-1489.

[37] K. Kuivila and M. L. Hladik, "Understanding the Occurrence and Transport of Current-Use Pesticides in the San Francisco Estuary Watershed," *San Francisco*

Estuary and Watershed Science, vol. 6, no. 3, 2008, ISSN: 15462366. DOI: 10.15447/sfews.2008v6iss3art2.

[38] B. Hong and J. Shen, "Responses of estuarine salinity and transport processes to potential future sea-level rise in the Chesapeake Bay," *Estuarine, Coastal and Shelf Science*, vol. 104-105, pp. 33–45, 2012, ISSN: 02727714. DOI: 10.1016/j.ecss.2012.03.014.

[39] C. Nilsson, C. A. Reidy, M. Dynesius, and C. Revenga, "Fragmentation and flow regulation of the world's large river systems," *Science*, vol. 308, no. 5720, pp. 405–408, 2005, ISSN: 00368075. DOI: 10.1126/science.1107887.

[40] K. F. Drinkwater, "On the Role of Freshwater Outflow on Coastal Marine Ecosystems - A Workshop Summary," in *The Role of Freshwater Outflow in Coastal Marine Ecosystems*, S. Skreslet, Ed., Berlin, Heidelberg: Springer Berlin Heidelberg, 1986, pp. 429–438, ISBN: 978-3-642-70886-2.

[41] H. B. Fischer, E. J. List, R. C. Y. Koh, J. Imberger, and N. H. Brooks, *Mixing in Inland and Coastal Waters*. San Diego, CA: Academic Press, 1979, ISBN: 978-0-12-258150-2.

[42] J. J. Gibson and R. Reid, "Water balance along a chain of tundra lakes: A 20-year isotopic perspective," *Journal of Hydrology*, vol. 519, no. PB, pp. 2148–2164, 2014, ISSN: 00221694. DOI: 10.1016/j.jhydrol.2014.10.011. [Online]. Available: http://dx.doi.org/10.1016/j.jhydrol.2014.10.011.

[43] L. S. Sherman, J. D. Blum, J. T. Dvonch, L. E. Gratz, and M. S. Landis, "The use of Pb, Sr, and Hg isotopes in Great Lakes precipitation as a tool for pollution source attribution," *Science of the Total Environment*, vol. 502, pp. 362–374, 2015, ISSN: 18791026. DOI: 10.1016/j.scitotenv.2014.09.034. [Online]. Available: http://dx.doi.org/10.1016/j.scitotenv.2014.09.034.

[44] D. P. Krabbenhoft, C. J. Bowser, C. Kendall, and J. R. Gat, "Use of Oxygen-18 and Deuterium To Assess the Hydrology of Groundwater-Lake Systems," pp. 67–90, 1994, ISSN: 0065-2393. DOI: 10.1021/ba-1994-0237.ch003.

[45] T. Vitvar, D. A. Burns, G. B. Lawrence, J. J. Mcdonnell, and D. M. Wolock, "Estimation of baseflow residence times in watersheds from the runoff hydrograph recession : method and application in the Neversink watershed , Catskill Mountains , New York," vol. 1877, no. April, pp. 1871–1877, 2002. DOI: 10.1002/hyp.5027.

[46] C. Marchina, G. Bianchini, C. Natali, M. Pennisi, N. Colombani, R. Tassinari, and K. Knoeller, "The Po river water from the Alps to the Adriatic Sea (Italy): new insights from geochemical and isotopic (δ18O-δD) data," *Environmental Science and Pollution Research*, vol. 22, no. 7, pp. 5184–5203, 2015, ISSN: 16147499. DOI: 10.1007/s11356-014-3750-6.

[47] D. Penna, G. Zuecco, S. Crema, S. Trevisani, M. Cavalli, L. Pianezzola, L. Marchi, and M. Borga, "Response time and water origin in a steep nested catchment in the Italian Dolomites," *Hydrological Processes*, vol. 31, no. 4, pp. 768–782, 2017, ISSN: 10991085. DOI: 10.1002/hyp.11050.

[48] C. Marchina, V. Lencioni, F. Paoli, M. Rizzo, and G. Bianchini, "Headwaters' isotopic signature as a tracer of stream origins and climatic anomalies: Evidence from the Italian Alps in summer 2018," *Water (Switzerland)*, vol. 12, no. 2, 2020, ISSN: 20734441. DOI: 10.3390/w12020390.

[49] J. Halder, L. Decrouy, and T. W. Vennemann, "Mixing of Rhône River water in Lake Geneva (Switzerland-France) inferred from stable hydrogen and oxygen isotope profiles," *Journal of Hydrology*, vol. 477, pp. 152–164, 2013, ISSN: 00221694. DOI: 10.1016/j.jhydrol.2012.11.026.

[50] K. T. Peter, C. Wu, Z. Tian, and E. P. Kolodziej, "Application of Nontarget High Resolution Mass Spectrometry Data to Quantitative Source Apportionment," *Environmental Science and Technology*, vol. 53, pp. 12 257–12 268, 2019, ISSN: 15205851. DOI: 10.1021/acs.est.9b04481.

[51] V. K. Sridharan, S. G. Monismith, D. A. Fong, and J. L. Hench, "One-dimensional particle tracking with streamline preserving junctions for flows in channel net-

works," *Journal of Hydraulic Engineering*, vol. 144, no. 2, pp. 1–10, 2018, ISSN: 19437900. DOI: 10.1061/(ASCE)HY.1943-7900.0001399.

[52] H. Bai, Y. Chen, D. Wang, R. Zou, H. Zhang, R. Ye, W. Ma, and Y. Sun, "Developing an EFDC and numerical source-apportionment model for nitrogen and phosphorus contribution analysis in a Lake Basin," *Water (Switzerland)*, vol. 10, no. 10, 2018, ISSN: 20734441. DOI: 10.3390/w10101315.

[53] J. Lund, E. Hanak, W. Fleenor, W. Bennett, R. Howitt, J. Mount, and P. Moyle, *Envisioning Futures for the Sacramento-San Joaquin Delta*. San Francisco, CA: Public Policy Institute of California, 2007, ISBN: 9781582131269. DOI: 10.1007/s13398-014-0173-7.2. arXiv: 9809069v1 [gr-qc]. [Online]. Available: http://ideas.repec.org/b/ppi/ppirpt/deltaa.html.

[54] J. Mount, W. Bennett, J. Durand, W. Fleenor, E. Hanak, J. Lund, and P. Moyle, "Aquatic Ecosystem Stressors in the Sacramento San Joaquin Delta," Tech. Rep., 2012.

[55] E. S. Gross, P. H. Hutton, and A. J. Draper, "A comparison of outflow and salt intrusion in the pre-development and contemporary San Francisco estuary," *San Francisco Estuary and Watershed Science*, vol. 16, no. 3, 2018, ISSN: 15462366. DOI: 10.15447/sfews.2018v16iss3art6.

[56] J. Lund, E. Hanak, W. Fleenor, W. Bennett, R. Howitt, J. Mount, and P. Moyle, *Comparing Futures for the Sacramento-San Joaquin Delta*. Berkely, CA: University of California Press, 2010, ISBN: 0520261976.

[57] K. J. Brown and G. B. Pasternack, "The geomorphic dynamics and environmental history of an upper deltaic floodplain tract in the Sacramento-San Joaquin Delta, California, USA," *Earth Surface Processes and Landforms*, vol. 29, no. 10, pp. 1235–1258, 2004, ISSN: 01979337. DOI: 10.1002/esp.1088.

[58] A. A. Whipple, J. H. Viers, and H. E. Dahlke, "Flood regime typology for floodplain ecosystem management as applied to the unregulated Cosumnes River of Califor-

nia, United States," *Ecohydrology*, vol. 10, no. 5, pp. 1–18, 2017, ISSN: 19360592. DOI: 10.1002/eco.1817.

[59] J. R. Gat, "Oxygen and Hydrogen Isotopes in the Hydrologic Cycle," *Annual Review of Earth and Planetary Sciences*, vol. 24, no. 1, pp. 225–262, 1996, ISSN: 0084-6597. DOI: 10.1146/annurev.earth.24.1.225.

[60] V. Casulli and R. A. Walters, "An unstructured grid, three-dimensional model based on the shallow water equations," *International Journal for Numerical Methods in Fluids*, vol. 32, no. 3, pp. 331–348, 2000, ISSN: 02712091.

[61] R. A. Walters and V. Casulli, "A robust, finite element model for hydrostatic surface water flows," *Communications in Numerical Methods in Engineering*, vol. 14, no. 10, pp. 931–940, 1998, ISSN: 10698299. DOI: 10.1002/(SICI)1099-0887(1998100)14:10<931::AID-CNM199>3.0.CO;2-X.

[62] David Ford Consulting Engineers, "Cosumnes and Mokelumne River watersheds Design storm runoff analysis," David Ford Consulting Engineers, Inc, Sacramento, CA, Tech. Rep., 2004.

[63] C. J. Willmott, "On the Validation of Models," *Physical Geography*, vol. 2, no. 2, pp. 184–194, 1981. DOI: 10.1080/02723646.1981.10642213.

[64] V. Casulli and P. Zanolli, "Semi-implicit numerical modeling of nonhydrostatic free-surface flows for environmental problems," *Mathematical and Computer Modelling*, vol. 36, no. 9-10, pp. 1131–1149, 2002, ISSN: 08957177. DOI: 10.1016/S0895-7177(02)00264-9.

[65] G. B. Pasternack, C. L. Wang, and J. E. Merz, "Application of a 2D hydrodynamic model to design of reach-scale spawning gravel replenishment on the Mokelumne River, California," *River Research and Applications*, vol. 20, no. 2, pp. 205–225, 2004, ISSN: 15351459. DOI: 10.1002/rra.748.

[66] G. M. Kondolf, P. L. Angermeier, K. Cummins, T. Dunne, M. Healey, W. Kimmerer, P. B. Moyle, D. Murphy, D. Patten, S. Railsback, D. J. Reed, R. Spies, and R. Twiss, "Projecting cumulative benefits of multiple river restoration projects:

An example from the Sacramento-San Joaquin river system in California," *Environmental Management*, vol. 42, no. 6, pp. 933–945, 2008, ISSN: 0364152X. DOI: 10.1007/s00267-008-9162-y.

[67] S. S. Parker, E. J. Remson, and L. N. Verdone, "Restoring conservation nodes to enhance biodiversity and ecosystem function along the santa clara river," *Ecological Restoration*, vol. 32, no. 1, pp. 6–8, 2014, ISSN: 15434079. DOI: 10.3368/er.32.1.6.

[68] B. Hassett, M. Palmer, E. Bernhardt, S. Smith, J. Carr, and D. Hart, "Restoring watersheds project by project: Trends in Chesapeake Bay tributary restoration," *Frontiers in Ecology and the Environment*, vol. 3, no. 5, pp. 259–267, 2005, ISSN: 15409309. DOI: 10.1890/1540-9295(2005)003[0259:RWPBPT]2.0.CO;2.

[69] R. L. Vannote, G. W. Minshall, K. W. Cummins, J. R. Sedell, and C. E. Cushing, "The River Continuum Concept," *Canadian Journal of Fisheries and Aquatic Sciences*, vol. 37, pp. 130–137, 1980.

[70] R. O. Swenson, K. Whitener, and M. Eaton, "Restoring floods on floodplains: riparian and floodplain restoration at the Cosumnes River Preserve," *California Riparian Systems: Processes and Floodplain Management, Ecology and Restoration*, pp. 224–229, 2003. [Online]. Available: http://www.sjrdotmdl.org/concept_model/phys-chem_model/documents/300001823.pdf.

[71] J. J. Opperman, R. Luster, B. A. McKenney, M. Roberts, and A. W. Meadows, "Ecologically functional floodplains: Connectivity, flow regime, and scale," *Journal of the American Water Resources Association*, vol. 46, no. 2, pp. 211–226, 2010, ISSN: 1093474X. DOI: 10.1111/j.1752-1688.2010.00426.x.

[72] California Natural Resources Agency, California Department of Food and Agriculture, and California Environmental Protection Agency, "California Water Action Plan: 2016 Update," Tech. Rep., 2016, p. 22. [Online]. Available: http://resources.ca.gov/docs/california_water_action_plan/Final_California_Water_Action_Plan.pdf.

[73] L. Farly, C. Hudon, A. Cattaneo, and G. Cabana, "Seasonality of a Floodplain Subsidy to the Fish Community of a Large Temperate River," *Ecosystems*, vol. 22, no. 8, pp. 1823–1837, 2019, ISSN: 14350629. DOI: 10.1007/s10021-019-00374-w. [Online]. Available: https://doi.org/10.1007/s10021-019-00374-w.

[74] M. Bormans, P. W. Ford, and L. Fabbro, "Spatial and temporal variability in cyanobacterial populations controlled by physical processes," *Journal of Plankton Research*, vol. 27, no. 1, pp. 61–70, 2005, ISSN: 01427873. DOI: 10.1093/plankt/fbh150.

[75] N. Niquil, E. Chaumillon, G. A. Johnson, X. Bertin, B. Grami, V. David, C. Bacher, H. Asmus, D. Baird, and R. Asmus, "The effect of physical drivers on ecosystem indices derived from ecological network analysis: Comparison across estuarine ecosystems," *Estuarine, Coastal and Shelf Science*, vol. 108, no. 2012, pp. 132–143, 2012, ISSN: 02727714. DOI: 10.1016/j.ecss.2011.12.031.

[76] P. B. Shafroth, A. C. Wilcox, D. A. Lytle, J. T. Hickey, D. C. Andersen, V. B. Beauchamp, A. Hautzinger, L. E. McMullen, and A. Warner, "Ecosystem effects of environmental flows: Modelling and experimental floods in a dryland river," *Freshwater Biology*, vol. 55, no. 1, pp. 68–85, 2010, ISSN: 00465070. DOI: 10.1111/j.1365-2427.2009.02271.x.

[77] W. T. Flatley and P. Z. Fulé, "Are historical fire regimes compatible with future climate? Implications for forest restoration," *Ecosphere*, vol. 7, no. 10, pp. 1–21, 2016, ISSN: 21508925. DOI: 10.1002/ecs2.1471.

[78] B. Ainslie, N. Alexander, N. Johnston, J. Bradley, A. C. Pomeroy, P. L. Jackson, and K. A. Otter, "Predicting spatial patterns of eagle migration using a mesoscale atmospheric model: A case study associated with a mountain-ridge wind development," *International Journal of Biometeorology*, vol. 58, no. 1, pp. 17–30, 2014, ISSN: 00207128. DOI: 10.1007/s00484-012-0620-0.

[79] J. E. Cloern, "Habitat connectivity and ecosystem productivity: implications from a simple model.," *The American naturalist*, vol. 169, no. 1, 2007, ISSN: 15375323. DOI: 10.1086/510258.

[80] D. Aksnes and J. Egge, "A theoretical model for nutrient uptake," *Marine Ecology Progress Series*, vol. 70, no. 1, pp. 65–72, 1991, ISSN: 0171-8630. DOI: 10.3354/meps070065. [Online]. Available: http://www.jstor.org/stable/24816799.

[81] L. V. Lucas, J. K. Thompson, and L. R. Brown, "Why are diverse relationships observed between phytoplankton biomass and transport time?" *Limnology and Oceanography*, vol. 54, no. 1, pp. 381–390, 2009, ISSN: 00243590. DOI: 10.4319/lo.2009.54.1.0381. [Online]. Available: http://doi.wiley.com/10.4319/lo.2009.54.1.0381.

[82] N. Mladenov, D. M. McKnight, P. Wolski, and L. Ramberg, "Effects of annual flooding on dissolved organic carbon dynamics within a pristine wetland, the Okavango Delta, Botswana," *Wetlands*, vol. 25, no. 3, pp. 622–638, 2005, ISSN: 02775212. DOI: 10.1672/0277-5212(2005)025[0622:EOAFOD]2.0.CO;2.

[83] A. I. Robertson, S. E. Bunn, P. I. Boon, and K. F. Walker, "Sources, sinks and transformations of organic carbon in Australian floodplain rivers," *Marine & Freshwater Research*, vol. 50, pp. 813–829, 1999. DOI: 10.1071/MF99112.

[84] N. J. Corline, T. Sommer, C. A. Jeffres, J. Katz, C. Salmon, and. C.. Rice, "Zooplankton ecology and trophic resources for rearing native fish on an agricultural floodplain in the Yolo Bypass," *Wetlands Ecology and Management*, vol. 25, no. 5, pp. 547–559, 2017, ISSN: 1572-9834. DOI: 10.1007/s11273-017-9534-2.

[85] M. L. Pace, K. G. Porter, and Y. S. Feig, "Species- and age-specific differences in bacterial resource utilization by two co-occuring cladocerans," *Ecology*, vol. 64, no. 5, pp. 1145–1156, 1983.

[86] J. F. Saunders and W. M. Lewis, "Zooplankton abundance in the lower Orinoco River, Venezuela," *Limnology and Oceanography*, vol. 34, no. 2, pp. 397–409, 1989, ISSN: 19395590. DOI: 10.4319/lo.1989.34.2.0397.

[87] W. A. Bennett and P. B. Moyle, "Where have all the fishes gone? Interactive factors producing fish declines in the Sacramento-San Joaquin estuary," in *San Francisco Bay: The Ecosystem*, J. T. Hollibaugh, Ed., San Francisco, CA, 1996, pp. 519–542.

[88] P. B. Bayley, "Understanding large river-floodplain ecosystems - Significant economic advantages and increased biodiversity and stability would result from restoration of impaired systems," *BioScience*, vol. 45, no. 3, pp. 153–158, 1995, ISSN: 0006-3568. DOI: 10.2307/1312554.

[89] W. J. Junk, P. B. Bayley, and R. E. Sparks, "The flood pulse concept in river-floodplain systems," in *International Large River Symposium (LARS)*, vol. 106, Honey Harbour, Ontario, Canada: Canadian Special Publication of Fisheries and Aquatic Sciences, 1989, pp. 110–127, ISBN: 0-660-13259-1. DOI: 10.1371/journal.pone.0028909.

[90] J. V. E. Katz, C. Jeffres, J. L. Conrad, T. R. Sommer, J. Martinez, S. Brumbaugh, N. Corline, and P. B. Moyle, "Floodplain farm fields provide novel rearing habitat for Chinook salmon," pp. 1–16, 2017.

[91] K. Tockner and J. A. Stanford, "Riverine flood plains: Present state and future trends," *Environmental Conservation*, vol. 29, no. 3, pp. 308–330, 2002, ISSN: 03768929. DOI: 10.1017/S037689290200022X.

[92] R. E. Sparks, "Need for ecosystem management of large rivers and their floodplains," *BioScience*, vol. 45, no. 3, pp. 168–182, 1995, ISSN: 08860882. DOI: 10.2307/1312556. [Online]. Available: https://www.jstor.org/stable/1312556.

[93] L. A. James and M. B. Singer, "Development of the Lower Sacramento Valley Flood-Control System : Historical Perspective," no. August, pp. 125–135, 2008.

[94] G. H. Golet, M. D. Roberts, R. A. Luster, G. Werner, E. W. Larsen, R. Unger, and G. G. White, "Assessing societal impacts when planning restoration of large alluvial rivers: A case study of the Sacramento River Project, California," *Environmental Management*, vol. 37, no. 6, pp. 862–879, 2006, ISSN: 0364152X. DOI: 10.1007/s00267-004-0167-x.

[95] R. A. Camacho and J. L. Martin, "Hydrodynamic modeling of first-order transport timescales in the St. Louis Bay Estuary, Mississippi," *Journal of Environmental Engineering (United States)*, vol. 139, no. 3, pp. 317–331, 2013, ISSN: 07339372. DOI: 10.1061/(ASCE)EE.1943-7870.0000647.

[96] . J. Delhez, A. W. Heemink, and. Deleersnijder, "Residence time in a semi-enclosed domain from the solution of an adjoint problem," *Estuarine, Coastal and Shelf Science*, vol. 61, no. 4, pp. 691–702, 2004, ISSN: 02727714. DOI: 10.1016/j.ecss.2004.07.013.

[97] B. L. Kimmel and D. M. Søballe, "A largescale comparison of factors influencing phytoplankton abundance in rivers, lakes, and impoundments," *Ecology*, vol. 68, no. 6, pp. 1943–1954, 1987.

[98] L. E. Schemel, T. R. Sommer, A. B. Müller-Solger, and W. C. Harrell, "Hydrologic variability, water chemistry, and phytoplankton biomass in a large floodplain of the Sacramento River, CA, U.S.A.," *Hydrobiologia*, vol. 513, no. 1, pp. 129–139, 2004, ISSN: 0018-8158. DOI: 10.1023/B:hydr.0000018178.85404.1c.

[99] T. A. Doane and W. R. Horwáth, "Spectrophotometric Determination of Nitrate with a Single Reagent," *Analytical Letters*, vol. 36, no. 12, Jan. 2003, ISSN: 0003-2719. DOI: 10.1081/AL-120024647.

[100] R. B. Baird, A. D. Eaton, and E. W. Rice, Eds., *Standard Methods for the Examination of Water and Wastewater*, 23rd ed. Washington D.C.: American Public Health Association, 2017.

[101] R. Merritt, K. Cummins, and M. Berg, *An Introduction to the Aquatic Insects of North America*, 4th. Kendall Hunt Publishing, 2008.

[102] J. Thorp and A. Covich, *Ecology and Classification of North American Freshwater Invertebrates*. Elsevier, 2010, ISBN: 9780123748553. DOI: 10.1016/C2009-0-02669-5.

[103] C. C. Mischke, D. J. Wise, and R. L. Lane, "Zooplankton Size and Taxonomic Selectivity of Channel Catfish Fry," *North American Journal of Aquaculture*, 2003.

[104] E. P. Lemagie and J. A. Lerczak, "A Comparison of Bulk Estuarine Turnover Timescales to Particle Tracking Timescales Using a Model of the Yaquina Bay Estuary," *Estuaries and Coasts*, vol. 38, no. 5, pp. 1797–1814, 2015, ISSN: 15592731. DOI: 10.1007/s12237-014-9915-1.

[105] M. D. Rayson, E. S. Gross, R. D. Hetland, and O. B. Fringer, "Time scales in Galveston Bay: An unsteady estuary Matthew," *Journal of Geophysical Research: Oceans*, vol. 121, pp. 2268–2285, 2016, ISSN: 21699291. DOI: 10.1002/2015JC011516.

[106] J. Fowler, L. Cohen, and P. Jarvis, *Practical Statistics for Field Biology*, 2nd ed. West Sussex PO19 8SQ, England: John Wiley & Sons Ltd, 1998.

[107] N. J. Corline, R. A. Peek, J. Montgomery, J. V. Katz, and C. A. Jeffres, "Understanding community assembly rules in managed floodplain food webs," *Ecosphere*, vol. 12, no. 2, Feb. 2021, ISSN: 21508925. DOI: 10.1002/ecs2.3330.

[108] T. Fenchel, L. D. Kristensen, and L. Rasmussen, "Water column anoxia: vertical zonation of planktonic protozoa," *Marine Ecology Progress Series*, vol. 62, pp. 1–10, 1990.

[109] J. D. Allan, "Life History Patterns in Zooplankton," *The American Naturalist*, vol. 110, no. 971, Feb. 1976. [Online]. Available: https://about.jstor.org/terms.

[110] V. Podsetchine and G. Schernewski, "The influence of spatial wind inhomogeneity on flow patterns in a small lake," *Water Resources*, vol. 33, no. 15, pp. 3348–3356, 1999. [Online]. Available: www.elsevier.com/locate/watres.

[111] K. Bryan, "Geology and groundwater resources of Sacramento Valley, California," U.S. Geological Survey, Tech. Rep., 1923.

[112] T. Sommer, B. Harrell, M. Nobriga, R. Brown, P. Moyle, W. Kimmerer, and L. Schemel, "California's Yolo Bypass: Evidence that flood control Can Be compatible with fisheries, wetlands, wildlife, and agriculture," *Fisheries*, vol. 26, no. 8, pp. 6–

16, 2001, ISSN: 0363-2415. DOI: 10.1577/1548-8446(2001)026<0006:CYB>2.0.CO;2.

[113] M. Russo and DWR, "Fact Sheet: Sacramento River Flood Control Project Weirs and Flood Relief Structures," no. December, pp. 1–21, 2010. [Online]. Available: https://www.rd108.org/wp-content/uploads/2015/07/WeirsReliefStructures.pdf.

[114] E. Grosholz and E. Gallo, "The influence of flood cycle and fish predation on invertebrate production on a restored California floodplain," *Hydrobiologia*, vol. 568, no. 1, pp. 91–109, 2006, ISSN: 00188158. DOI: 10.1007/s10750-006-0029-z.

[115] R. E. Salcido, "The Success and Continued Challenges of the Yolo Bypass Wildlife Area: A Grassroots Restoration," *Ecology Law Quarterly*, vol. 39, no. 4, pp. 1085–1134, 2012, ISSN: 0046-1121. DOI: 10.15779/Z38B541.

[116] A. Brice, Y. B. Foundation, and P. O. Box, "The Yolo Bypass Wildlife Area : History , Management and Significance for Birds," pp. 2–13, 2015.

[117] F. Feyrer, T. Sommer, and W. Harrell, "Managing floodplain inundation for native fish: Production dynamics of age-0 splittail (Pogonichthys macrolepidotus) in California's Yolo Bypass," *Hydrobiologia*, vol. 573, no. 1, pp. 213–226, 2006, ISSN: 00188158. DOI: 10.1007/s10750-006-0273-2.

[118] K. D. Bovee, "Development and evaluation of habitat suitability criteria for use in the Instream Flow Incremental Methodology," U.S. Fish and Wildlife Service, Tech. Rep., 1986, p. 235.

[119] Y. Yi, X. Cheng, Z. Yang, S. Wieprecht, S. Zhang, and Y. Wu, "Evaluating the ecological influence of hydraulic projects: A review of aquatic habitat suitability models," *Renewable and Sustainable Energy Reviews*, vol. 68, no. September 2016, pp. 748–762, 2017, ISSN: 18790690. DOI: 10.1016/j.rser.2016.09.138.

[120] A. M. Mouton, M. Schneider, J. Depestele, P. L. Goethals, and N. De Pauw, "Fish habitat modelling as a tool for river management," *Ecological Engineering*, vol. 29, no. 3, pp. 305–315, 2007, ISSN: 09258574. DOI: 10.1016/j.ecoleng.2006.11.002.

[121] "Fremont Weir Adult Fish Passage Modification Project Final Initial Study/Environmental Assessment," California Department of Water Resources, Tech. Rep., Aug. 2017. [Online]. Available: https://www.usbr.gov/mp/nepa/includes/documentShow.php?Doc_ID=29941.

[122] cbec, Yolo Basin Foundation, Consero Solutions, and D. Environmental, "Yolo Bypass Drainage and Water Infrastructure Improvement Study - Final Report," Tech. Rep. April, 2014.

[123] "Chinook Salmon Habitat Quantification Tool User Guide," San Francisco Estuary Institute, Tech. Rep. December, Dec. 2019.

[124] G. C. Roegner, R. McNatt, D. J. Teel, and D. L. Bottom, "Distribution, Size, and Origin of Juvenile Chinook Salmon in Shallow-Water Habitats of the Lower Columbia River and Estuary, 20022007," *Marine and Coastal Fisheries*, vol. 4, no. 1, pp. 450–472, 2012, ISSN: 19425120. DOI: 10.1080/19425120.2012.675982.

[125] G. E. Davis, J. Foster, C. E. Warren, and P. Doudoroff, "The Influence of Oxygen Concentration on the Swimming Performance of Juvenile Pacific Salmon at Various Temperatures," *Transactions of the American Fisheries Society*, vol. 92, no. 2, pp. 111–124, Apr. 1963, ISSN: 0002-8487. DOI: 10.1577/1548-8659(1963)92[111:tiooco]2.0.co;2.

[126] "Southern Pacific Shorebird Conservation Plan - A Strategy for Supporting Californias Central Valley and Coastal Shorebird Populations," PRBO Conservation Science, Stinson Beach, CA, Tech. Rep., Dec. 2003. [Online]. Available: www.prbo.org.

[127] "Wetland Management for Waterfowl Handbook," Mississippi River Trust, Tech. Rep., 2007. [Online]. Available: http://plants.usda.gov/plants.

[128] R. G. Suddeth and J. R. Lund, "Multi-purpose optimization for reconciliation ecology on an engineered floodplain: Yolo Bypass, California," *San Francisco Estuary and Watershed Science*, vol. 14, no. 1, 2016, ISSN: 15462366. DOI: 10.15447/sfews.2016v14iss1art5.